DEVELOPING OPTIMUM OPERATION STRATEGIES FOR WIND-HYDRO HYBRID SYSTEMS

A THESIS SUBMITTED TO
THE GRADUATE SCHOOL OF NATURAL AND APPLIED SCIENCES
OF
MIDDLE EAST TECHNICAL UNIVERSITY

BY

ERAY ERCAN

IN PARTIAL FULFILLMENT OF THE REQUIREMENTS
FOR
THE DEGREE OF MASTER OF SCIENCE
IN
CIVIL ENGINEERING

JUNE 2020

Approval of the thesis:

DEVELOPING OPTIMUM OPERATION STRATEGIES FOR WIND-HYDRO HYBRID SYSTEMS

submitted by **ERAY ERCAN** in partial fulfillment of the requirements for the degree of **Master of Science in Civil Engineering Department, Middle East Technical University** by,

Prof. Dr. Halil Kalıpçılar
Dean, Graduate School of **Natural and Applied Sciences** ________________

Prof. Dr. Ahmet Türer
Head of Department, **Civil Engineering** ________________

Prof. Dr. Elçin Kentel Erdoğan
Supervisor, **Civil Engineering, METU** ________________

Examining Committee Members:

Prof. Dr. Ayşe Burcu Altan Sakarya
Civil Engineering, METU ________________

Prof. Dr. Elçin Kentel Erdoğan
Civil Engineering, METU ________________

Prof. Dr. İsmail Yücel
Civil Engineering, METU ________________

Prof. Dr. Ayşegül Aksoy
Environmental Engineering, METU ________________

Assist. Prof. Dr. Gökçen Uysal
Civil Engineering, Eskişehir Technical University ________________

Date: 18.06.2020

I hereby declare that all information in this document has been obtained and presented in accordance with academic rules and ethical conduct. I also declare that, as required by these rules and conduct, I have fully cited and referenced all material and results that are not original to this work.

Name, Surname: Eray Ercan

Signature :

ABSTRACT

DEVELOPING OPTIMUM OPERATION STRATEGIES FOR WIND-HYDRO HYBRID SYSTEMS

Ercan, Eray
M.S., Department of Civil Engineering
Supervisor: Prof. Dr. Elçin Kentel Erdoğan

June 2020, 124 pages

In today's world, energy is one of the most important drivers for the continuation of civilization. Until recent years, the energy demands of the countries have been mainly supplied by fossil fuels. However, the negative effects of using fossil fuels in energy generation shifted the focus to renewable energy resources. In addition to this, the popularity of renewable energy resources increased as their costs decreased and efficiencies increased. Therefore, the integration of renewable energy systems to national grids increased in recent years. However, this integration is challenging due to the intermittent nature of renewable energy sources. In addition to the uncertainty in the generation of energy from the renewables, the uncertainty in the electricity spot markets increases the difficulty in the management of the renewables. To deal with the intermittent nature of the renewables, energy storage systems have to be implemented. Pumped storage hydropower is currently the most viable form of large scale energy storage. The operation of renewable systems, together with pumped storage hydropower plants, increases the efficiency of the hybrid system. In this study, a wind-hydro hybrid system (WHHS) is considered, and optimum daily operation strategies for a hypothetical case study is developed. To increase the revenue of the

WHHS, a long short-term memory (LSTM) network is developed to forecast electricity prices in the day-ahead spot electricity market. Apart from the LSTM network, an optimization model is developed to obtain optimum operation schedules and the maximum revenue of the WHHS by using the electricity price and available wind energy as inputs. To investigate the effects of the LSTM network and the optimization model, different scenarios are created and run. According to the results, it is observed that wind turbines compensate the loss due to the poor forecasting of the electricity price. Thus, the higher the installed capacity of wind turbines in the WHHS, the better compensation it provides. However, within the studied range (i.e., 25 MW to 500 MW), the operation schedules of the pump and the hydro turbine of the WHHS are not affected from increasing the installed capacity of wind turbines. Once enough energy is generated by wind turbines to be used to pump the water to the upper reservoir, the rest of the wind energy is directly sold to the grid.

Keywords: Renewable Energy, Optimization, LSTM, Electricity Price Forecasting, Wind-Hydro Hybrid Systems

ÖZ

RÜZGAR-HİDRO HİBRİT SİSTEMLER İÇİN OPTİMUM ÇALIŞMA STRATEJİLERİNİN GELİŞTİRİLMESİ

Ercan, Eray
Yüksek Lisans, İnşaat Mühendisliği Bölümü
Tez Yöneticisi: Prof. Dr. Elçin Kentel Erdoğan

Haziran 2020 , 124 sayfa

Günümüz dünyasında enerji, uygarlıkların devamı için en önemli unsurlardan biridir. Geçtiğimiz yıllara kadar ülkelerin enerji talepleri çoğunlukla fosil yakıtlar tarafından karşılanmıştır. Ancak, fosil yakıtların enerji üretiminde kullanılmasının olumsuz etkileri, ilgiyi yenilenebilir enerji kaynaklarına kaydırmıştır. Buna ek olarak, yenilenebilir enerji kaynaklarının popülaritesini maliyetlerdeki düşüş ve verimlilikteki artış olumlu etkilemiştir. Bu nedenle, yenilenebilir enerji sistemlerinin elektrik şebekelerine entegrasyonu son yıllarda artış göstermiştir. Ancak, yenilenebilir enerji kaynaklarının sürekli olmaması entegrasyonu zorlu bir hale getirmektedir. Yenilenebilir enerji kaynaklarındanki belirsizliğe ek olarak, elektrik spot piyasalarındaki belirsizlik, yenilenebilir enerji kaynaklarının yönetimindeki zorluğu arttırmaktadır. Yenilenebilir enerji kaynaklarının süreksizliği ile başa çıkmak için enerji depolama sistemlerinin uygulanması gerekmektedir. Pompaj depolamalı hidroelektrik santralleri şu anda büyük ölçekli enerji depolamanın en uygun şeklidir. Yenilenebilir enerji sislemlerinin pompaj depolamalı hidroelektrik santraller ile birlikte çalıştırılması hibrit sistemlerin verimliliğini arttırmaktadır. Bu çalışmada, bir rüzgar-hidro hibrit sistemi (RHHS) ele alınmış ve varsayımsal bir vaka çalışması için optimum çalışma stratejileri geliştirilmiştir. RHHS'nin gelirini artırmak için, gün öncesi spot elektrik piyasasındaki elektrik fiyatlarını tahmin etmek için uzun kısa vadeli hafıza (UKVH) ağı geliştirilmiştir. UKVH ağının yanı sıra, elektrik fiyatını ve mevcut rüzgar enerjisini girdi olarak kullanarak optimum çalışma programları sunan ve RHHS'nin maksimum gelirini elde eden bir optimizasyon modeli geliştirilmiştir. UKVH ağının ve optimizasyon modelinin etkilerini araştırmak için farklı senaryolar oluşturulmuş ve çalıştırılmıştır. Elde edilen sonuçlara göre, rüzgar türbinlerinin elektrik fiyatının başarısız tahmininden kaynaklanan kaybı telafi ettiği görülmektedir. Bu nedenle, rüzgar türbini sayısındaki artış, kaybın azalmasını sağlamaktadır. Ancak, bu çalışmada analiz edilen rüzgar türbin enerji aralığında (10 MW ile 500 MW arası), RHHS'deki pompa ve hidrolik türbinin operasyonel programlarının değişmediği görülmüştür. Rüzgar türbinleri tarafından üretilen enerji, suyu üst rezervuara pompalamak için kullanıldıktan sonra geriye kalanının doğrudan şebekeye satıldığı gözlemlenmiştir.

Anahtar Kelimeler: Yenilenebilir Enerji, Optimizasyon, UKVH, Elektrik Fiyat Tahmini, Rüzgar-Hidro Hibrit Sistemler

To my family

ACKNOWLEDGMENTS

I would like to thank my supervisor Prof. Dr. Elçin Kentel Erdoğan for her guidance, continuous encouragement, patience, support, and sharing her knowledge throughout all my thesis study. It was a great chance to study with her, who improved my engineering perspective.

I would like to express my deepest appreciation to my family and friends for their endless care and motivation.

TABLE OF CONTENTS

LIST OF TABLES

TABLES

LIST OF FIGURES

FIGURES

CHAPTER 1

INTRODUCTION

The development of nations depends on the energy used. Thus, energy demand is increasing continuously. Conventional energy sources do not exist everywhere, and they will be even scarcer in the future. Also, due to the negative impacts of conventional energy sources on the environment, their use keeps on decreasing globally (Panwar, Kaushik and Kothari, 2011). One of the most current concerns of the World is climate change. One of the reasons for climate change is greenhouse gases that are the result of fossil fuel power plants. Instead of conventional energy sources, renewable energy sources have risen to prominence in recent years. Currently, many governments support renewable energy investments since they are environmentally friendly and infinite. Also, the integration of renewable energy into the energy budget of a country increases its energy security by reducing energy imports from other countries. However, renewable energy sources depend on season, weather conditions, and time. Likewise, energy demand is variable. Thus, the storage of renewable energy sources is a necessity, and their direct storage is not possible.

The cost of renewable energy systems was higher than the cost of fossil fuels, so renewable energy systems could not compete in the market for many years (Timmons, Harris and Roach, 2014). Only hydropower has competed with fossil fuels for a long time, but unless the necessary precautions are taken, hydropower projects have some negative social and ecological effects on people and the project area (Kentel and Alp, 2013; Somaraki, 2003). On the other hand, they have many benefits such as flood control, water supply, low-cost energy generation, and recreation lands (Hogeboom, Knook and Hoekstra, 2018).

Apart from hydropower, wind energy become a key renewable energy option due to technology advancement and cost reduction in its establishment (IRENA, 2019). However, the intermittent nature of the wind brings serious problems and decreases the efficiency of energy systems. It negatively affects the grid stability and decreases the revenue of the energy seller due to not fulfilling the proposed operational schedule in the electricity spot market (Angarita and Usaola, 2007). The operation of wind power plants should be coupled with energy storage systems in a hybrid manner to provide the maximum benefit.

Energy storage systems are powerful solutions to cope with the intermittent nature of wind power. They allow storage of the generated wind energy to be used whenever needed or the most beneficial. Currently, there are many energy storage technologies, including pumped storage hydropower, thermal energy storage, compressed air energy storage, flow battery storage, flywheel energy storage, superconductor magnetic energy storage, supercapacitor energy storage and electrochemical batteries (Antal, 2014). However, pumped storage hydropower among all is the only commercially proven large scale energy storage technology (Deane, Gallachóir and McKeogh, 2010; Kapsali and Kaldellis, 2010; Sivakumar, Das, Padhy, Kumar and Bisoyi, 2013). In this study, the pumped storage hydropower is used as the storage system. In pumped storage hydropower, water is pumped to the upper reservoir to allow the storage of surplus electricity in the form of the potential energy, and water is released through a turbine to allow the transformation back to electricity (Gimeno-Gutiérrez and Lacal-Arántegui, 2013). In this way, the pumped storage hydropower sells the energy when the prices and the demand are high, and buys the energy when the prices and the demand are low to make a profit. When the pumped storage hydropower and the wind power are combined in a system, the pumped storage hydropower can benefit the availability of free energy generated by wind turbines to pump the water to the upper reservoir (Ghaisi Rad, Rahmani, Gharghabi, Zoghi, Hossein Hosseinian and Hossein, 2017). The described system, which is called the wind-hydro hybrid system (WHHS), provides the efficient management of wind energy. In addition to that, it increases the revenue of the pumped storage hydropower plant by decreasing the energy that is bought from the grid.

In Turkey, according to OECD (2019), energy import satisfies more than 80% of the total energy demand. To decrease the energy import, the integration of the wind and other renewables to the national grid is important. One of the alternatives to the convenient integration of wind power is WHHS that can be built by using current cascade hydropower plants or building new pumped storage hydropower plants.

In the scope of this thesis, a hypothetical WHHS is considered, and an optimization model is developed to maximize the revenue of the WHHS. Moreover, to increase the performance of the WHHS in the electricity spot market, a long short-term memory network (LSTM) is developed, and electricity prices in the market are forecasted. In the electricity spot market, only day-ahead operations are considered to maximize the revenue. In addition to that, the designed WHHS is assumed to be a closed-loop (off-stream) system. In other words, all inflows and outflows to and from the system are ignored.

To investigate the results of the optimization model and LSTM network, different scenarios are created and run. It is found that the LSTM network is beneficial when the electricity prices do not have abrupt changes and increases revenue. However, in Turkey, the abrupt changes are very common, and future electricity price prediction is challenging. Second, it is observed that the increasing penetration of the wind turbines decreases the grid dependency and increases the revenue of the WHHS.

The thesis consists of six chapters. In Chapter 2, the literature review is presented. In Chapter 3 the methodology of developed models and mathematical representations are provided. In Chapter 4, an implementation of the methodology on a case study is presented. Results and discussions of the case study are provided in Chapter 5 and finally, conclusions are given in Chapter 6.

CHAPTER 2

LITERATURE REVIEW

In the scope of this thesis, an optimization model to determine the best daily operation strategy is developed for a WHHS. The optimization model takes hourly electricity price and hourly wind energy as inputs. The first input, hourly electricity prices are declared in the Turkish Electricity Market. We forecast the electricity prices with the LSTM, which is a special type of artificial neural network. The second input, the wind energy, is taken from NASA MERRA-2 database. A brief information about these concepts and previous studies are presented in this chapter. In Section 2.1, pumped storage hydropower plants, wind power plants and WHHS are explained. The energy generated or used in power plants can be bought or sold in the electricity spot markets. In Section 2.2, Turkish Electricity Spot Markets are described. The LSTM model, which is used to forecast the electricity prices in the spot market, is introduced Section 2.3. Lastly, a literature review of the wind-hydro optimization model is presented in Section 2.4.

2.1 Pumped Storage Hydropower Plants, Wind Power Plants, Wind-Hydro Hybrid Systems

Pumped storage hydropower plants are the most viable large scale electricity storage alternatives. They are especially necessary to regulate the intermittent character of renewable energy sources such as wind and solar. Wind power plants are used for converting the mechanical energy of wind to electricity. Wind energy is a renewable energy resource that has less environmental impact compared to fossil fueled power plants. WHHS combines the pumped storage hydropower plant and wind power plant and provides more efficient energy generation. These power plants are explained in the following sections.

2.1.1 Pumped Storage Hydropower Plants

Pumped storage hydropower plant (PSHP) has two reservoirs unlike conventional hydropower plants. Water moves from the lower reservoir to the upper one or vice versa. This can be achieved by a pump hydro turbine. A pump hydro turbine is a machine that can work in the turbine mode or the pump mode. The key idea behind PSHPs is that when electricity prices are low, it pumps the water from the lower reservoir to the upper reservoir, and when electricity prices are high, it turbines the water from the upper reservoir. In this way, although the net energy generation is negative, more revenue can be achieved from the same amount of water.

A typical PSHP layout, shown in Figure 2.1, has the following components: Two reservoirs that are linked, turbine shutoff valves, tunnels for water movement in reservoirs, a transmission switchyard, transmission link and hydro machinery that includes transformers, a motor-generator and a pump-turbine (U.S. Army Corps of Engineers, 2009). Motor-generator is used to convert electrical energy into mechanical energy or vice versa. Pump-turbine moves fluids or extracts energy from it depending on the working mode.

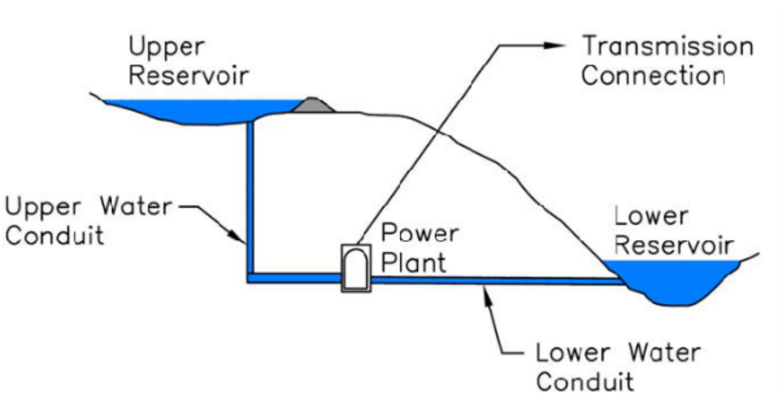

Figure 2.1. Typical PSHP Layout (U.S. Army Corps of Engineers, 2009)

PSHPs are net energy consumers. Yang and Jackson (2011) states that typical PSHP recaptures 70-80% of the input energy. So, it means that if water with a potential of 100 MWh energy exists, approximately 70 to 80 MWh will be recaptured after the PSHP operations. The main reason for this loss is friction losses in waterways and pump-turbine equipment. Since PSHPs generate negative energy overall, they can be thought as transmission facilities (Miller, 2009).

Formerly, PSHPs are used to provide a balanced load on a system. They help to manage considerable energy generated from thermal power plants. According to Miller (2009), it is the largest and most effective grid energy storage. It also provides network frequency control by adjusting power operations immediately.

There are two main types of PSHP, pure PSHP and pump-back PSHP (Deane et al., 2010). Pure PSHP is named as 'closed-loop' or 'off-stream', as well. In the pure PSHP, there is no inflow to the upper reservoir other than water pumped from the lower reservoir. A pure PSHP could be fully separated from the natural water system. Pump-back PSHP uses both the natural flows and pumped water to fill its upper reservoir. Types of PSHPs are shown in Figure 2.2. In this thesis, added value of electricity price estimation on the revenue of a closed-loop PSHP is evaluated. Since it is simpler to model a closed-loop, and research on wind hydro hybrid systems for Turkey is limited, we choose to initially work on this system.

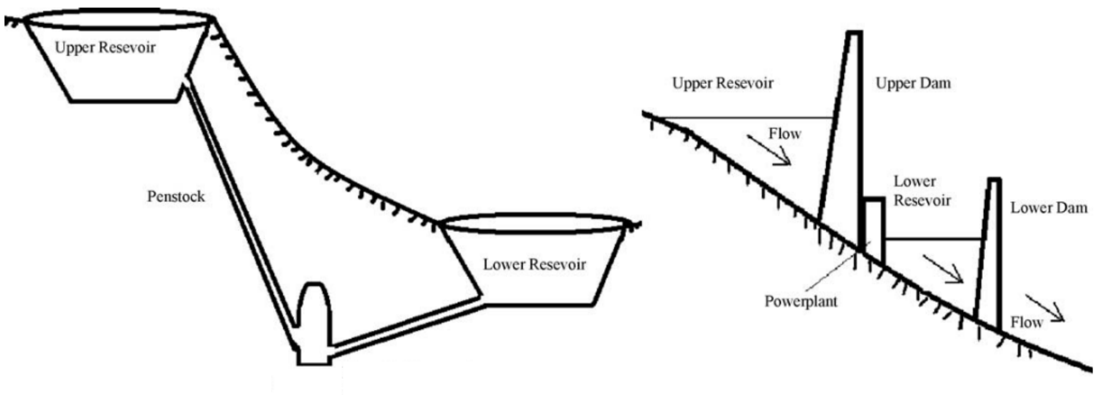

Figure 2.2. Pure PSHP on left and pump-back PSHP on right (?)

According to IHA (2018), there exist a high interest in PSHPs in many countries, especially in China. PSHPs are thought of as key elements to integrate renewable energy sources into grid systems. The total global capacity of PSHP was stated as roughly

161 GW in the World by IHA (2018). Figure 2.3 shows 5 largest total PSHP installed capacities. Due to planned high integration of wind and solar energy resources, there will be a need for operational flexibility. To provide this flexibility, the total installed capacity of PSHP is expected to increase. Figure 2.4 shows projected PSHPs installed capacities by IHA (2018) up to 2030. Also, PSHPs will be installed in Turkey in order to eliminate the constraints of increasing renewable energy on the grid, as stated in the eleventh development plan (Presidency of the Republic of Turkey, 2019).

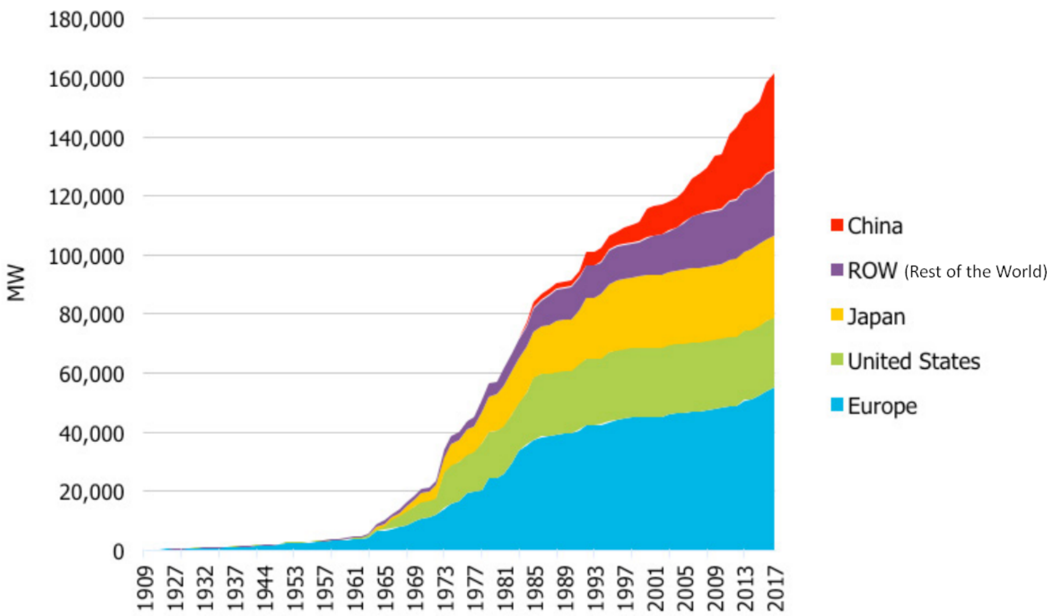

Figure 2.3. PSHP Installed Capacities Trend in the World (IHA, 2018)

2.1.2 Wind Power Plants

The wind turbine is a machine that is used for converting the natural energy resource, wind into electricity. It is kwown as one of the oldest energy resources, and used for drainage and irrigation purposes, initially (Ragheb, 2012). A typical modern wind turbine's capacity changes in the range of 1.5 to 5 MW. Wind turbines having larger capacities are used in a large grid system, frequently in the United States and Europe (James F. Manwell, Jon G. McGowan, 2009).

Wind creates an aerodynamic force on the rotating shaft that leads to the production of torque and mechanical energy. This mechanical energy is converted to electricity by

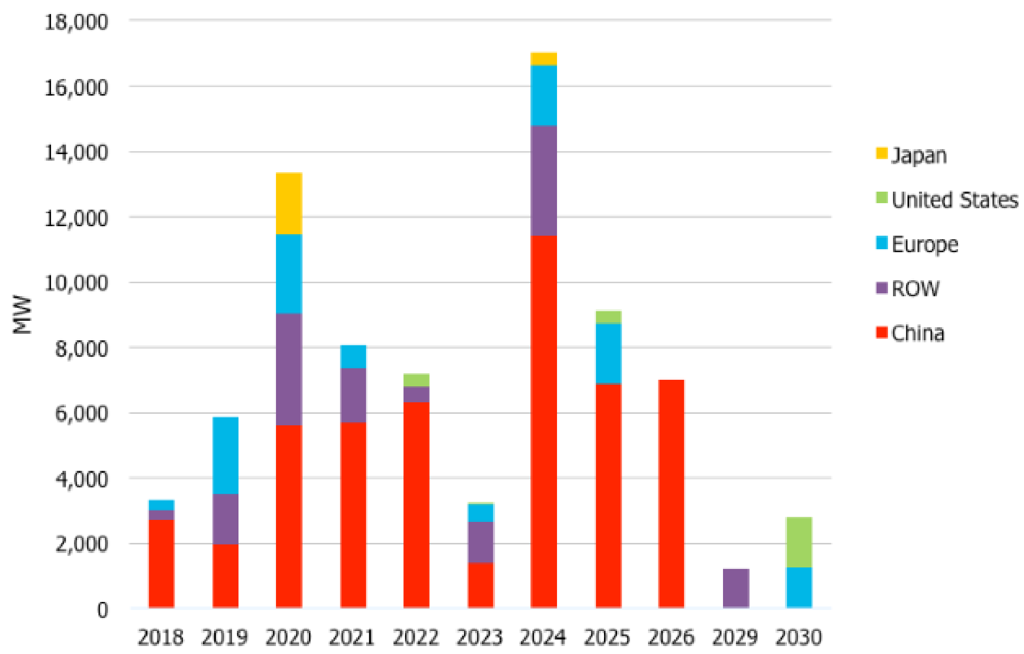

Figure 2.4. PSHP Projected Installed Capacities in the World (IHA, 2018)

a generator. The wind turbine can generate electricity instantly if enough wind speed exists. However, wind energy can not be stored to be used afterward, unlike most other fossil-fueled power plants. Therefore, energy generated from wind turbines oscillates parallel to wind speed. A typical wind turbine has the following components: the rotor (includes the support hub and blades), the electrical system (includes cables, switchgear, transformers, electronic power converters), the drive train (includes shafts, gearbox, mechanical brake, and the generator), the main frame, the tower and the foundation. The main components of the wind turbine are shown in Figure 2.5.

A typical wind turbine power curve is shown in Figure 2.6. To generate useful energy from a wind turbine, there should be a minimum sufficient wind speed, the cut-in speed. The maximum power output from a wind turbine is named as rated wind speed. There is a cubic relationship between wind speed and energy. That is, as wind speed doubles, the turbine generates eight times more power. However, during the blowing of high wind speed, there could be machine damage, so the turbine's maximum speed is limited by the cut-out speed. These cut-in, rated and cut-out speeds are determined by engineering designs considering safety constraints.

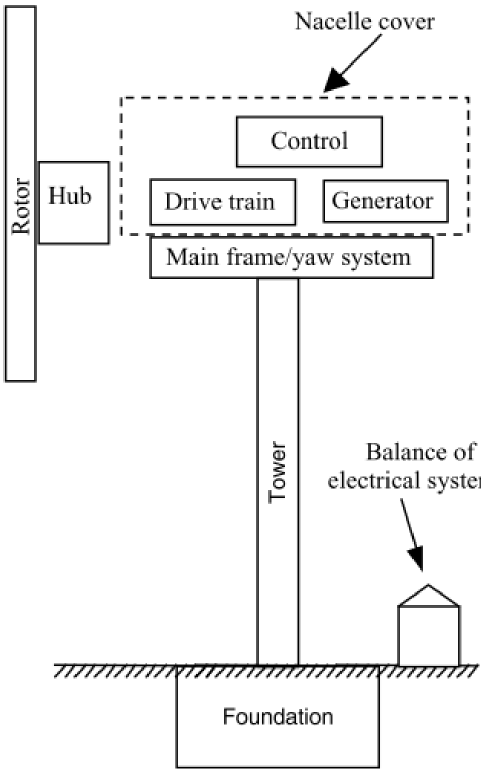

Figure 2.5. Main Components of a Wind Turbine (James F. Manwell, Jon G. McGowan, 2009)

According to GWEC (Wind Global Council Energy) (2019), the global wind energy capacity is 591 GW in 2018. Figure 2.7 shows the total wind power plant installations by countries for onshore and offshore types. China and the United Kingdom has the largest shares for the onshore and offshore installations, respectively. Figure 2.8 shows the historic development of wind power plants total installations in the World. While Compound Annual Growth Rate (CAGR) is decreasing with years, share of offshore in total installations increases. In Turkey, 497 MW onshore wind power plant installations is added in 2018. The total installed capacity of Turkey is 7370 MW, with no offshore installations.

2.1.3 Wind-Hydro Hybrid Systems

Wind power plants and PSHPs can be operated as a combined system with the joint operation. This joint operation is called a WHHS. WHHS has many advantages when

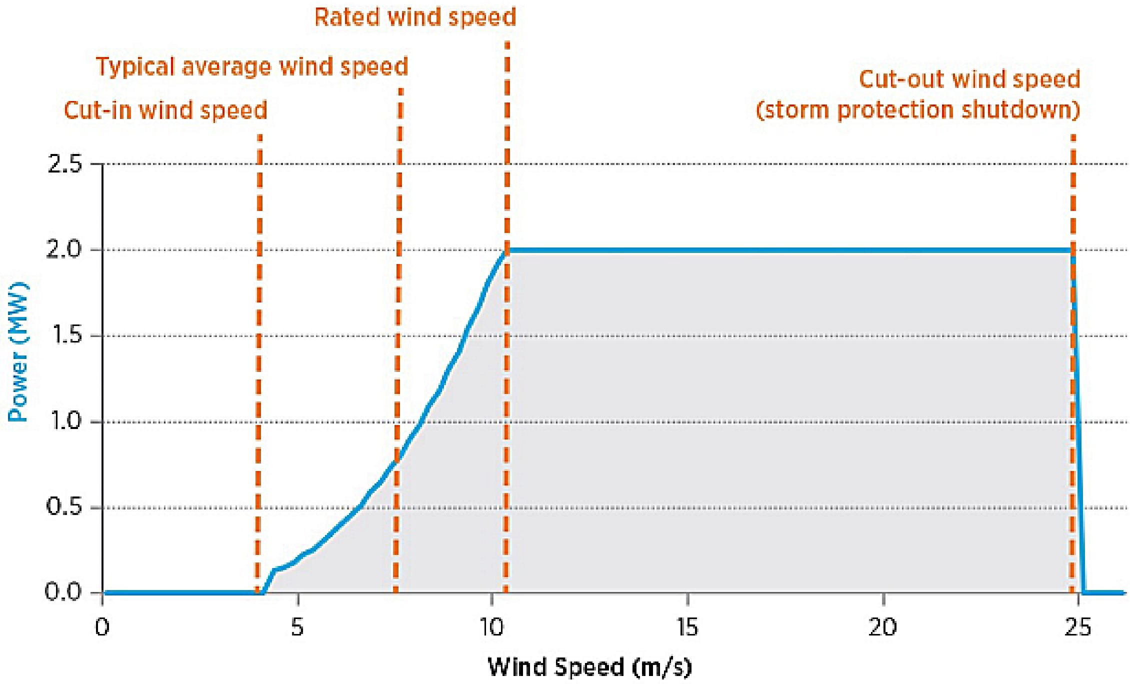

Figure 2.6. Typical Wind Turbine Curve (Zayas et al., 2015)

compared to the uncoordinated operations of PSHP and wind power plant. In this section, the working mechanism of the WHHS is explained, and some example studies are presented. Figure 2.9 shows a typical WHHS. It includes a higher reservoir, a lower reservoir, a pump-turbine, penstocks, and wind turbines (Anagnostopoulos and Papantonis, 2012).

Korpaas, Holen and Hildrum (2003) points out that wind energy is an important support for conventional energy resources. However, the intermittency characteristic of wind power limits its maximum integration to the grids. Wind power plant owners can not foresee the hourly production amounts, and this creates a compelling situation during the market operations. An energy storage system will give flexibility to the owner, and market operations can be carried out in an improved manner.

To increase the efficiency of PSHP and to overcome to the storage of wind energy problem, the WHHS is a powerful alternative solution. According to Benitez, Benitez and van Kooten (2008), to provide power, when the wind is not blowing and there is a need for peak-load power, wind power plant with hydraulic energy storage is an ideal system. In this way, continuous energy supply to the grid can be achieved.

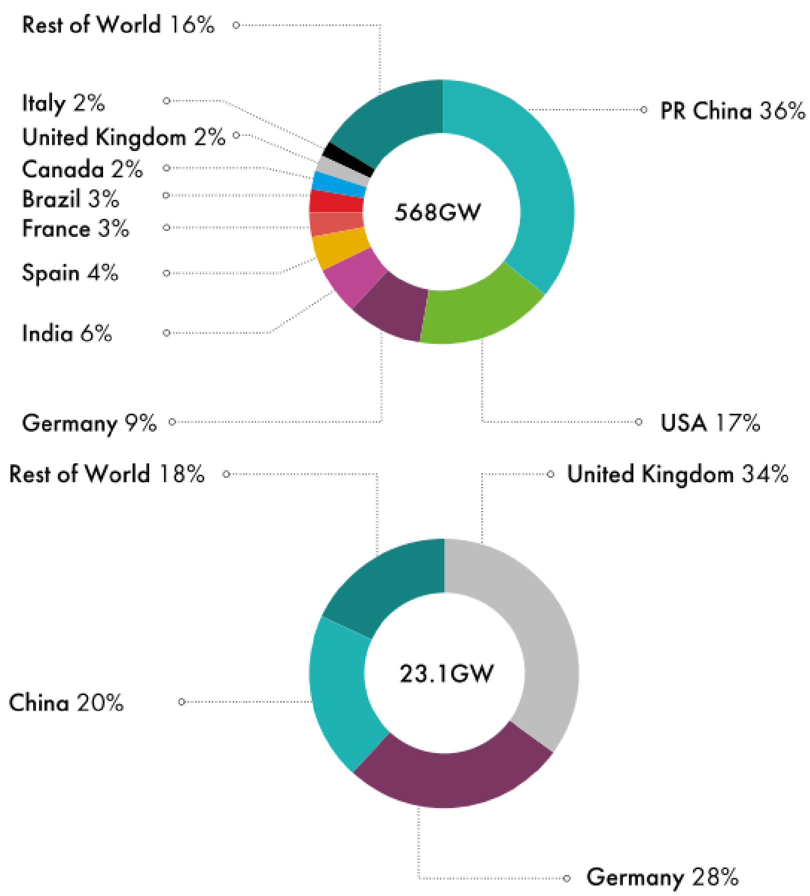

Figure 2.7. Total Installations of Wind Power Plants (onshores at the top, offshores at the bottom) (GWEC, 2019)

Typically, during the daytime, hourly electricity prices are low while they are high in the nighttime. So, if the energy generated from wind turbines is used to pump the water to the upper reservoir during low electricity price hours, and energy generated through releasing the water from the upper reservoir to the lower reservoir is sold to the grid when the prices are high, then more revenue can be achieved.

Integration of wind turbines to the storage facilities provides the following benefits (Loutan and Hawkins, 2007): making more revenue by taking advantage of the price difference in off-peak and on-peak hours, providing ancillary services like regulation, giving flexibility to grid operations and mitigating large wind energy ramps. Moreover, storing energy smooths the system demand curve, and make a more stable grid (see Figure 2.10). Storing energy when the system demand is low, decreases the peak

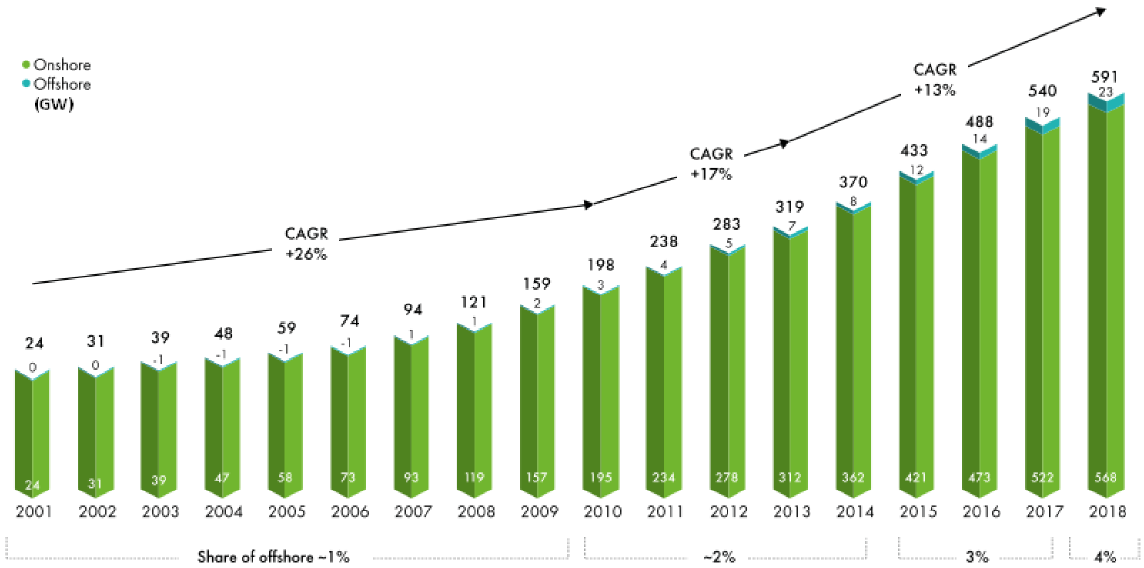

Figure 2.8. Development of Wind Power Plant Total Installations (GWEC, 2019)

demand. Smoother system demand curve provides easier management of the grid and integration of wind energy to the grid (Ibrahim et al., 2011).

There are existing and ongoing studies about WHHS both in the World and Turkey. In the following paragraphs, example studies are presented. These studies explain the advantages of WHHS through case studies.

Jaramillo, Borja and Huacuz (2004) investigated hypothetical facilities in Mexico. They studied the performance of the WHHS by taking into account the capacity factors of the wind farm and the hydroelectric power plant. They concluded that the renovation of hydro projects with wind energy integration is an important opportunity for WHHS in Mexico.

Bueno and Carta (2006) proposed the installation of a wind power integrated PSHP on the Island of Gran Canaria. Their main purpose was to solve the problem of restricted penetration of wind sources to the grid system. They created an economically optimal model for the wind-powered hydro pump system by using existing water reservoirs. They specified that when all alternative external approaches were analyzed, the proposed system is the most efficient one, also it is clean energy. They suggested applying these systems in the other Canary Islands as well.

Al Zohbi, Hendrick, Renie, Bouillard and Zohbi (2015) presented a wind power inte-

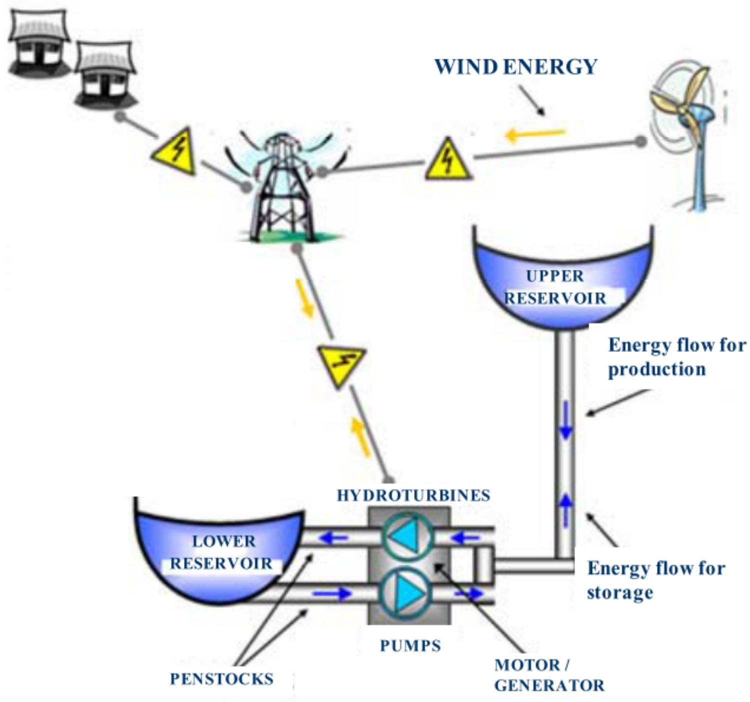

Figure 2.9. Schematic Representation of WHHS (Anagnostopoulos and Papantonis, 2012)

grated PSHP to supply energy demand in Lebanon. Their study is the first application of wind-hydro PSHP in Lebanon. They specified that the proposed system performed well in terms of supplying energy demand. They claimed that the integration of wind power enhanced the sustainability of the Lebanese electricity system.

Kapsali and Kaldellis (2010) applied a wind-hydro model for the Island of Lesbos. Their model solves restricted wind energy contribution problem, and exploits wind energy rejection by the help of the PSHP. The authors specified that this model paves the way for future wind energy investments in the Island.

Papaefthymiou, Karamanou, Papathanassiou and Papadopoulos (2010) investigated the operation of the hybrid power station with a simulation model in Ikaria for 2012. They run the simulations for different hydrological and wind scenarios. Their work showed that wind energy penetration in the Island's energy balance is highly efficient with the hybrid power station. Also, they stated that instead of expensive conventional peak power plants, the hybrid power station could provide the firm capacity to the

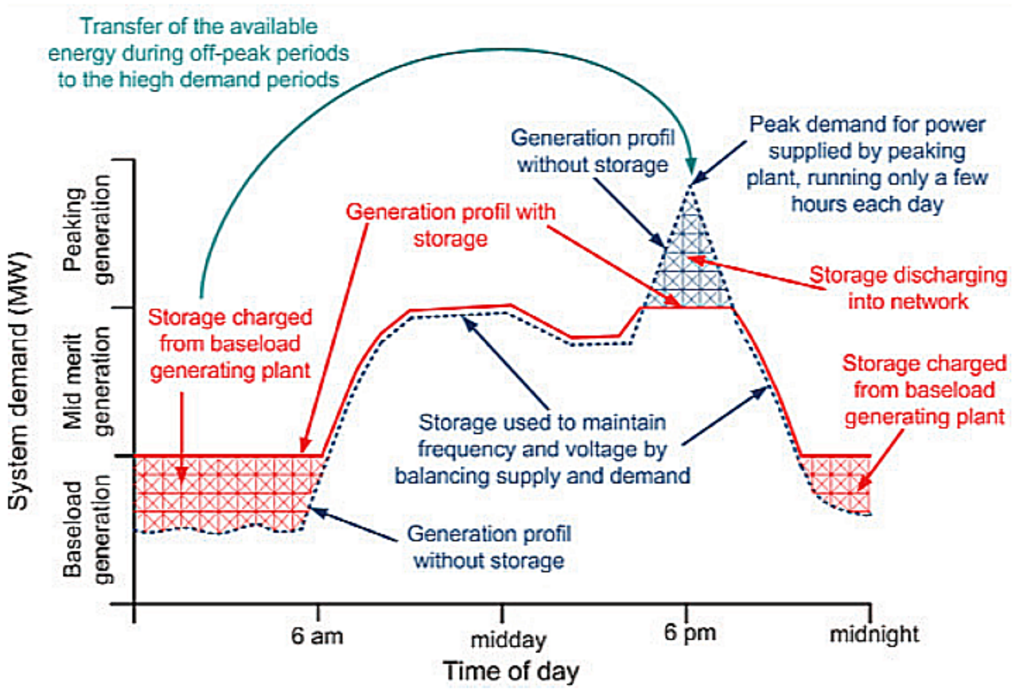

Figure 2.10. Effect of Energy Storage on System Demand (Ibrahim et al., 2011)

Island.

As can be seen from the studies that are presented in the above paragraphs, wind-hydro hybrid applications were analyzed in Islands, mostly. Since islands are isolated systems, hybrid systems can be applied in an easier way. In general, islands have high wind energy potential, and they can benefit from the sea for the pumped storage hydropower plant. In addition to that, since islands have smaller grid systems, WHHS can be integrated smoothly. In this thesis, the WHHS is suggested for a region in Turkey. Since Turkey has a much more complicated grid system compared to an island, the integration of these hybrid systems to the grid is more compelling. This is one of the reasons for the evaluation of a closed-loop PSHP in this project. A few studies about the WHHS in Turkey are presented in the following paragraphs.

Dursun, Alboyaci and Gokcol (2011) evaluated the efficiency of a combined WHHS to the Marmara region intending to supply the energy demand. In their system, after meeting the demand, excess energy is stored to be used when it is needed. It is realized that the proposed system fulfills the energy demand with less cost compared to the existing systems. This study is the first scientific study of a WHHS in Turkey.

Kose and Kaya (2013) proposed a WHHS to supply the energy demand of the Konya water treatment plant. They found that their proposed hybrid model can cover the energy demand of the plant. They noticed that the energy demand in 10 months in a year could be provided only from the hydropower plant operation. For the other two months, the wind power plant operation is necessary. Also, just 4 of 10 months, the hydropower plant can provide the energy demand with 10% safety margin. Therefore, they stated that the hybrid system operation is essential to guarantee uninterrupted energy production for the demand.

Kaya (2012) studied on supplying of the energy need of Alibeyhüyüğü irrigation pumps by a WHHS. He determined the most efficient wind turbine and PSHP capacity. In addition to that, a feasibility study was performed. He concluded that the WHHS is quite a suitable solution to prevent fluctuations in wind energy. In Turkey, there is not any WHHS yet, and research on efficiency of these systems is limited. Also, a limited research study exists about these systems. Therefore, we think that this study will be important guidance for the integration of these systems in Turkey.

2.2 Turkish Electricity Spot Markets

There are two main challenges of electricity. Firstly, its storage is difficult and expensive. Secondly, supply and demand amounts must be equal all the time (Yarici, 2018). To balance the supply and demand considering the system constraints, there should be spot markets. Turkish electricity spot market consists of three markets; intraday, day-ahead and balancing markets. While the balancing market is operated by TEIAS, day-ahead and intraday markets are operated by EPIAS. TEIAS is the market operator, and TEIAS is the transmission operator in Turkey.

In the day-ahead market, all the trading activities are performed for the next day. The purpose of this market is to plan and balance the generation and consumption values in the previous day (i.e., one day ahead). In the day-ahead market, energy sellers deliver their offers for each hour of the next day. In the same manner, energy buyers submit their needs for each hour of the next day. The market operator takes these bids, and sort them from the lowest to the highest for each hour. After intersecting the supply and demand curves, shown in Figure 2.11, Market Clearing Price (MCP) is determined. The day-ahead market offer period covers 24 hours of the next day from 00.00 to the following day 24.00. The due date for the submission of the offers is today's 12.30. The results are announced at 13.30. After half an hour of objection time, final results are declared at 14.00 (Yarici, 2018).

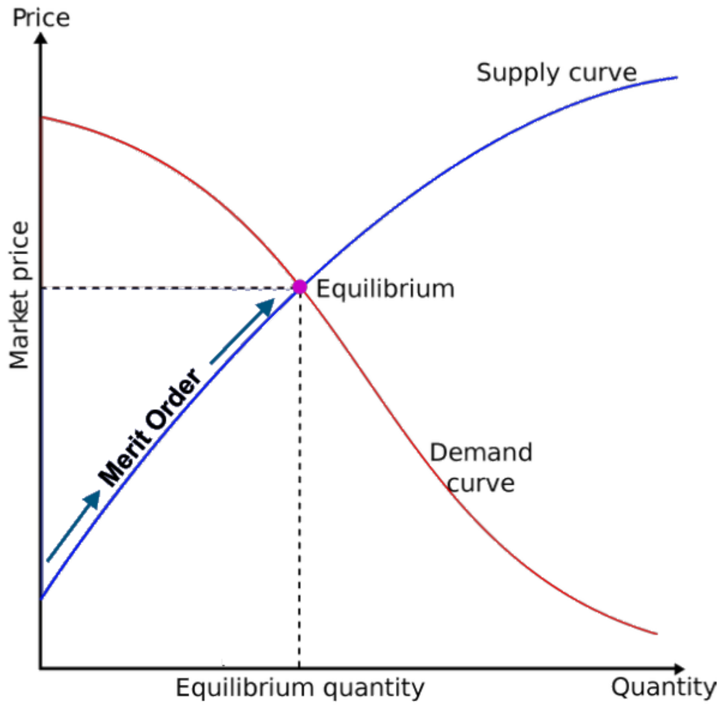

Figure 2.11. Determination of MCP (Kur, 2019)

The intraday market provides additional opportunities to market players. It is the extension of the day-ahead market. Its main purpose is the mitigation of imbalances. Agreements in the intraday market could be performed up to one hour before the physical delivery. Market players have a chance to adjust their positions after the day-ahead market closes. The intraday market opens four hours after the final results are announced in the day-ahead market. In the intraday market, market players offer new prices and quantities for desired hours.

The balancing market's primary purpose is to guarantee system security. After system supply and demand are balanced in the day-ahead market, energy producers could face some problems (i.e., malfunctioning of turbines or other equipment, etc.), and they could not fulfill their commitment. In this case, imbalances occur in the system. TEIAS operates the balancing market, so that system frequency is kept in the desired value. The market players that are capable of buying or selling a minimum of 10 MW within 15 minutes are compulsory to take part in the balancing market. Trading operations in the balancing market are performed with System Marginal Price (SMP). An example timeline for the spot markets is shown in Figure 2.12. This timeline shows the market operations schedule for 02.01.2020.

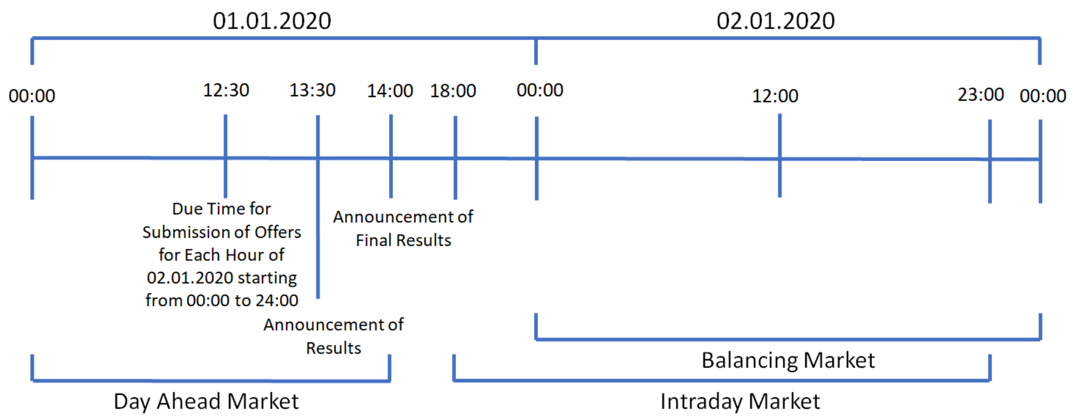

Figure 2.12. Scheduling of Market for 02.01.2020

If the system has an energy surplus, MCP is greater than SMP; otherwise, SMP is greater than MCP. If offered productions in the day ahead and balancing markets could not be fulfilled, then some penalties are applied to the market players who cause the imbalances. Market players get maximum revenue by fulfilling their offers in the day ahead and balancing markets (Aksoy, Eryigit, Hashimova, Isbilir, Avsar, Koksal and Terciyanli, n.d.).

2.3 Long Short-Term Memory Networks

Conventional artificial neural networks (ANN) have been used for the solution of real-life problems for a long time. They are powerful tools to simulate non-linear relationships. A recurrent neural network (RNN) is a type of ANN. RNN creates feedback connections in input data, and this provides significant improvements compared to conventional ANN. RNN has the ability to execute more complicated computations

(Garrido, 2012) and RNN has been widely used to predict time series.

RNN is trained using input data that are in the form of a sequence. It can learn time-dependent relationships in different sections of the input. For instance, when a sentence is given as an input, RNN can recognize the relationship between different words. In this way, it can learn the grammar rules of the used language (Veselý, Burget and Grézl, 2010).

During the training of standard RNN, some problems may occur, such as vanishing or exploding of the gradients (Pascanu, Mikolov and Bengio, 2012). Gradients are the sum of the derivatives of the cost function, which measure the performance of the network, with respect to the model parameters such as weights and biases through timesteps. Gradients are used to update the model parameters and are propagated from the last layer to the initial layer in a backward sweep. They are exposed to many matrix multiplications due to the chain rule. When they are carried to earlier layers, if they are smaller than one, they have the potential to shrink exponentially. This leads to the vanishing gradient problem, and learning of the model becomes impossible. The other scenario occurs when the gradient has a value larger than one, then it has the potential to get too large. This creates an exploding gradient problem. These problems decrease the capability of RNN's learning of long time relations in the input patterns. To suppress these problems, Hochreiter and Schmidhuber (1997) developed a special type of RNN, which is the LSTM. Operations in LSTM networks are controlled by its gates, and this prevents the gradient problems. LSTM network also has the capability to build a relationship between a wide range of time steps, even in noisy data by making use of short term dependencies.

Roche and Mcnally (2016) applied RNN and LSTM models to predict the price of Bitcoin. The LSTM model achieved a higher accuracy value than the standard RNN. They also implemented a popular ARIMA model for the same data. Non-linear models, LSTM and RNN, outperformed the ARIMA model.

Sak, Senior and Beaufays (2014) compared the performance of the deep neural network (DNN) and LSTM networks on a large vocabulary speech recognition project, which is the Google English Voice Search. This is the first implementation of LSTM networks on an extensive vocabulary speech recognition. They indicated that LSTM architecture resulted in better performance than the DNN model.

Mandal, Senjyu, Member and Urasaki (2007) tried to forecast short-term electricity prices using RNN based on similar days (SD) method in PJM, which is a regional transmission organization in the District of Columbia. SD method takes the information of days similar to the forecast day. So, the authors create an architecture that integrates the RNN model with the SD method to obtain better results. At the end of their study, they found that the RNN technique outperforms the SD method. The proposed RNN model is capable of forecasting the peak values but not the large ones. Also, they notice that the model predicts weekend better than weekdays due to high volatility in PJM prices.

Jiang and Hu (2018) used an LSTM model for 24 hours ahead of price forecast in Australia and Singapore markets. They used system demands, historical prices, hour of the day, day of the week, week of the year and holidays information as inputs. The performance of the LSTM model is compared with the performance of four popular methods, which are BP-ANN, WT-ANN, PSO-ANFIS and SARIMA. The results indicated that the LSTM model outperforms the other methods.

Anbazhagan and Kumarappan (2013) applied an RNN model to forecast electricity market prices in Spain. The created RNN model is compared with different approaches to evaluate its accuracy. They used 16 different sets of lagged prices as input features based on correlation analysis. According to their results, the RNN model is selected as the best model in terms of accuracy, computation time and model complexity. In this thesis, various models are built using different lagged prices and evaluated in terms of their price estimation performances. The one that shows higher performance is used for the optimization model input.

Hong and Hsiao (2001) developed three RNN models to forecast locational marginal prices (LMP) on weekdays, Saturday and Sunday. They selected historical LMPs, system loads, system operating conditions, transaction periods and net-tie flows as inputs of the RNN model. Due to the similar shape of the LMP pattern on weekdays, Saturdays and Sundays individually, three different models were created. It was found that the proposed RNN models could efficiently forecast LMPs.

2.4 Optimization Models for Wind-Hydro Hybrid Systems

To analyze benefits of WHHS, many studies are performed in the literature. This section briefly explains the important points of these previous studies.

Crespo-Vazquez, Carrillo, Diaz-Dorado, Martinez-Lorenzo and Noor-E-Alam (2018) developed a model to attend to the day-ahead, intraday and balancing markets under the uncertainties of intermittent wind and unforeseen electricity prices. They generate scenarios for market prices. The scenario based on LSTM network model performed the best results in terms of net income. Scenarios are also generated for wind energy. Their analysis showed that both uncertainties in wind energy and market price affect the net income in a similar manner. They explored that the proposed scenario generation techniques could be combined with a model predictive control framework to create a dynamic decision-making tool for an extensive pool market. They also suggested that scenario generation methods combined with machine learning techniques are powerful to cope with uncertainties in wind speed and electricity prices.

Castronuovo and Lopes (2004a) created an optimization model to maximize the 24-h operational profit of the wind-hydro power plant. The solution of the optimization problem gives an operational schedule of wind, hydro turbine and pump units for the next 24 hours. Since the system is assumed to be a closed-loop system, no inflow and outflow are considered. The wind power was assumed to be a stochastic quantity with two hourly series, such as average and standard deviation of the wind power. Based on the model, random samples are generated. Each sample represented a wind power scenario. For each scenario, the optimization model was solved. The integration of the water storage increased the wind power plant profit. While during the high price periods, the hydro generation supports the wind park to provide more energy to the grid, during the low price periods, the pump units increased the water reservoir level.

Benitez et al. (2008) proposed an optimization model to evaluate the integration of intermittent energy into the grid. Their model firstly found the best allocation of power generation from a variety of sources by minimizing the total operational costs. Secondly, the energy storage capabilities of reservoirs and the intermittency of wind power was integrated with the constrained optimization method. Since storage facilities are necessary for wind penetrations to the grid, the model leads to the design of profitable electricity systems. Thirdly, the model predicts the best level of new capacity for any level of wind penetration.

Ghaisi Rad et al. (2017) suggested a new approach to determine the optimum number of wind turbines to be integrated with the hydro pump storage unit, to get maximum net income. To generate wind and price data, the Monte Carlo method was applied, and the scheduled operation presented. The shorter payback period of the pump storage power plant enhanced the longer payback period of the wind power plant. The approach was applied to various electricity prices and wind energies. It is concluded that the results of the study can help the wind hydro hybrid plant owners to find the exact electricity price and wind energy.

Castronuovo and Lopes (2004b) described an optimization model to find the best operation strategy of combined wind-hydro pumping storage power plants. The solution to the optimization problem gave the hourly operation of wind-hydro pumping storage power plants. They concluded that the proposed model could be used to help the hydraulic design of the plant by computing the optimal equipment properties by neglecting all inflows and outflows.

Cruz, Pousinho, Melício and Mendes (2014) proposed a mixed-integer linear programming model to have the optimal scheduling of a closed-loop pumped-hydro system with a wind farm. The results showed that this coordinated operation provides more profit to the generation company during trading in the day-ahead market. Additionally, the proposed model highly reduces wind energy curtailments and decreases penalty risks due to energy deviations.

Song, Zhang, Li, Zeng and Zhang (2013) depicted the joint operation mode of the wind farm and the closed-loop pumped storage hydropower plant to cope with errors in predicting wind power values that affect wind power integration negatively. The purpose of their study was to reduce the operational risks and increase financial benefits. Also, the proposed optimization models showed that total revenues are higher in the joint operation mode rather than independent operations.

Kaldellis and Kavadias (2001) developed a methodology for the optimal closed-loop wind-hydro solution to find the most beneficial configuration of renewable stations. The study showed that this methodology has multiple advantages. Firstly, the potential for renewable energy penetration reaches high values. Secondly, exchange losses were minimized, including fuel imports. Thirdly, the environmental effects of combustion engines were mitigated. Lastly, a high amount of the wind energy surplus was diverted to the desalination plant to be used in clean-water production.

Hering, Mošna, Janecek and Hrycej (2013) compared the use of a hydropower plant with a reservoir and pumped storage hydropower (PSH) in a WHHS. Selection among these two options depends on the average load to supply, the cost of energy and hydrological constraints. The authors stated that PSH is efficient for minimizing costs. Also, PSH brings environmental benefits. For instance, the same installed capacity PSH uses less reservoir area and can be operated with smaller reservoir volume.

García-González, de la Muela, Santos and Gonzalez (2008) demonstrated an optimization model for the joint operation of a wind farm and a closed-loop pumped storage hydropower plant. To deal with uncertainties in the spot market, a two-stage stochastic programming approach was suggested as a powerful tool for the decision-making process. The proposed model could guide the investors about the wind farm and pumped storage facilities during the market operations.

CHAPTER 3

METHODOLOGY

In the scope of this thesis, an optimization model is built to determine the daily operation schedule of a WHHS to obtain maximum revenue. Figure 3.1 shows the flowchart of the methodology. The two important inputs of the optimization model are hourly available wind energy and hourly electricity price. The first input, hourly wind energy, is derived using wind speed data that is taken from NASA Modern-Era Retrospective Analysis for Research and Applications, Version 2 (MERRA-2), which is available on the Internet database. The second input, hourly electricity price, is forecasted by a LSTM network, which is a special type of recurrent neural network. Calculating wind energy from wind speed is described in Section 3.1. Forecasting hourly electricity prices with the LSTM network is explained in detail in Section 3.2. Lastly, the development of the optimization model for the WHHS is presented in Section 3.3.

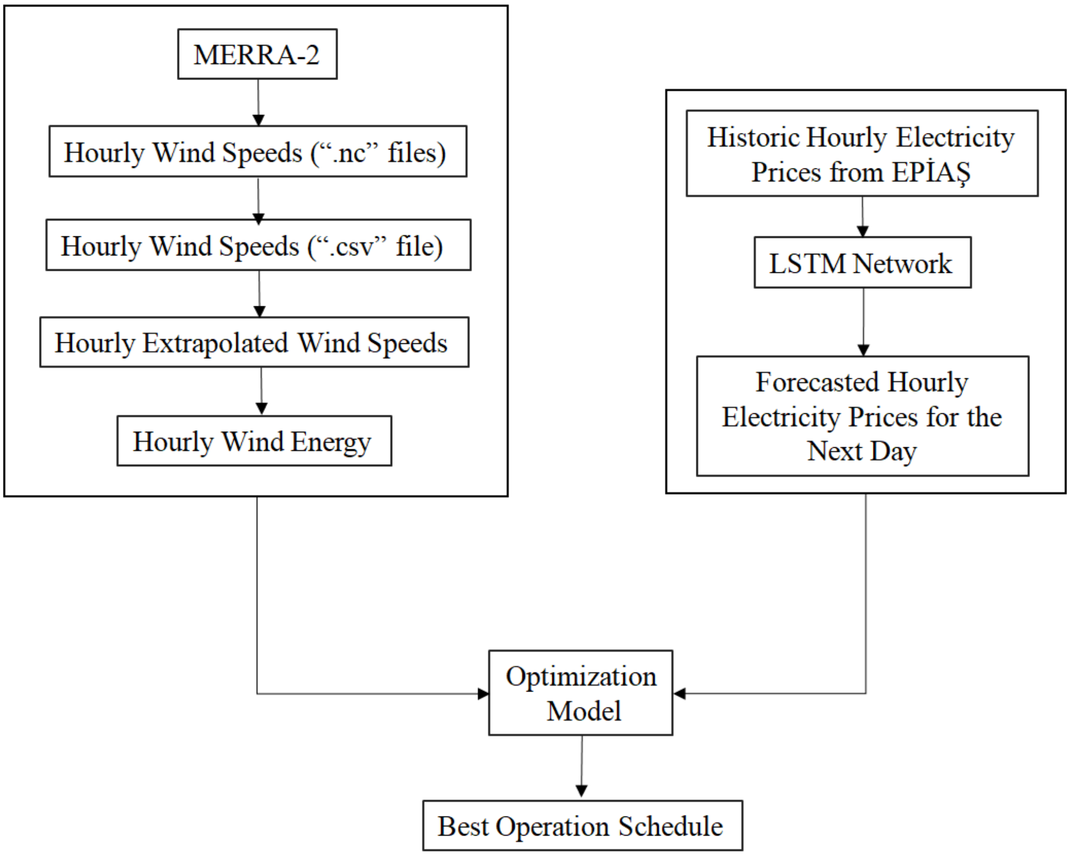

Figure 3.1. Methodology Flowchart

3.1 Calculation of Wind Energy from Wind Speed Data

The sun is the beginning source of the earth's wind resource. Solar radiation induces unbalanced heating of the earth, and that generates pressure differences across the earth's surface. These pressure differences on earth's surface constitute winds. Movement of air in the atmosphere, due to unbalanced heating of the earth, is affected by the rotational movement of the earth. In addition to that, variations in the atmosphere movements are increased by seasonal changes (James F. Manwell, Jon G. McGowan, 2009). Eventually, wind speeds change with respect to both the location and the time. To obtain wind energy to be used in the optimization model, MERRA-2 data is used as the source of wind speed at the desired location. In the following paragraphs, information about MERRA-2 data, wind speed extrapolation and estimation of wind energy are explained.

MERRA-2 data covers data from 1980's to a few weeks behind real-time. MERRA-2 uses a modern satellite database for the meteorological data assimilation (Aeronautics and Information, 2017). MERRA-2 data contains a large number of products. Among all products, we used M2T1NXSLV (MERRA-2 tavg1_2d_slv_Nx: 2d, 1-Hourly, Time-Averaged, Single-Level, Assimilation, Single-Level Diagnostics V5.12.4) for the wind speed. The spatial resolution of the data is $0.5° \times 0.625°$. This resolution is quite low to be used in a wind power plant system design. However, since this study deals with the comparative evaluation of the revenue of a hypothetical WHHS when electricity prices are estimated by an LSTM network, low-resolution wind data was sufficient. MERRA-2 data set has been used in the literature for similar studies (Ritter, Shen, Cabrera, Odening and Deckert, 2015; Olauson and Bergkvist, 2015).

Wind speed data is in the netCDF format, and NASA's Goddard Earth Sciences Data and Information Services Center (GES DISC) website allows us to download files in a subset form. The desired time and the spatial coverage or points are specified, and then the website creates download links for each day for the defined time interval. Each netCDF file contains 24 records and five parameters, which are the latitude, the longitude, the time, the eastward wind speed at 50 meters (U50M), and the northward wind speed at 50 meters (V50M). After all netCDF files are downloaded, wind speed data for September 2017 to August 2018 period are extracted with a Python code. The main library used in the Python code is defined in Table 3.1.

Table 3.1. Used Library for Wind Speed Data Extraction

Library	Description	Application
netCDF4	Python interface to the netCDF C library.	Wind speed data is extracted from MERRA-2 netCDF file.

As explained in Aeronautics and Information (2017), the downloaded wind data is composed of eastward and northward wind vectors at 50 meters, respectively U50 and V50. The U wind component is parallel to the x-axis, which is the longitude. Positive U wind values represent the wind coming from the west, and negatives represent the wind coming from the east. The V wind component is parallel to the y-axis, which is the latitude. Positive V wind values represent the wind coming from the south, and negatives represent the wind coming from the north. Wind vector components are shown in Figure 3.2. Wind speeds are calculated using the Pythagorean Theorem:

$$Wind\ Speed = \sqrt{U^2 + V^2} \tag{3.1}$$

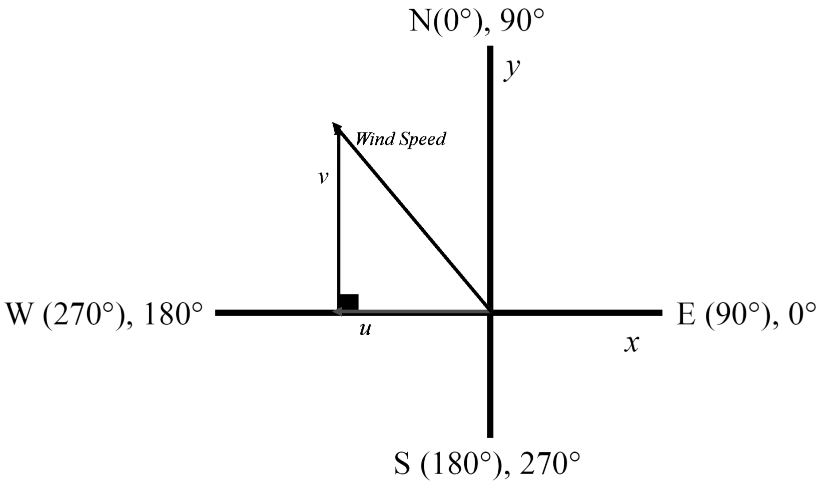

Figure 3.2. Wind Vector Components

According to Kragh and Fleming (2012), to extract the maximum possible amount of energy from the wind, the wind turbine should adjust its alignment so that the rotor axis is aligned with the wind direction. In the modern wind turbines, there are instruments for this adjustment. They adjust the nacelle, providing that the rotating blades are always facing directly into the wind. In this way, the maximum possible energy is generated. In this study, the calculated wind speeds are directly used in wind energy estimation without considering their direction since it is assumed that wind turbines adjust their alignment according to the direction of wind speed.

The attained wind speeds are at 50 meters above the surface. They need to be extrapolated to the height of the wind turbine hub. To extrapolate the wind speed to the hub height, the power-law expression is used in this study. The power law is a simple model used to calculate the vertical wind speed profile. The power law is defined by the following equation (James F. Manwell, Jon G. McGowan, 2009):

$$\frac{U(z)}{U(z_r)} = \left(\frac{z}{z_r}\right)^{\alpha} \tag{3.2}$$

where $U(z)$ is the wind speed at height z, $U(z_r)$ is the reference wind speed at the reference height z_r, and α is the power-law exponent. The power-law exponent changes with many parameters, such as elevation, time of the day, season, nature of the terrain, wind speed, temperature, and several thermal and mechanical parameters. However, these parameters affect the power-law exponent in a complicated manner, so they reduce the simplicity and applicability of the power law (James F. Manwell, Jon G. McGowan, 2009). Therefore, an empirical expression proposed by Justus (1978) is used in this study:

$$\alpha = \frac{0.37 - 0.088\, ln(U(z_r))}{1 - 0.088\, ln\left(\frac{z_r}{10}\right)} \tag{3.3}$$

where the unit of $U(z_r)$ is m/s, and the unit of z_r is m.

After wind speeds are extrapolated to the hub height, they can be used for calculating wind energy to be used in the optimization model. Wind power of a turbine changes with wind speed, and every wind turbine has a unique power curve that depends on the technical details of the turbine. By using a power curve, the energy production of a wind turbine can be determined without technical calculations of each component of the wind turbine (e.g., the wind turbine rotor, electrical generator, gearbox gear ratios). Wind turbine manufacturers derive a wind power curve for each manufactured wind turbine by carrying out field tests. In this study, the power curve of a selected wind turbine, General Electric (GE) 2.5 MW wind turbine (General Electric, n.d.), is found from the catalog of the wind turbine manufacturers and used to calculate wind energy. Wind energy is calculated by multiplying the power by the time interval. In this study, the time interval equals one hour. For example, the power of 2 MW in the one hour time interval produces 2 MWh energy. A Python code is written to fit a polynomial function to the wind power curve (see Table 3.2). By using this polynomial function, available wind energy is obtained for all time intervals of the downloaded MERRA-2 wind speed data (i.e., from September 2017 to August 2018).

Table 3.2. Used Library to Fit a Function to the Power Curve

Library	Description	Application
NumPy	Python package for scientific computing.	A polynomial function is fitted to the power curve.

3.2 Electricity Price Forecasting

The second input of the optimization model is hourly electricity prices. Hourly electricity prices are forecasted by using an LSTM network. The developed LSTM network forecasts 24-hours time period forward (i.e., for the next day) by using 48-hour time series. One LSTM network is developed to forecast electricity prices at each hour of the next day. Thus, 24 LSTM networks are developed. However, all LSTM networks have the same architecture and use the same input (i.e., electricity prices of past 48 hours). The only difference is the output. First, some definitions are given for a better understanding of the LSTM network. Then the selected hyperparameters for this study are given. The hyperparameters are selected based on a trial-and-error procedure and considering the duration of the simulations of the LSTM network.

Time series size specifies the number of hourly electricity prices that will be used in forecasting. In this study, the time series size is selected as 48 hours. So, the LSTM network takes 48 hours of hourly electricity prices as inputs to forecast the next day's electricity prices (see Figure 3.3). A diagram explaining the LSTM network is given in Figure 3.4. In Figure 3.4, the second subscript of the $\boldsymbol{x}$ and $\boldsymbol{h}$ vectors, ranging between 1 and S, represents the time series size. In our problem $S = 48$.

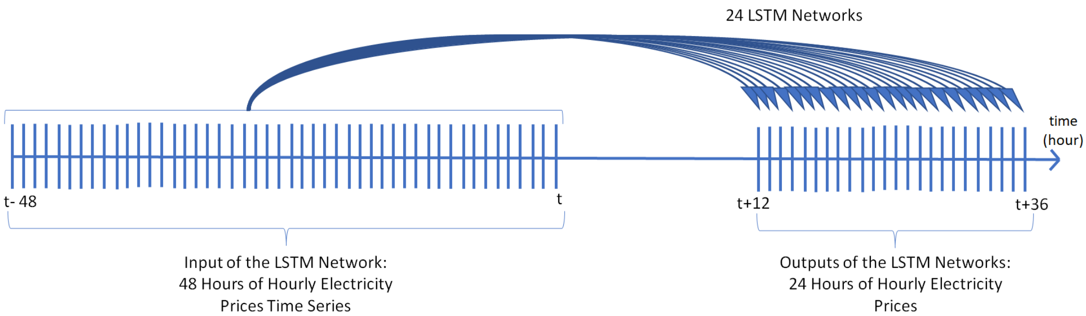

Figure 3.3. LSTM Networks Input and Output

Batch size is the number of samples per gradient update (Chollet et al., 2015). All training data is not preferred to be passed at once as suggested in Tan, Xiang and Zhou (2015) and Merity, Keskar and Socher (2017) (see Figure 3.5). Thus, the training dataset is divided into batches. The number of batches or the batch size is a parameter that needs to be specified by the user. Also, it controls the frequency of the weight

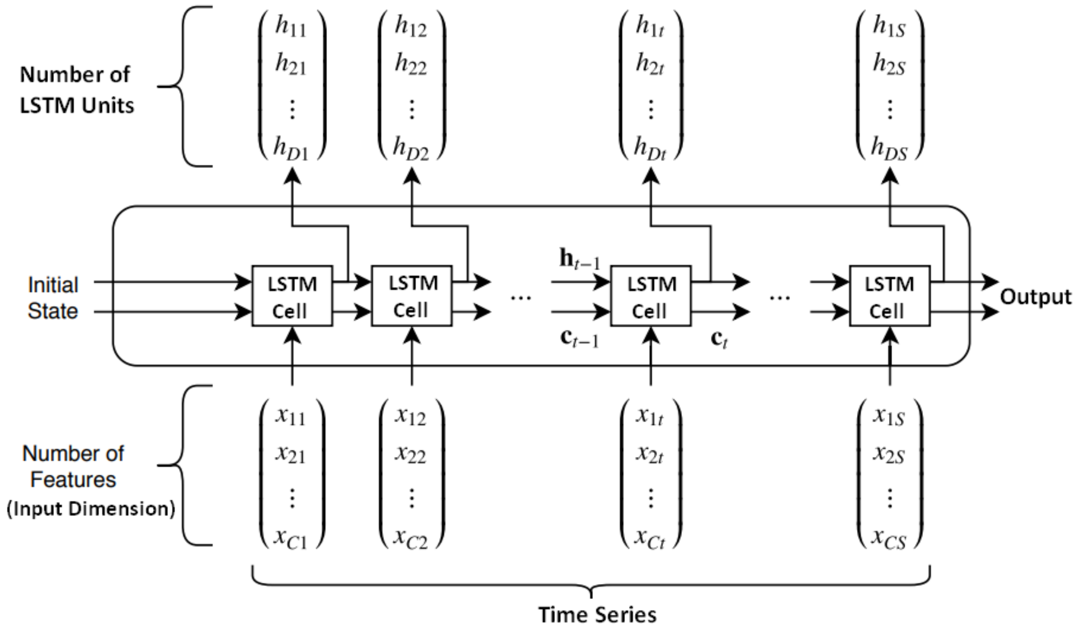

*Figure 3.4. LSTM Diagram (*Long Short-Term Memory Networks*, n.d.)*

update. At the end of each batch, the LSTM network updates the weights. In our problem, we are using a total of 49680 patterns for training, and the batch size of the LSTM network is selected as 128 based on trial and error. So, in one complete pass of the training dataset, the weights are updated around 388 times.

The number of the LSTM units determines the size of the LSTM network output (see Figure 3.4). It affects the learning capacity of the network. A large number of LSTM units provides a higher number of learned parameters, such as weights and biases. In Figure 3.4, the first subscript of the h, ranging between 1 and D, represents the number of LSTM units. In our problem, three LSTM units are used to build the LSTM network, so $D = 3$.

The number of the features is called the input dimension, as well. It is used to specify how many features affect the LSTM network output. The developed LSTM model takes four inputs. In this study, lagged time serieses of electricity prices are used as inputs. In Figure 3.4, the first subscript of the x, shown as C, represents the number of features. If the architecture given in Figure 3.4 is used (i.e, $y_j = f(y_t, y_{t-1}, ..., y_{t-48})$ for $j = t + 12, t + 13, ..., t + 36$) then the LSTM network

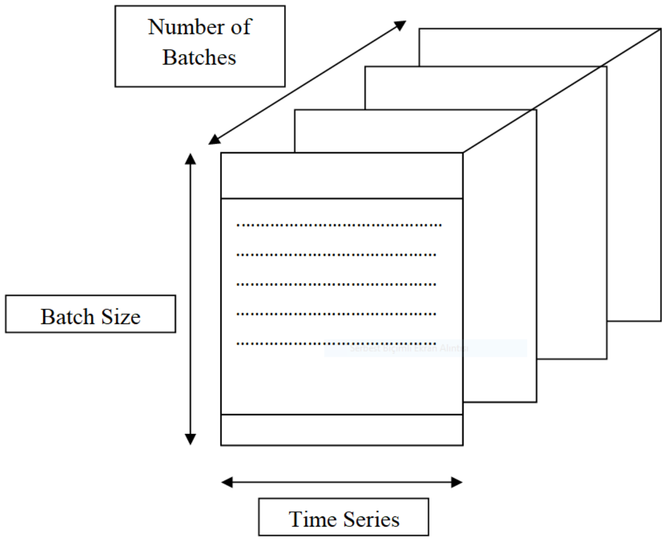

Figure 3.5. Batch Size and Time Series Schematic View

has one feature. If a series of e hour lagged price values are added as a second input (i.e, $y_j = f((y_t, y_{t-1}, ..., y_{t-48}), (y_{t-e}, y_{t-e-1}, ..., y_{t-e-48}))$, then the LSTM network has two features. We used unlagged plus three additional lagged price time series as inputs, so, in our problem, the number of features, C is four.

The number of epoch controls the number of the forward and backward pass of all training samples in the LSTM network. For instance, one epoch means one forward and one backward pass of all batches to update the weight matrix. In our problem, the number of the epoch of the developed LSTM network is set to 5000. So, if all epochs are completed, the number of updates of the weight matrix can be found by multiplying the number of batches by 5000. However, a property of the coding library, called early stopping, is used in this study. Early stopping is used to end the training of the network if training is below a set threshold rate. That is, if the training loss, which is the measurement of the discrepancy between the real value and the forecasted value (Smola and Vishwanathan, 2008), cannot be improved, the LSTM network stops the training and restore the best model weights. In this LSTM network, the value of the early stopping is set to 25. That means, if the LSTM network cannot improve the loss value more than the set threshold in 25 consecutive iterations, then it stops. The effect of the number of epochs is investigated to avoid overfitting, as explained in Section

5.1.

The LSTM network is trained using the default optimizer of the library, Adam optimizer, and mean square error (MSE) loss function. MSE is defined in Equation (3.4). During the training, the best model parameters that minimizes the training data error are found.

$$MSE = \frac{1}{K}\sum_{i=1}^{K}(x_i - y_i)^2 \tag{3.4}$$

where x_i is the real value, y_i is the output of the LSTM network and K is the total number of the outputs or samples in a batch.

The LSTM Architecture

The LSTM network is introduced by Hochreiter and Schmidhuber (1997), and explained in this section. LSTM networks can be thought of as a chain that is formed by repeated LSTM cells. The length of the chain is determined by time series size. An LSTM cell can carry out its state over time, and includes systems of gating units to control the flow of information (Goodfellow, Bengio and Courville, 2016). The main idea of the LSTM is to keep under control the cell state (c_t), which is the memory of the LSTM, with input, forget, and output gates. Gates consist of sigmoid and point-wise multiplication operators. The cell state information is controlled by adding or multiplying the input data by the hidden state (h_t), which is the output of the current LSTM cell. The structure of an LSTM cell is shown in Figure 3.6.

In a neural network, to obtain an output, forward and backward passes are carried out. The forward pass computes values from inputs to the output. The backward pass performs backpropagation that starts at the end of the forward pass and updates the weights by minimizing the error between the real value and the output of the forward pass. During the forward pass, the cell state c_t and the hidden state h_t, output, of the LSTM cell at timestep t are calculated as follows (Fischer and Krauss, 2017):

- In the first step, the LSTM cell decides which information should be discarded from its previous cell states (c_{t-1}). The activation values of the forget gates at timestep t are calculated based on the current input and the output of the LSTM

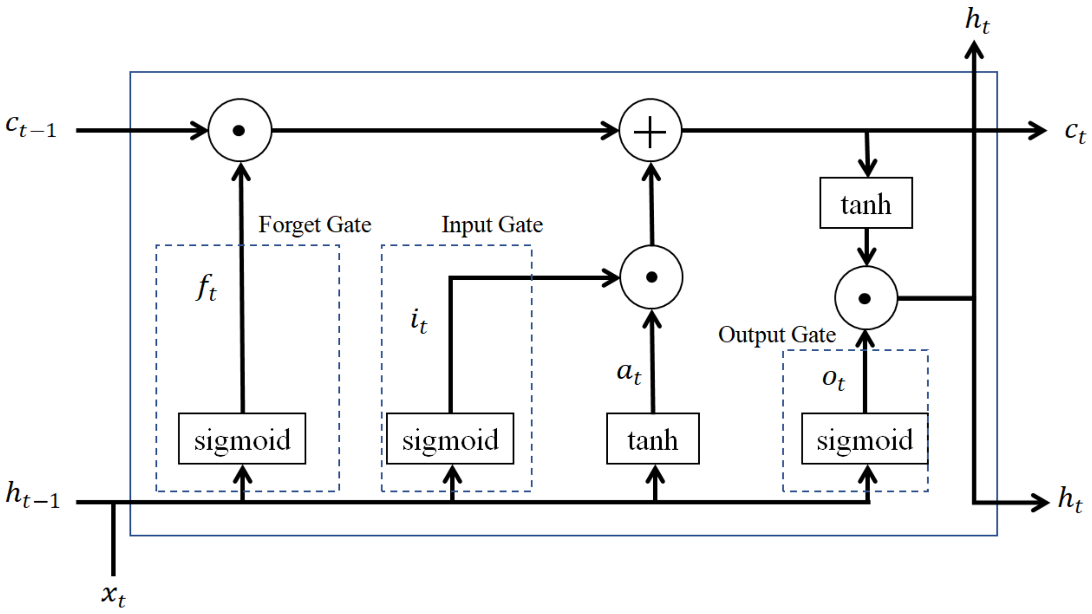

Figure 3.6. Structure of a LSTM Cell

cell at the previous timestep (h_{t-1}). After that, the sigmoid function scales all activation values into the range between zero, which means completely forget, and one, which means completely remember (see Equation (3.5)).

- In the second step, the LSTM cell decides which information should be added to the cell state (c_t). This decision depends on two computations. First, the candidate cell state that has potentitial to be added to the cell state is calculated using Equation (3.6). Second, the activation values of the input gate is calculated using Equation (3.7).

- In the third step, the new cell state is calculated based on the results of the previous two steps with the Hadamard product (see Equation (3.8)).

- In the last step, the hidden state, the output of the LSTM cell, is computed by Equations (3.9) and (3.10).

Forward pass equations are collectively provided as follows (Fischer and Krauss, 2017):

$$f_t = sigmoid(W_f x_t + U_f h_{t-1} + b_f) \tag{3.5}$$

$$a_t = tanh(W_a x_t + U_a h_{t-1} + b_a) \tag{3.6}$$

$$i_t = sigmoid(W_i x_t + U_i h_{t-1} + b_i) \tag{3.7}$$

$$c_t = f_t \odot c_{t-1} + i_t \odot a_t \tag{3.8}$$

$$o_t = sigmoid(W_o x_t + U_o h_{t-1} + b_o) \tag{3.9}$$

$$h_t = o_t \odot tanh(c_t) \tag{3.10}$$

where x_t is the input vector at timestep t; c_t is the cell state; a_t is the candidate cell state that preserves the information of the hidden state across the time steps (i.e., adds information to the cell state); i_t is the input gate that defines which information to add to the cell state; f_t is the forget gate that defines which information to remove from the cell state; o_t is the output gate that defines which information from the cell state to use as output; W_i is the weight matrix for the input gate for the input vector; W_a is the weight matrix for the candidate cell state for the input vector; W_f is the weight matrix for the forget gate for the input vector; W_o is the weight matrix for the output gate for the input vector; U_i is the weight matrix for the input gate for the hidden state; U_a is the weight matrix for the candidate cell state for the hidden state; U_f is the weight matrix for the forget gate for the hidden state; U_o is the weight matrix for the output gate for the hidden state; b_i is the bias for the input gate; b_a is the bias for the candidate cell state; b_f is the bias for the forget gate; b_o is the bias for the output gate. The element-wise or Hadamard product is represented by $\odot$.

After completion of the forward pass, the backward pass computations of the LSTM network to update the weights are carried out as follows:

- In the first step, the difference in the hidden state (the output) is found (see Equation (3.11)). This difference is composed of five components. The first component Δ_t is the derivative of the loss function, which is the mean square error, with respect to the hidden state at t. Summation of other components corresponds to the difference in the hidden state at $t+1$.

- In the second step, the differences in the output gate, the cell state, the forget gate, the input gate and the candidate cell state are computed using Equations (3.12), (3.13), (3.14), (3.15) and (3.16), respectively.
- In the last step, the cell state, weight matrices for the input vector, weight matrices for the hidden state, and biases are updated to their new values by using the computed differences in gates. The differences in the candidate cell state weight matrix, the input gate weight matrix, the forget gate weight matrix and the output gate weight matrix for the input vector are computed using Equations (3.17), (3.18), (3.19), and (3.20), respectively. Next, the differences in the candidate cell state weight matrix, the input gate weight matrix, the forget gate weight matrix and the output gate weight matrix for the hidden state are computed using Equations (3.21), (3.22), (3.23) and (3.24), respectively. Next, the differences in the bias for the candidate cell state, the input gate, the forget gate and the output gate are computed using Equations (3.25), (3.26), (3.27) and (3.28), respectively.

Backward pass equations are collectively provided as follows (Greff, Srivastava, Koutnik, Steunebrink and Schmidhuber, 2017):

$$\delta h_t = \Delta_t + U_a^T \, \delta a_{t+1} + U_i^T \, \delta i_{t+1} + U_f^T \, \delta f_{t+1} + U_o^T \, \delta o_{t+1} \tag{3.11}$$

$$\delta o_t = \delta h_t \odot tanh(c_t) \odot o_t \odot (1 - o_t) \tag{3.12}$$

$$\delta c_t = \delta h_t \odot o_t \odot (1 - tanh^2(c_t)) + \delta c_{t+1} \odot f_{t+1} \tag{3.13}$$

$$\delta f_t = \delta c_t \odot c_{t-1} \odot f_t \odot (1 - f_t) \tag{3.14}$$

$$\delta i_t = \delta c_t \odot a_t \odot i_t \odot (1 - i_t) \tag{3.15}$$

$$\delta a_t = \delta c_t \odot i_t \odot (1 - a_t^2) \tag{3.16}$$

$$\delta W_a = \sum_{t=0}^{T} \delta a_t \otimes x_t \tag{3.17}$$

$$\delta W_i = \sum_{t=0}^{T} \delta i_t \otimes x_t \tag{3.18}$$

$$\delta W_f = \sum_{t=0}^{T} \delta f_t \otimes x_t \tag{3.19}$$

$$\delta W_o = \sum_{t=0}^{T} \delta o_t \otimes x_t \tag{3.20}$$

$$\delta U_a = \sum_{t=0}^{T-1} \delta a_{t+1} \otimes h_t \tag{3.21}$$

$$\delta U_i = \sum_{t=0}^{T-1} \delta i_{t+1} \otimes h_t \tag{3.22}$$

$$\delta U_f = \sum_{t=0}^{T-1} \delta f_{t+1} \otimes h_t \tag{3.23}$$

$$\delta U_o = \sum_{t=0}^{T-1} \delta o_{t+1} \otimes h_t \tag{3.24}$$

$$\delta b_a = \sum_{t=0}^{T} \delta a_t \tag{3.25}$$

$$\delta b_i = \sum_{t=0}^{T} \delta i_t \tag{3.26}$$

$$\delta b_f = \sum_{t=0}^{T} \delta f_t \tag{3.27}$$

$$\delta b_o = \sum_{t=0}^{T} \delta o_t \tag{3.28}$$

where δh_t is the difference in the hidden state; Δ_t is the derevative of the loss function with respect to h_t at t; U_a^T is the transpoze of the candidate cell state weight matrix for the hidden state; U_i^T is the transpoze of the input gate weight matrix for the hidden state; U_f^T is the transpoze of the forget gate weight matrix for the hidden state; U_o^T is the transpoze of the output gate weight matrix for the hidden state; δa_{t+1} is the difference in the candidate cell state at $t+1$; δi_{t+1} is the difference in the input gate at $t+1$; δf_{t+1} is the difference in the forget gate at $t+1$; δi_{t+1} is the difference in the output gate at $t+1$; δo_t is the difference in the output gate at t; δc_t is the difference in the cell state at t; δf_t is the difference in the forget gate at t; δa_t is the difference in the candidate cell state at t; δW_a is the difference in candidate cell state weight matrix for the input vector to update; δW_i is the difference in the input gate weight matrix for the input vector to update; δW_f is the difference in the forget gate weight matrix for the input vector to update; δW_o the difference in is the output gate weight matrix for the input vector to update; δU_a is the difference in the candidate cell state weight matrix for the hidden state to update; δU_i the difference in is the input gate weight matrix for the hidden state to update; δU_f the difference in is the forget gate weight matrix for the hidden state to update; δU_o the difference in is the output gate weight matrix for the hidden state to update; δb_a is the difference in the bias for the candidate cell state to update; δb_i is the difference in the bias for the input gate to update; δb_f is the difference in the bias for the forget gate to update; δb_o is the difference in the bias for the output gate to update; T is the number of timesteps.

Sigmoid and hyperbolic tangent functions(tanh) are defined as:

$$sigmoid(x) = \frac{1}{1 + e^{-x}} \tag{3.29}$$

$$tanh(x) = \frac{e^{x} - e^{-x}}{e^{x} + e^{-x}} \tag{3.30}$$

Curves corresponding to sigmoid and hyperbolic tangent functions are shown in Figure 3.7.

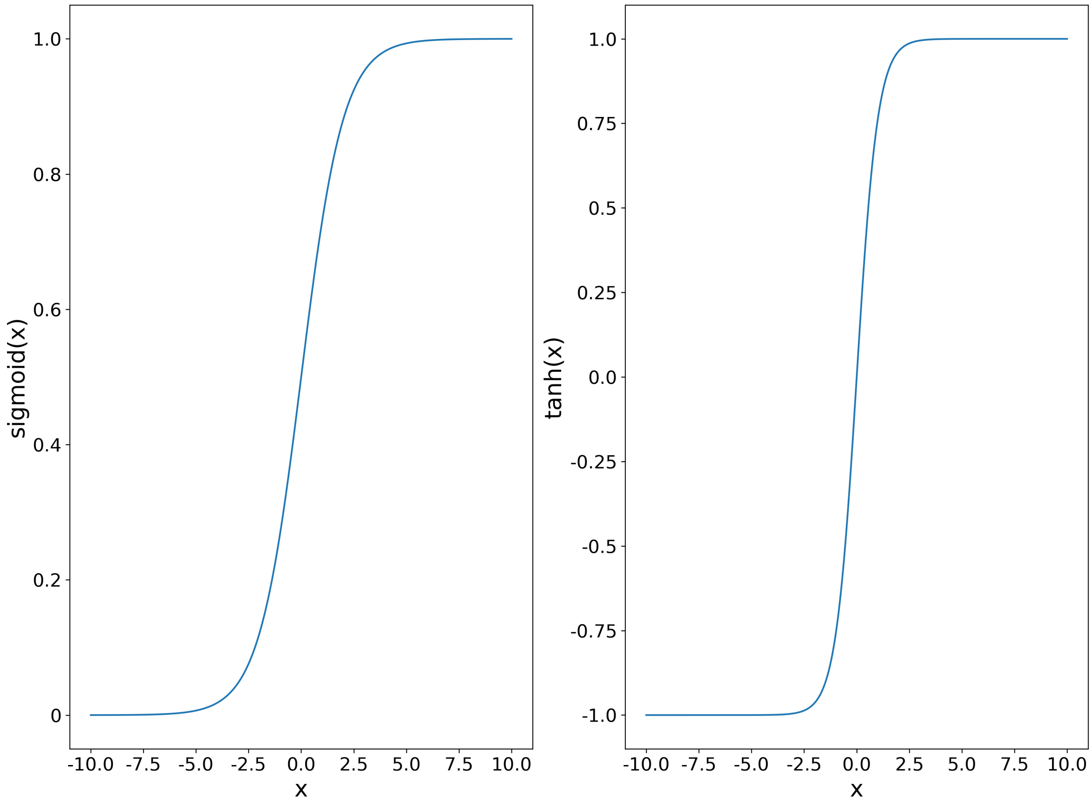

Figure 3.7. Sigmoid and Hyperbolic Tangent Curves

The total number of parameters N in an the LSTM layer is found by using the following expression:

$$N = 4\, n_u(n_u + n_d + 1) \tag{3.31}$$

where n_u is the number of LSTM units in the LSTM layer; n_d is the input dimension or the number of features.

In our problem, the LSTM layer is developed for a four-dimensional input vector and has three units, so the total number of parameters is 96. At the end of the network, there is a dense layer that is connected to the LSTM layer. The dense layer takes the output vector of the LSTM layer and produces the final output of the LSTM network. The dense layer of this LSTM network has one unit and a sigmoid activation function. So, the dense layer takes three-dimensional output vector (i.e., the number of LSTM units equals to three) of the LSTM layer, applies the element-wise product with the weight of the dense layer, adds the bias of the dense layer, and passes through the element-wise sigmoid function. As a result, it produces one value as the output. The number of parameters of the dense layer is four, three from the weights and one from the bias. Thus, in our problem the total number of parameters of the LSTM network is 96+4=100.

An LSTM code is developed in the Python environment, and libraries given in Table 3.3 are used in the code. The developed LSTM network code executes the following main steps:

- Hourly electricity price data is splitted into three parts, as data for training, validation and test.
- All data is normalized to a range [0,1] to prevent the effect of the scale of the data.
- The normalized data is converted to the necessary format according to the time series size, the input dimension and the batch size.
- The LSTM network is trained by trying various hyperparameters (e.g., number of LSTM units, batch size, number of epoch) to improve the forecasting performance of the validation data. The hyperparameters that show the best forecast performance are determined and fixed as final hyperparameters of the LSTM network.
- Final LSTM network model is used to simulate the test data which is not seen by the trained model previously.

Table 3.3. Used Libraries for the LSTM Network

Library	**Description**	**Application**
NumPy	Python package for scientific computing.	Data operations are carried on to create the right formats.
Matplotlib	Comprehensive Python library to create visualizations.	Results of the simulations are plotted.
Pandas	Powerful Python library for data analysis and manipulation.	Inputs and results of the simulations are tabulated and organized.
Scikit-learn	Python library for machine learning.	Data is scaled between zero and one.
Keras	Python library for high-level neural networks.	LSTM network model is built and simulated.

3.3 The Optimization Model

In the scope of this thesis, an optimization model is developed to maximize the daily revenue of a WHHS. The WHHS considered here is a closed-loop systems. In other words, all inflows to and outflows from the reservoir are neglected; thus it is an isolated system. Available wind energy is calculated based on MERRA-2 data since it is a reliable database that provides hourly wind speed data. The optimization model takes wind energies and forecasted market prices for each hour in a day (i.e., practically the next day), and finds the daily schedule of the WHHS that maximizes the net revenue of that day. The schedule of the WHHS includes the amount of energy to be bought or sold to the grid, energy productions of wind turbines and hydro turbines, and the amount of energy used to pump water from the lower reservoir to the upper reservoir in each hour of the day. The optimization model does not allow to sell or buy energy from the grid at the same hour. This is valid for pump and turbine operations, as well.

Mathematical Formulation

The daily schedule of the WHHS that maximizes the net revenue of the day can be obtained from the solution of the following optimization problem modified from the formulation developed by Cruz et al. (2014):

$$Max.\, Z = \sum_{t=0}^{23} \lambda_t \, p_t \tag{3.32}$$

$$s.t.$$

$$p_t = p_t^{wdirect} + p_t^{hydro} - p_t^{fgrid} \tag{3.33}$$

$$p_t^{wdirect} + p_t^{hydro} \leq (p_{max}^{w} + p_{max}^{hydro})y_t \qquad \forall\, y_t \tag{3.34}$$

$$p_t^{fgrid} \leq p_{max}^{fgrid}(1 - y_t) \qquad \forall\, y_t \tag{3.35}$$

$$p_t^{w} = p_t^{wdirect} + p_t^{wpump} \tag{3.36}$$

$$p_t^{pump} = p_t^{wpump} + p_t^{fgrid} \tag{3.37}$$

$$0 \leq p_t^{w} \leq p_{max}^{w} \tag{3.38}$$

$$0 \leq p_t^{hydro} \leq p_{max}^{hydro}(1 - x_t) \qquad \forall\, x_t \tag{3.39}$$

$$0 \leq p_t^{pump} \leq p_{max}^{pump} x_t \qquad \forall\, x_t \tag{3.40}$$

$$p_t^{hydro} \leq min\{(E_t - E_{min})\eta_{hydro}, \quad p_{max}^{hydro}\} \tag{3.41}$$

$$p_t^{pump} \leq min\{(E_{max} - E_t)\frac{1}{\eta_{pump}}, \quad p_{max}^{pump}\} \tag{3.42}$$

$$E_{t+1} = E_t + \ \eta_{pump}\, p_{t+1}^{pump} - \frac{1}{\eta_{hydro}} p_{t+1}^{hydro} \qquad t = 0, 1, ..., 22 \tag{3.43}$$

$$E_0 = E_{initial} + \ \eta_{pump}\, p_0^{pump} - \frac{1}{\eta_{hydro}} p_0^{hydro} \tag{3.44}$$

$$E_{min} \leq E_t \leq E_{max} \tag{3.45}$$

$$y_t \in \{0, 1\} \tag{3.46}$$

$$x_t \in \{0, 1\} \tag{3.47}$$

$$p_t^{hydro}, p_t^{wdirect}, p_t^{fgrid}, p_t^{wpump}, p_t^{pump}, p_t^{W}, E_t \geq 0 \tag{3.48}$$

where the set is:

$t \, \epsilon \, \{0, 1, 2, .., 23\}$	the duration of each interval, hour;

where the variables are:

p_t	the energy output injected into the grid minus energy bought from the grid in t;
λ_t	the electricity price in t;
$p_t^{wdirect}$	the energy output of wind turbines that is sold directly to the grid in t;
p_t^{hydro}	the energy output of the hydro turbine that is sold directly to the grid in t;
p_t^{fgrid}	the energy bought from the grid in t;
p_t^{w}	the wind energy that is generated in t;
p_t^{wpump}	the energy that is generated by wind turbines and is used by the pump in t;
p_t^{pump}	the energy that is used for pumping in t;
E_t	the energy stored in the upper reservoir at the end of t;
y_t	the binary variable that represents the buying or selling mode of the system in t where $y_t = 0$ is the buying mode, and $y_t = 1$ is the selling mode;
x_t	the binary variable that represents the turbine or pump modes in t where $x_t = 0$ is the turbine mode, and $x_t = 1$ is the pump mode;

and the corresponding parameters are:

p^{w}_{max} the maximum energy that can be generated by the wind turbines in an hour;

p^{hydro}_{max} the maximum energy that can be generated by the hydro turbine in an hour;

p^{fgrid}_{max} the maximum energy that can be bought from the grid in an hour;

p^{pump}_{max} the maximum energy that can be used as pumping input in an hour;

E_{min} the minimum energy level in the upper reservoir;

E_{max} the maximum energy level that can be stored in the upper reservoir;

η_{hydro} the efficiency for the turbine mode;

η_{pump} the efficiency for the pump mode;

$E_{initial}$ the initial energy in the upper reservoir.

Equation (3.32) is the objective function of the optimization problem. It aims to maximize the revenue of one day. Equation (3.33) defines the net energy sold to the grid, which is the energy sold minus the energy bought. When $p^{wdirect}_{t}$ and p^{hydro}_{t} are positive values, p^{fgrid}_{t} cannot be a positive value. Because selling and buying energy from the grid at the same time is illogical and not allowed. This is achieved by Equations (3.34) and (3.35). If y_t equals one, the system sells energy to the grid in t; if it equals zero, the system buys energy from the grid in t. The wind energy that is generated in t p^{w}_{t}, can be sold directly to the grid or used to pump the water to the upper reservoir. This is defined in Equation (3.36). The energy that is used for pumping in t p^{pump}_{t}, can be supplied by wind turbines or can be bought from the grid. Equation (3.37) presents this constraint. The wind energy that is generated in t p^{w}_{t}, has a minimum value of zero, and its upper bound cannot exceed p^{w}_{max} as defined in Equation (3.38). The energy output of the hydro turbine in t p^{hydro}_{t}, and the energy used for pumping in t p^{pump}_{t} cannot be larger than their maximum installed capacities. Also, they cannot be positive values at the same hour since it is not possible to run the pump and the turbine at the same time. These limitations are defined in Equations (3.39) and (3.40).

The energy output of the hydro turbine in t p^{hydro}_{t} is limited by two components in Equation (3.41). In the first component, $E_t - E_{min}$ represents the energy in the upper reservoir than can be used to generate energy by the hydro turbine. When it is multiplied by n_{hydro}, it becomes the energy output of the hydro turbine. The second component is the maximum capacity of the hydro turbine. So, p^{hydro}_{t} is restricted to be at most the minimum of these two terms.

The energy that is used for pumping in t p_t^{pump} is limited by two components in Equation (3.42). In the first component, $E_{max} - E_t$ represents the available empty energy storage that can be filled by the water. When it is divided by n_{pump}, it becomes the pumping energy input. The second component is the maximum energy input for the pump. So, p_t^{pump} is restricted to be at most the minimum of these two terms.

The energy balance of the upper reservoir is defined in Equation (3.43). The energy stored in the upper reservoir at the end of $t+1$ is composed of three components. The first component is the stored energy from the previous hour. The second component is the energy used for pumping the water from the lower reservoir to the upper reservoir in $t+1$. The third component is the energy spend to run the hydro turbine to generate electricity in $t+1$. So, E_{t+1} equals the summation of the first two components minus the third component. For the first hour, $t = 0$, the energy stored in the upper reservoir is initialized based on the starting energy storage in the upper reservoir E_{-1}. Lastly, E_t must be between E_{min} and E_{max}, and that is defined in Equation (3.45).

Except binary variables, y_t and x_t, units of all decision variables (p_t, $p_t^{wdirect}$, p_t^{hydro}, p_t^{fgrid}, p_t^{wpump}, p_t^{pump}, p_t^{w}, E_t) are MWh. Units of all parameters (p_{max}^{hydro}, p_{min}^{hydro}, p_{max}^{pump}, p_{min}^{pump}, p_{min}^{W}, p_{max}^{w}, p_{max}^{fgrid}, $E_{initial}$, E_{max}, E_{min}) are MWh, except a few ones. The unit of λ_t is TL/MWh, and η_{hydro} and η_{pump} are unitless.

The optimization model involves three assumptions. First, head losses in the piping system of WHHS are not included explicitly. They are assumed to be included in the efficiency values of the turbine and pump modes. Second, there is no inflow to or outflow from the reservoir. So, the system is assumed to be a closed-loop system. Third, the cost of pumping operation is assumed to be the same value as the electricity price at that hour (Cruz et al., 2014).

The following modifications to the mathematical formulation suggested by Cruz et al. (2014) are carried out in this study:

- The energy that is generated by the wind turbines is allowed to be used for pumping and direct selling, and stored in two different variables (see Equation (3.36)).
- The energy that is used for pumping is allowed to be obtained from wind tur-

bines and grid, and stored in two different variables (see Equation (3.37)).

- To prevent buying and selling at the same time in each hour, a binary variable is defined (see Equations (3.34) and (3.35)).
- Considering the minimum and maximum water levels in the upper reservoir, water can be pumped or released from the upper reservoir, and the energy stored in the upper reservoir is updated (see Equations (3.41) and (3.42)).
- Equations (13) and (14) in Cruz et al. (2014) are not used since they are satisfied by Equations (3.41) and (3.42).
- In Cruz et al. (2014), the final energy level of the upper reservoir is taken as a fixed value. However, in our study, we used the reservoir level of the last hour of the previous day.

The formulated optimization problem is a mixed-integer linear programming problem since two of the decision variables (i.e., x_i and y_i) are restricted to be binary values. To solve the optimization problem, a code is written in Python. The code uses *Coin-or branch and cut* solver which is developed by Forrest, Ralphs, Vigerske, LouHafer, Kristjansson, Jpfasano, EdwinStraver, Lubin, Santos, Rlougee and Saltzman (2018). To apply this solver in Python, Google OR-Tools library is included in the code. Main libraries to write the Python code is given in Table 3.4.

Table 3.4. Used Libraries for the Optimization Model

Library	**Description**	**Application**
NumPy	Python package for scientific computing.	Data operations are carried on to create the right formats.
Matplotlib	Comprehensive Python library to create visualizations.	Results of the simulations are plotted.
Pandas	Powerful Python library for data analysis and manipulation.	Inputs and results of the simulations are tabulated and organized.
OR-Tools	Python library for optimization, integer and linear programming, and constraint programming.	Optimization model is built and simulated.

CHAPTER 4

CASE STUDY

A hypothetical WHHS as a case study is designed to demonstrate application of the models developed in this study. The hypothetical WHHS is assumed to be a wind farm integrated to the existing Uluabat Hydropower Plant. Moreover, the Uluabat Hydropower Plant is assumed to be a closed-loop system. There are two main purposes of this study. The first one is to forecast hourly electricity prices in the day-ahead market for each hour of the next day with the LSTM network. The second one is to produce an optimum daily schedule of the WHHS that maximizes the daily revenue by using the forecasted hourly electricity prices. The methodology introduced in Chapter 3 is applied for the hypothetical WHHS introduced in this chapter. This chapter describes the case study with the following sections; location of the WHHS, analysis of hourly electricity prices and hourly wind energy at the case study site, the LSTM network and the optimization model.

4.1 Location of the WHHS

Uluabat Hydropower Plant with its 100 MW installed capacity is located at Susurluk Basin on Orhaneli River in the Marmara Region of Turkey. Water at Çınarcık Dam's reservoir is released to Lake Uluabat to generate electricity. In this study, we considered a hypothetical case. Çınarcık Dam and Lake Uluabat are thought of as the upper reservoir and the lower reservoir of a pumped storage hydropower plant, respectively. In addition, it is assumed that there are wind turbines near the hydropower plant site owned and operated by the same company. Pumped storage hydropower plant plus wind turbines compose the hypothetical WHHS. Although Çınarcık Dam and Uluabat Hydropower Plant are located on a river, it is assumed that the hypothetical WHHS is a closed-loop. That is, all inflows and outflows to and from Çınarcık Dam are neglected. The location of the Uluabat Hydropower Plant is shown in Figure 4.1.

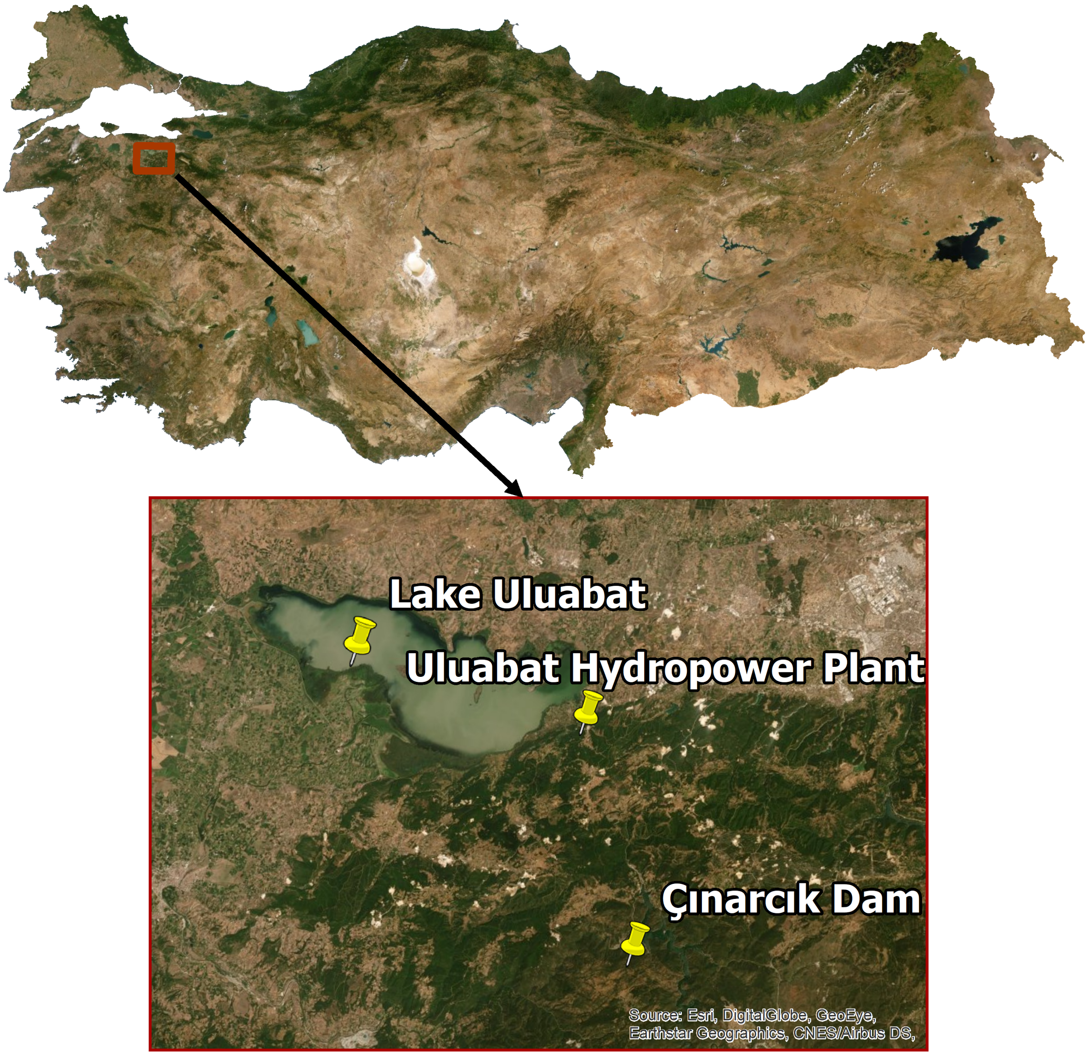

Figure 4.1. Location of the Case Study Site

4.2 Analysis of the Input Data

Two types of data are used in the case study. These are hourly wind speed data and hourly electricity price data. Hourly wind speed data is used to estimate hourly wind energy that can be generated by wind turbines. After hourly wind energy values are calculated, they are used as input to the optimization model. On the other hand, historical hourly electricity price data is used as the input of the LSTM network. The output of the LSTM network is the second input of the optimization model. The optimization model is run from September 2017 to August 2018, so the wind speed data is obtained for this time interval. Hourly electricity price data is obtained for the interval between January 2011 and August 2018. Since hourly electricity price data is used to train the LSTM network, the time interval of it is wider than the wind speed data.

4.2.1 Analysis of the Hourly Wind Speed Data

The hourly wind speed data is obtained from the NASA MERRA-2 database, which is described in Chapter 2. Figure 4.2 shows the variations in hourly wind speed data between September 2017 and August 2018. This distribution shows that the median of wind speeds are higher in afternoon hours, such as 14:00 and 15:00, and the number of outliers at this hours is lower than the other hours. So, it can be inferred that more electricity can be generated during the afternoon hours of most of the days.

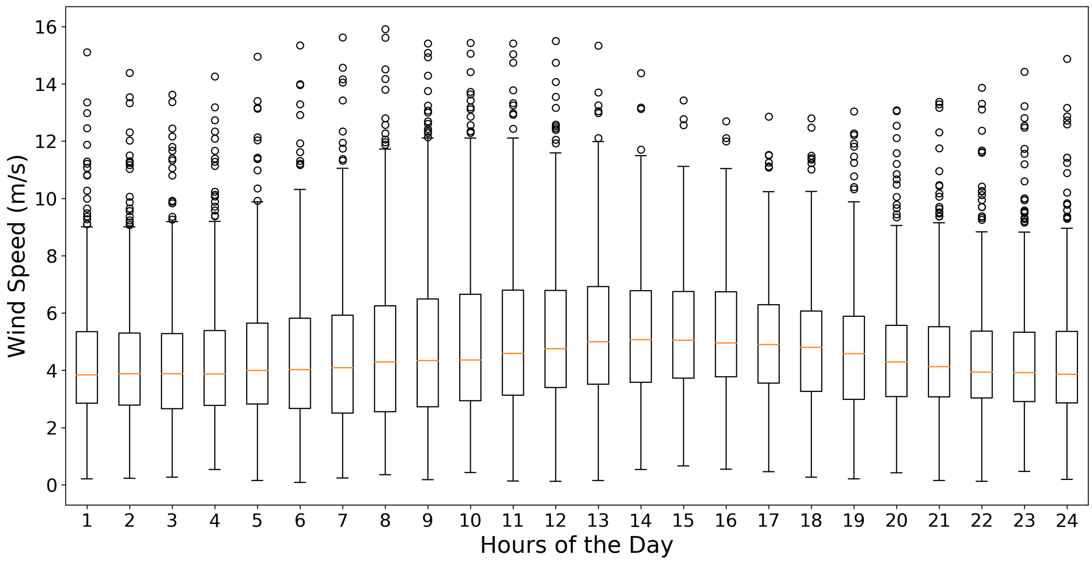

Figure 4.2. Variations in Hourly Wind Speed Data between 09/2017 and 08/2018

Varitions in hourly wind speed data for each month are investigated, as well. Since wind speed is affected by meteorological factors (e.g., temperature, moisture, atmospheric pressure) it has different characteristics in each month. Hourly wind speed variations for each month from September 2017 to August 2018 are presented in Figures 4.3 to 4.14, respectively. As can be seen from these figures, in September, May, June, July and August, wind speeds are higher in the afternoon hours, between 14:00 and 16:00. Also, there are not any outliers in May, whereas there are many in September. In November, the median values of the midnight hours, between 01:00 and 06:00, are higher. Wind speeds in December and March are higher than those in other months. Also, they do not have any outlier. In February, the variations of mid-day hours, between 11:00 and 13:00, are higher when compared to the other hours of the day and months. Wind speeds in April have smaller values. Also, the ranges of variations are smaller. As can be seen from Figures 4.3 to 4.14, hourly wind speed data show very large variations and there are many outliers. Based on these observations it is concluded that estimation of the future hourly wind speeds may not carried out effectively. Thus, instead of estimating wind speed data for future hours it is preferred to use previous years wind speed data in the optimization model.

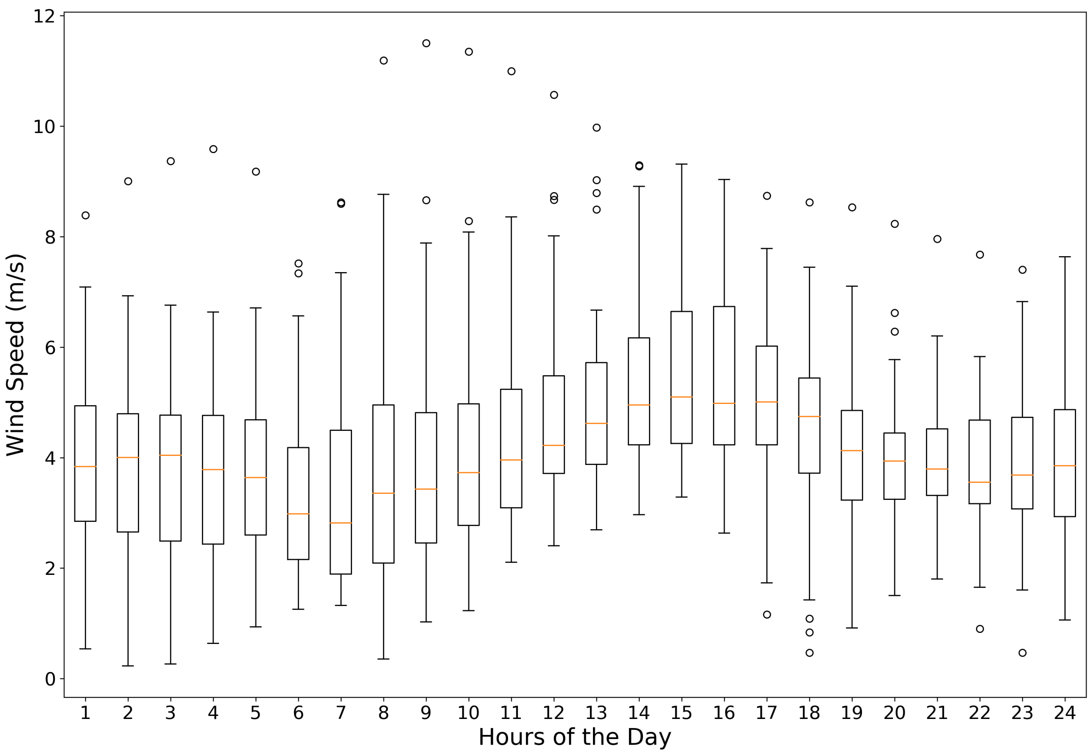

Figure 4.3. Hourly Wind Speed Variations in September

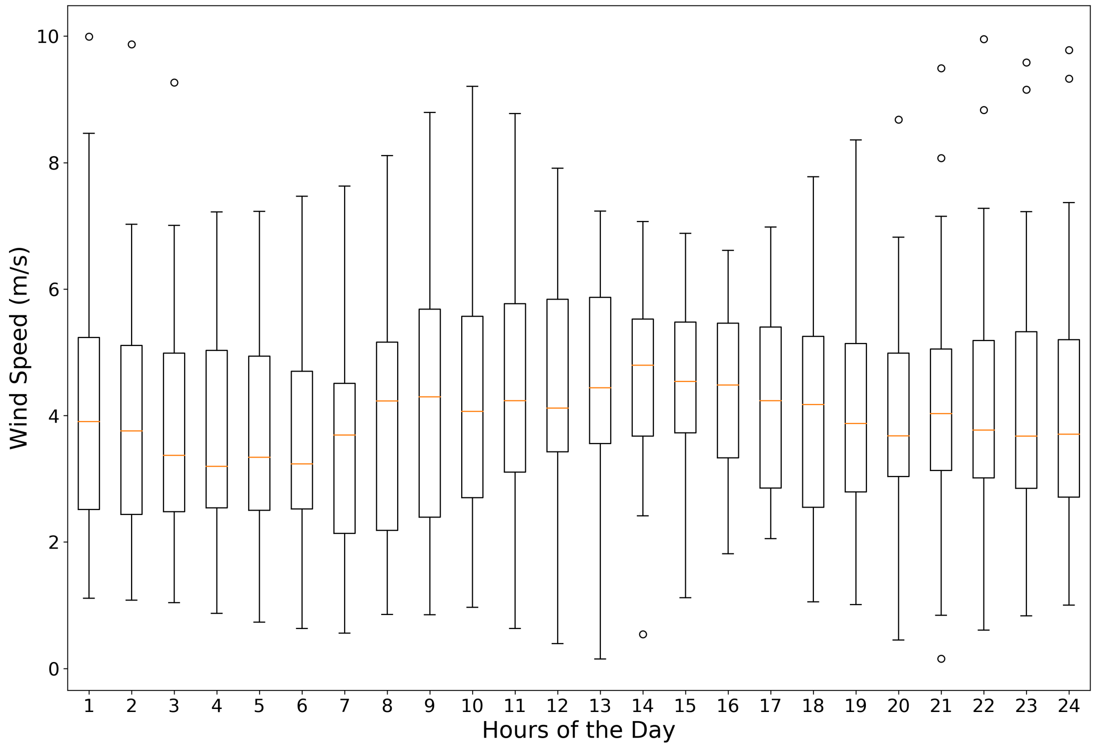

Figure 4.4. Hourly Wind Speed Variations in October

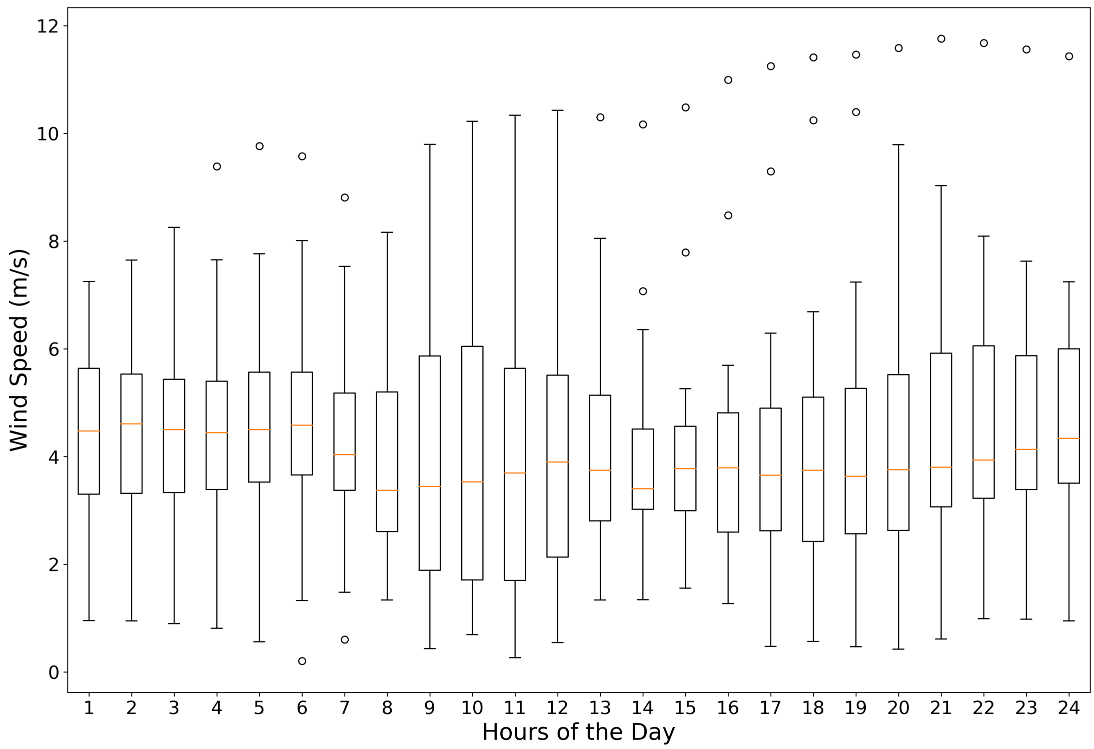

Figure 4.5. Hourly Wind Speed Variations in November

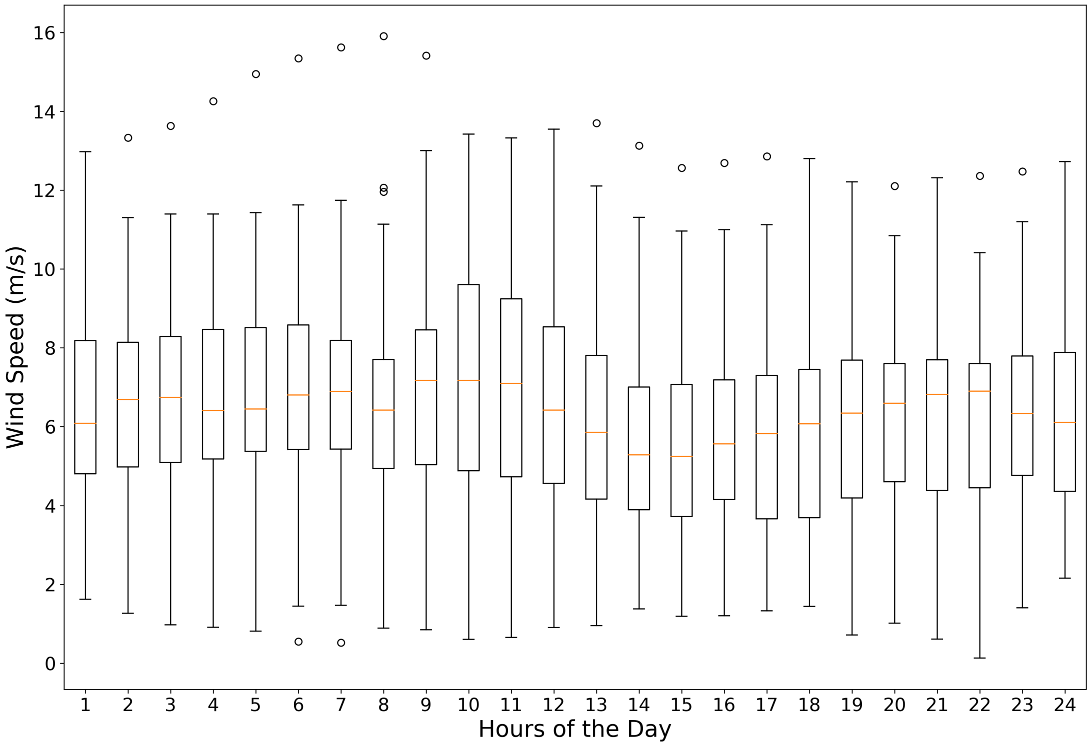

Figure 4.6. Hourly Wind Speed Variations in December

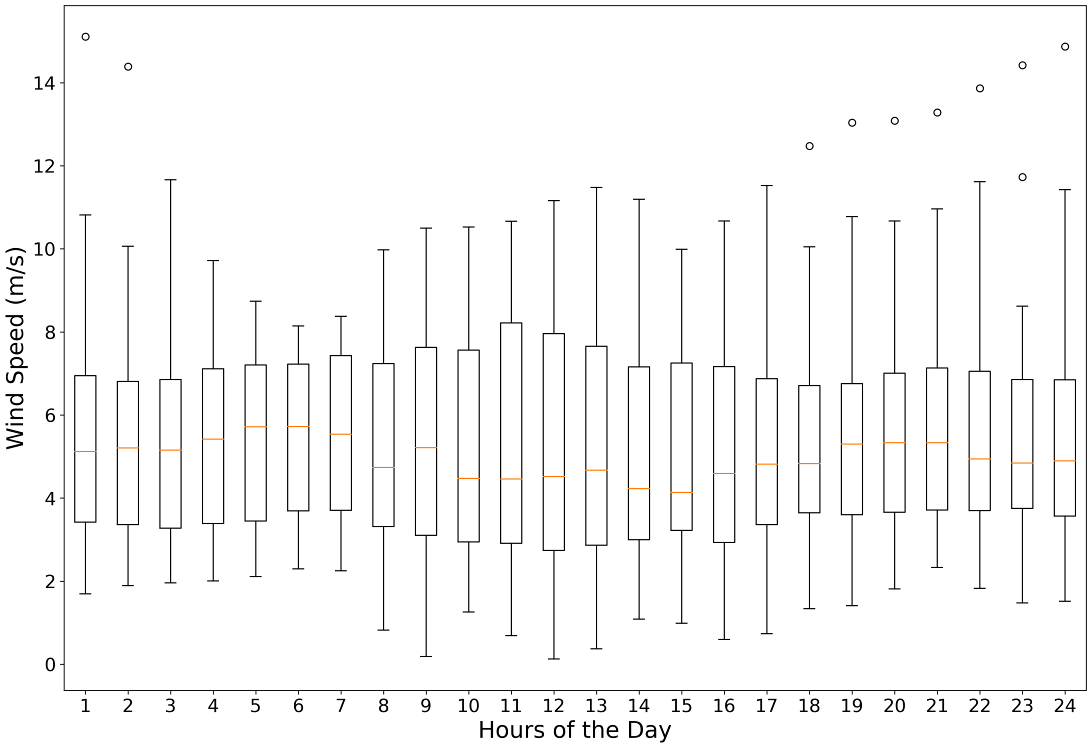

Figure 4.7. Hourly Wind Speed Variations in January

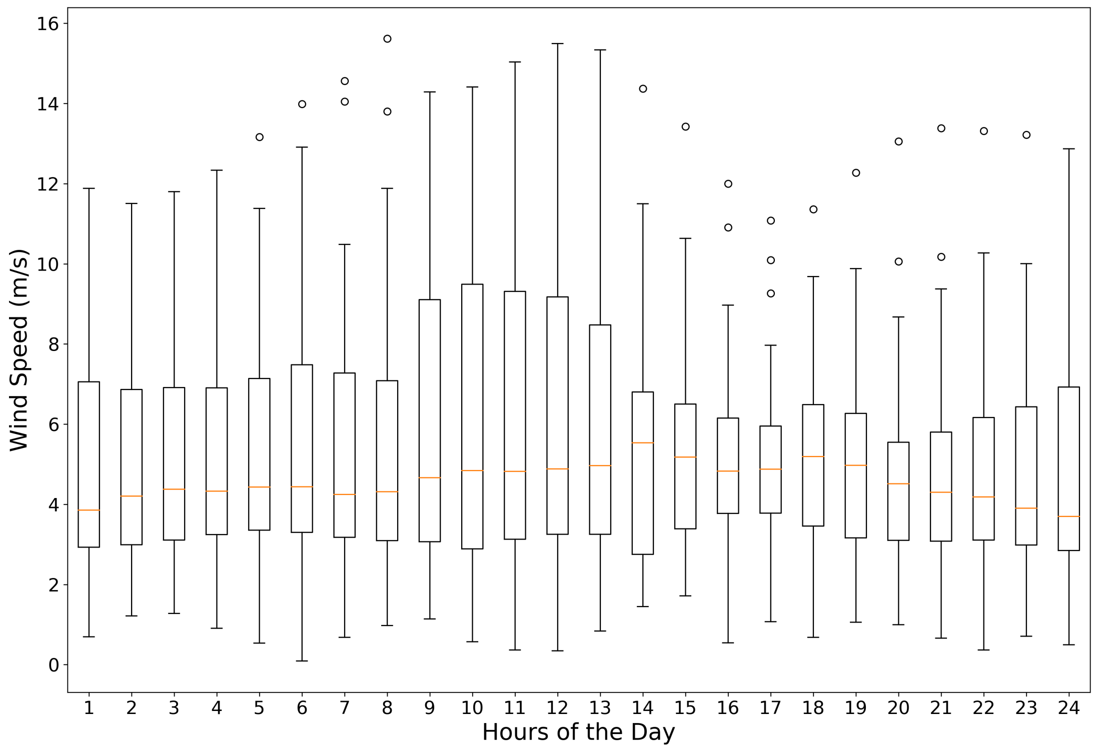

Figure 4.8. Hourly Wind Speed Variations in February

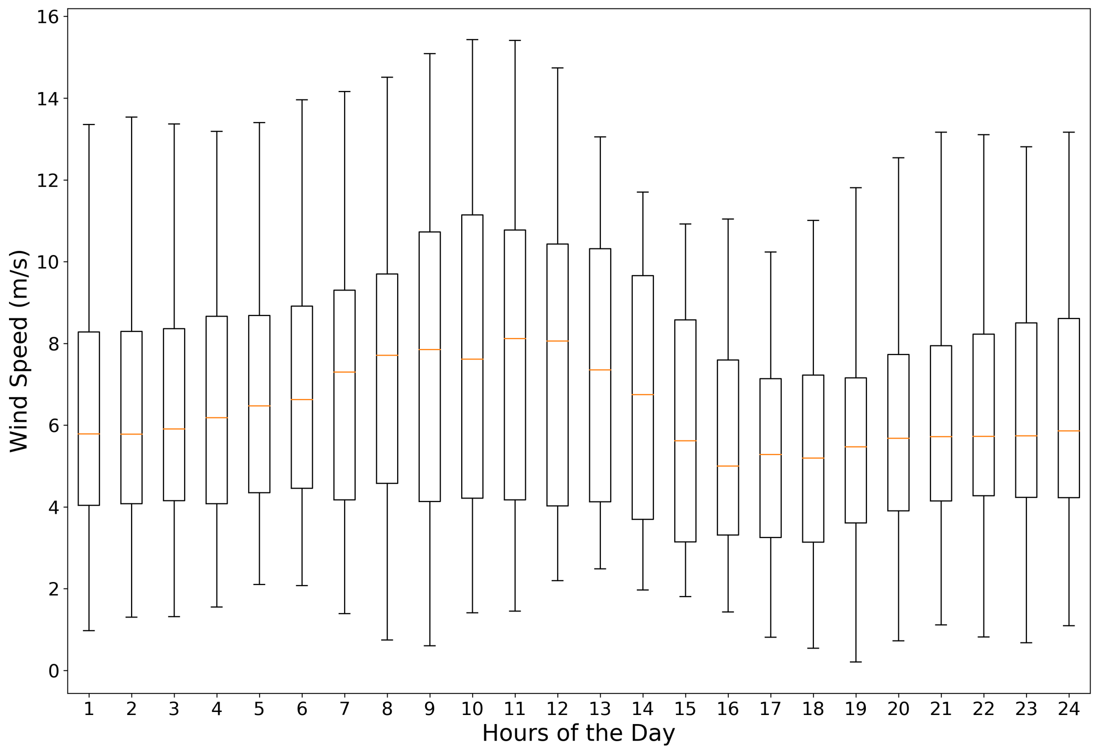

Figure 4.9. Hourly Wind Speed Variations in March

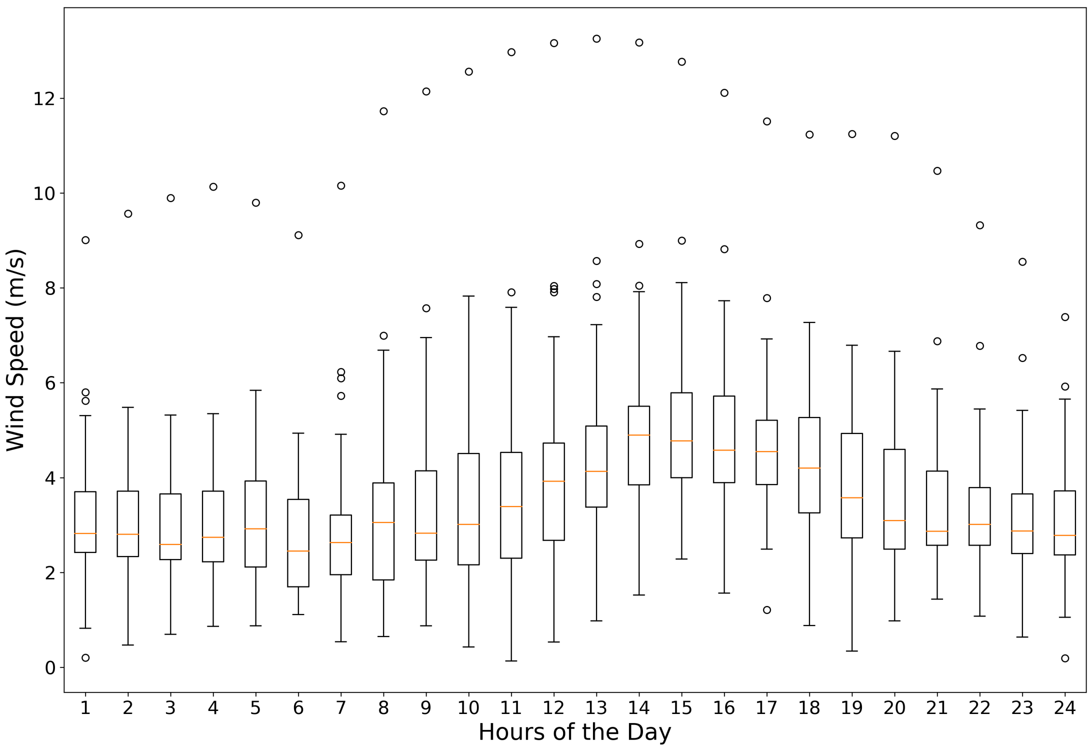

Figure 4.10. Hourly Wind Speed Variations in April

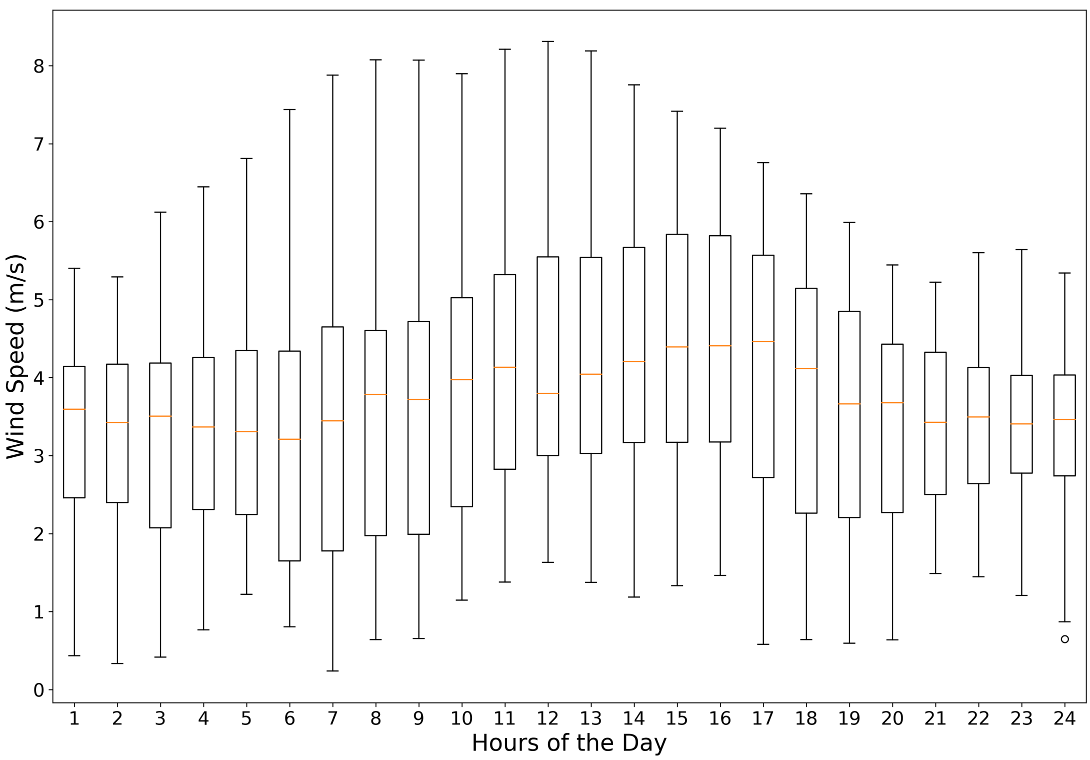

Figure 4.11. Hourly Wind Speed Variations in May

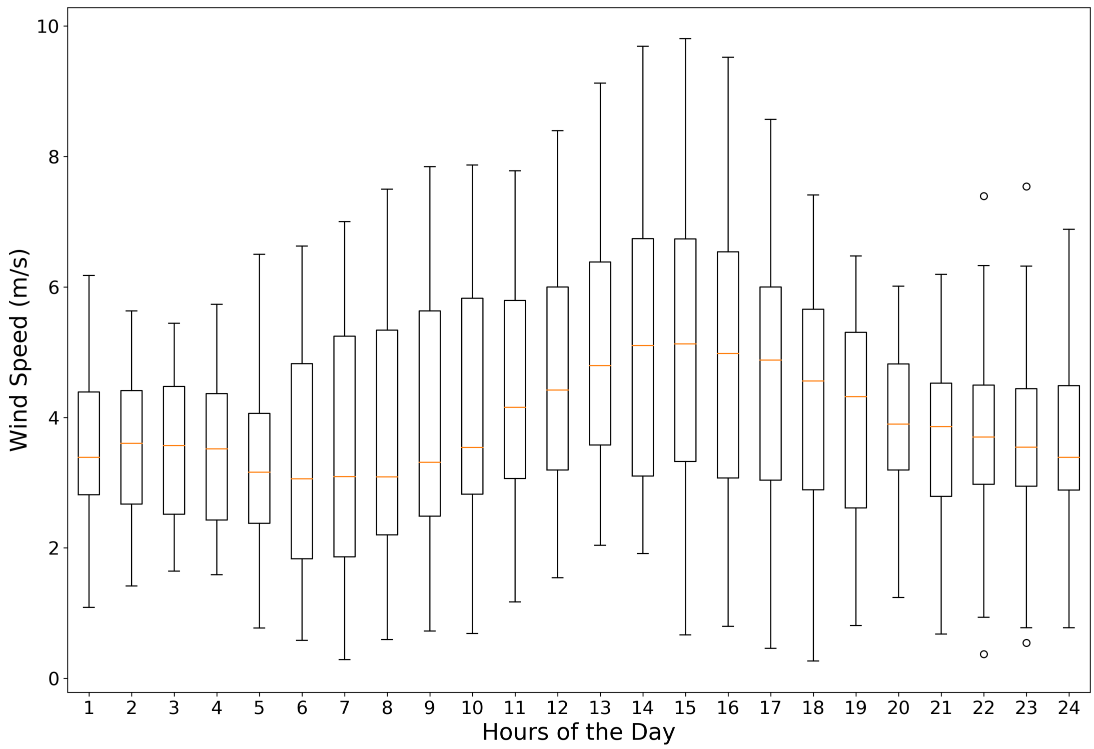

Figure 4.12. Hourly Wind Speed Variations in June

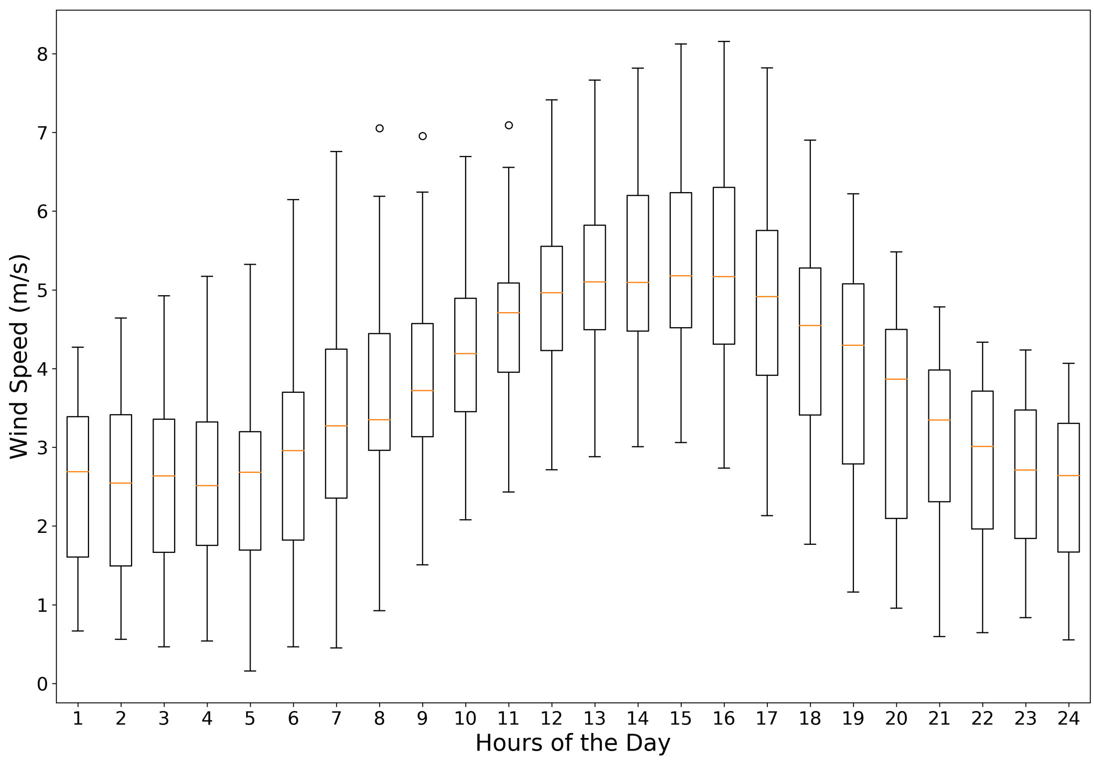

Figure 4.13. Hourly Wind Speed Variations in July

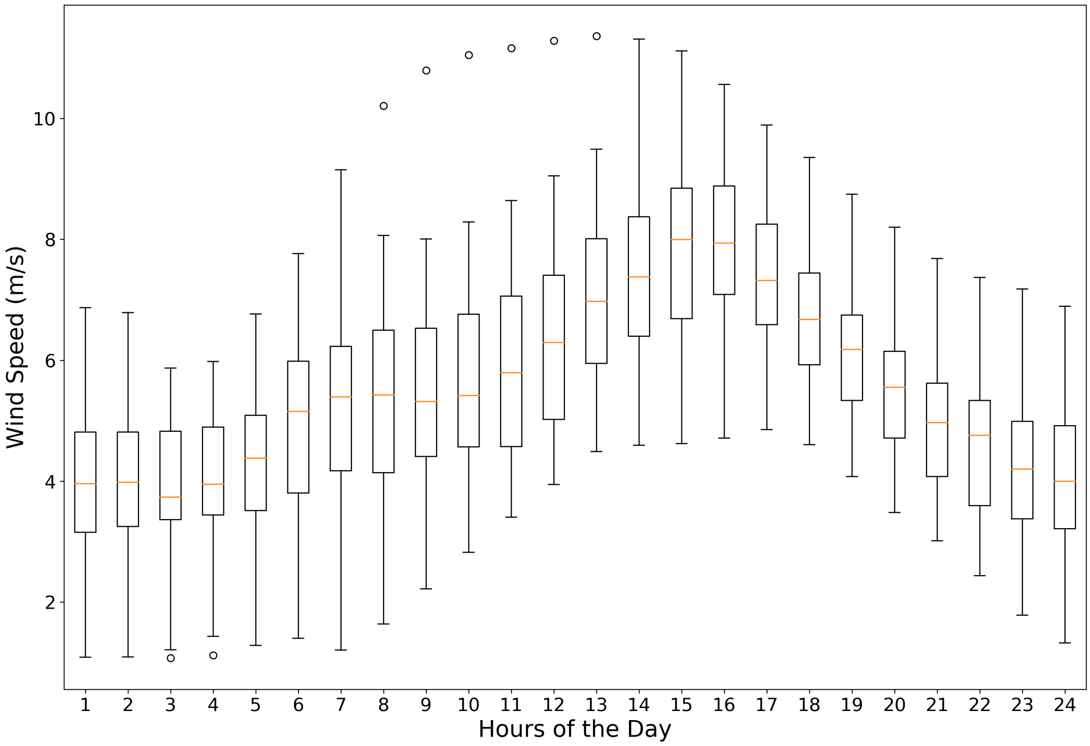

Figure 4.14. Hourly Wind Speed Variations in August

In addition to the hourly distributions of the wind speeds, correlations between wind speed at an hour and at previous hours are investigated, and presented in Figure 4.15. In Figure 4.15, the y-axis indicates the correlation coefficient, which is expressed as follows:

$$R = \frac{\sum_{i=1}^{n}(x_i - \bar{x})(y_i - \bar{y})}{\sqrt{\sum_{i=1}^{n}(x_i - \bar{x})^2}\sqrt{\sum_{i=1}^{n}(y_i - \bar{y})^2}} \tag{4.1}$$

where n is the sample size, x_i and y_i the individual sample points with index i, $\bar{x}$ and $\bar{y}$ are mean values of the samples. As can be seen in Figure 4.15, the correlation has a decreasing trend up to 60 hours before. After that, there is effectively no correlation (i.e., lower than 0.2). It shows a high correlation with the previous few hours and the correlation decreases rapidly. Thus, wind speeds especially for the future few hours might have been estimated using an LSTM network. However, the correlation drops below 0.6 for after 8 hours. Based on these observations, instead of estimating hourly wind speeds for the coming 24 hours, previous years wind speed data is used in this study. If hourly wind speed estimations become available from other sources such as State Meteorological Organization, they can be used as input in the optimization model.

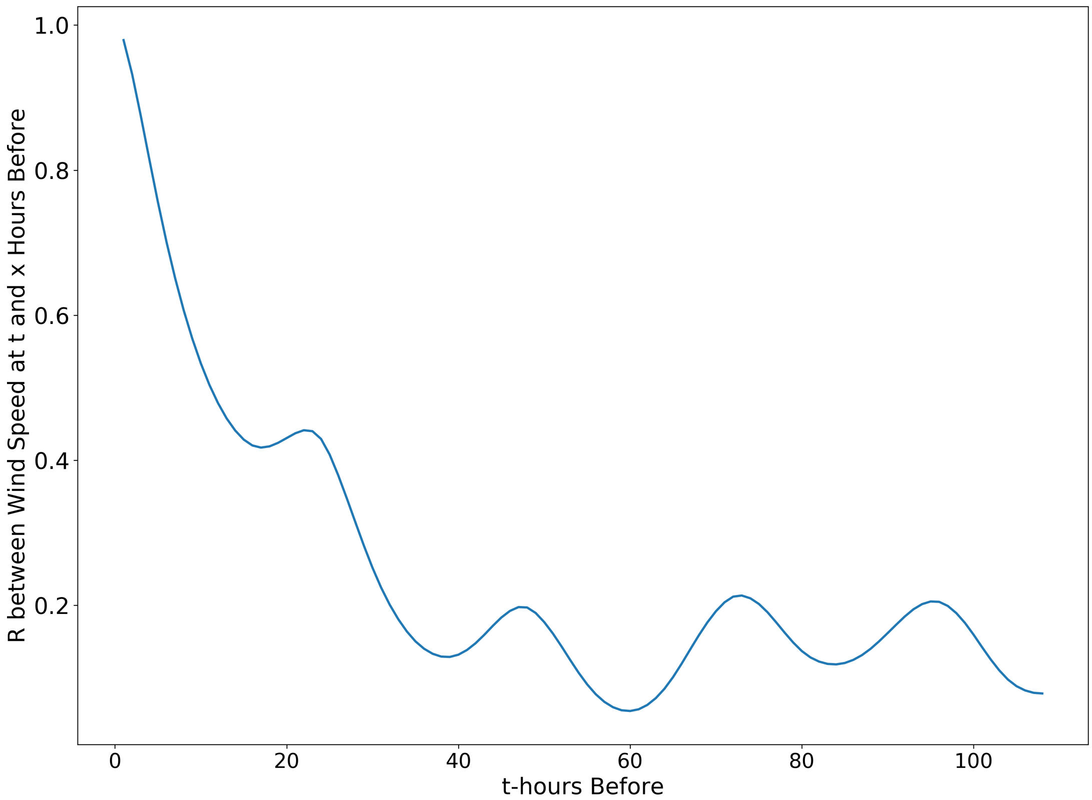

Figure 4.15. Variation in Wind Speed Correlation Coefficient with respect to Previous Hours

4.2.2 Analysis of the Hourly Electricity Price Data

The hourly electricity price data is obtained from EPİAŞ, which operates Turkish energy markets. Data from January 2011 to August 2017 is used to train the LSTM network, and the remaining data (i.e., from September 2017 to August 2018) is used for testing. The outputs of the LSTM network is used as the input of the optimization model. Variations in hourly electricity prices are presented for each year from 2011 to 2018 in Figures 4.16 to 4.23, respectively. In 2012, during daytime hours, many outliers are observed. At these hours (i.e., 11:00, 13:00, and 15:00), eight times higher daily median prices are observed. In 2015, quite low (i.e., close to zero) prices are observed at the hours from 00:00 to 12:00. 2018 includes the highest number of outliers among all years. The prices in four months (i.e., September, October, November and December) of 2017 and eight months (i.e., January, February, March, April, May, June, July and August) of 2018 are forecasted via the developed LSTM network. Due to the high number of outliers in 2017 and 2018, they are the most challenging year to be forecasted.

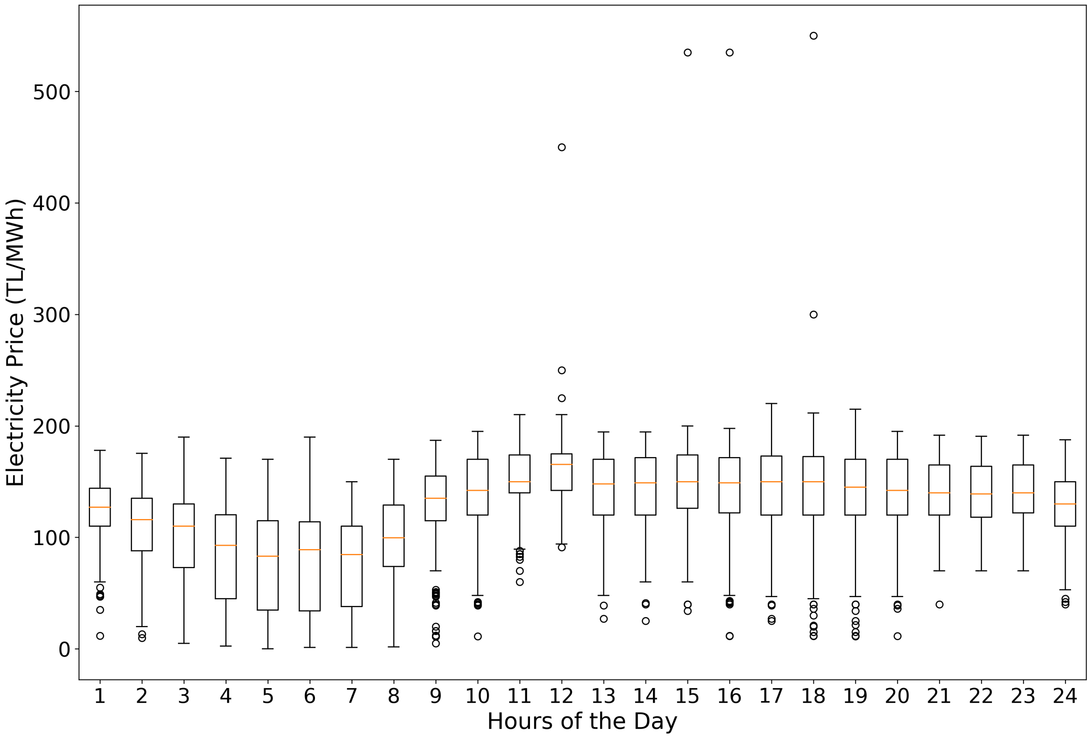

Figure 4.16. Variations in Electricity Prices in 2011

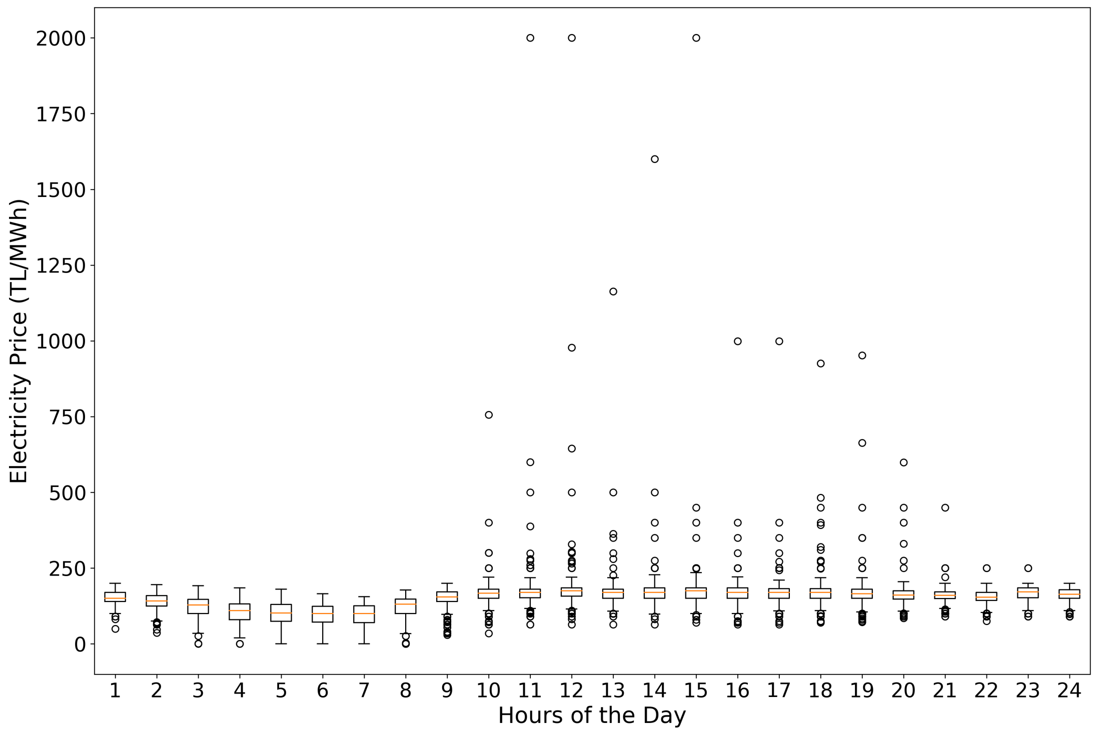

Figure 4.17. Variations in Electricity Prices in 2012

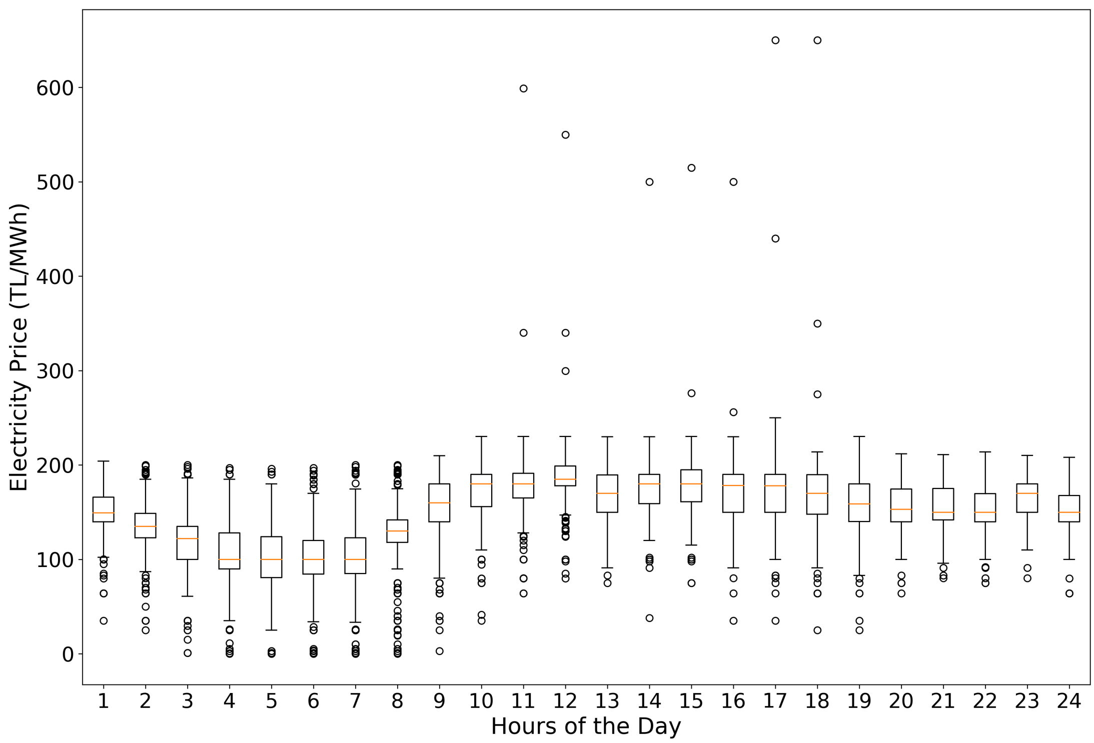

Figure 4.18. Variations in Electricity Prices in 2013

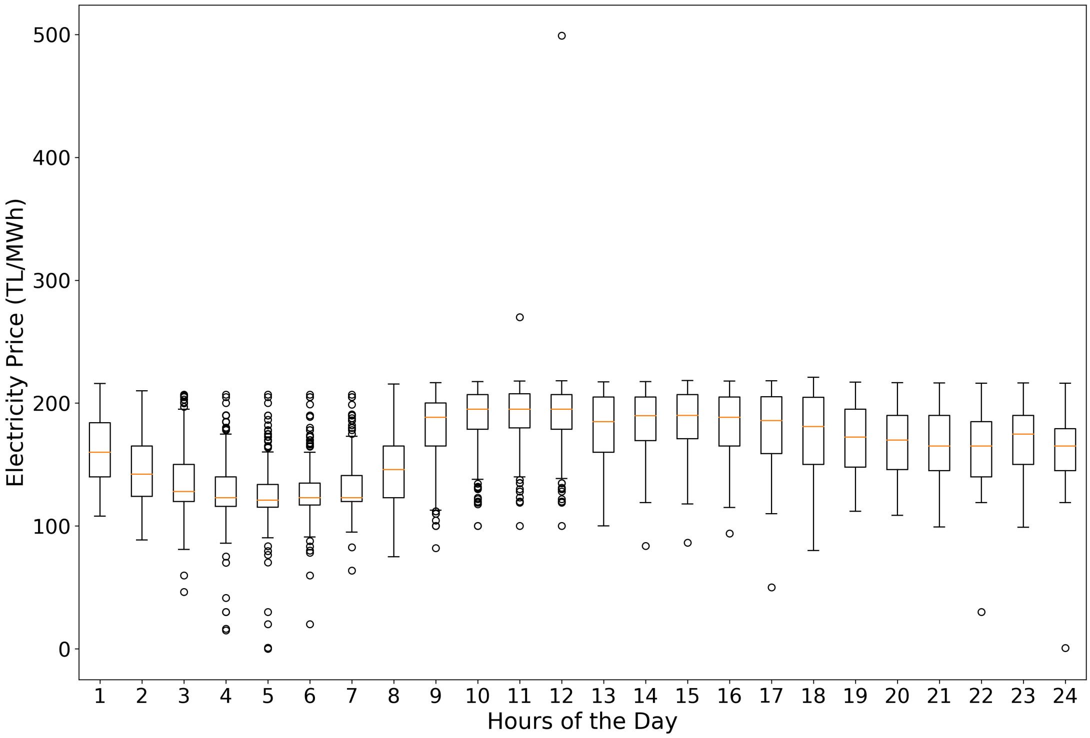

Figure 4.19. Variations in Electricity Prices in 2014

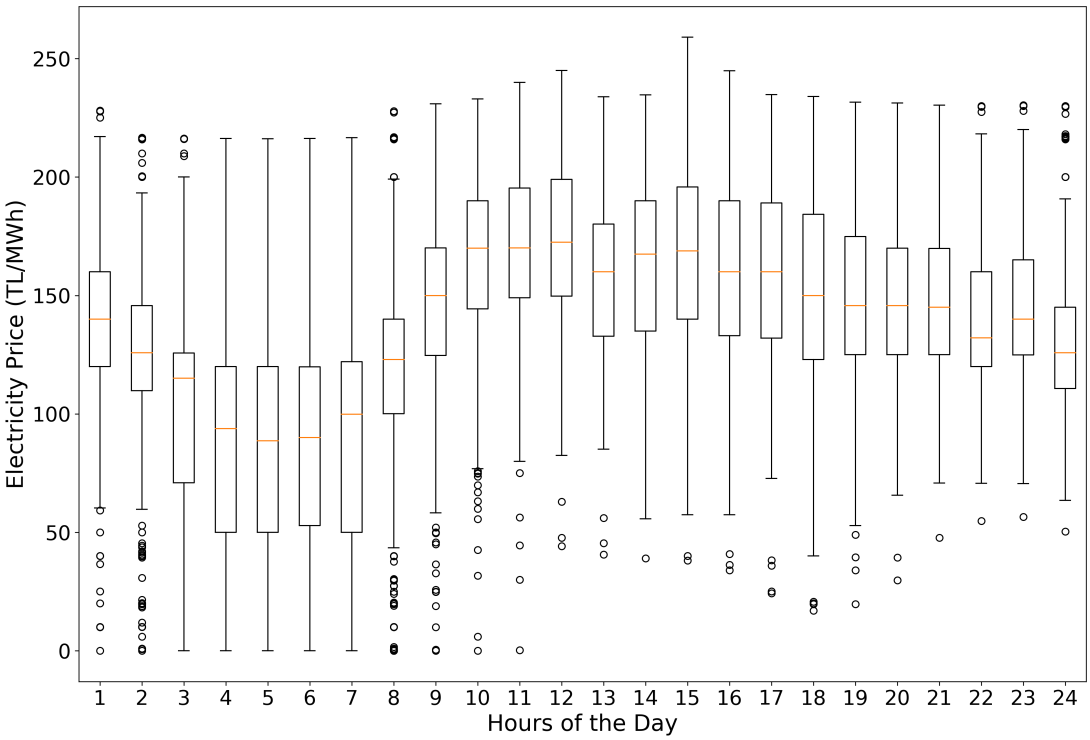

Figure 4.20. Variations in Electricity Prices in 2015

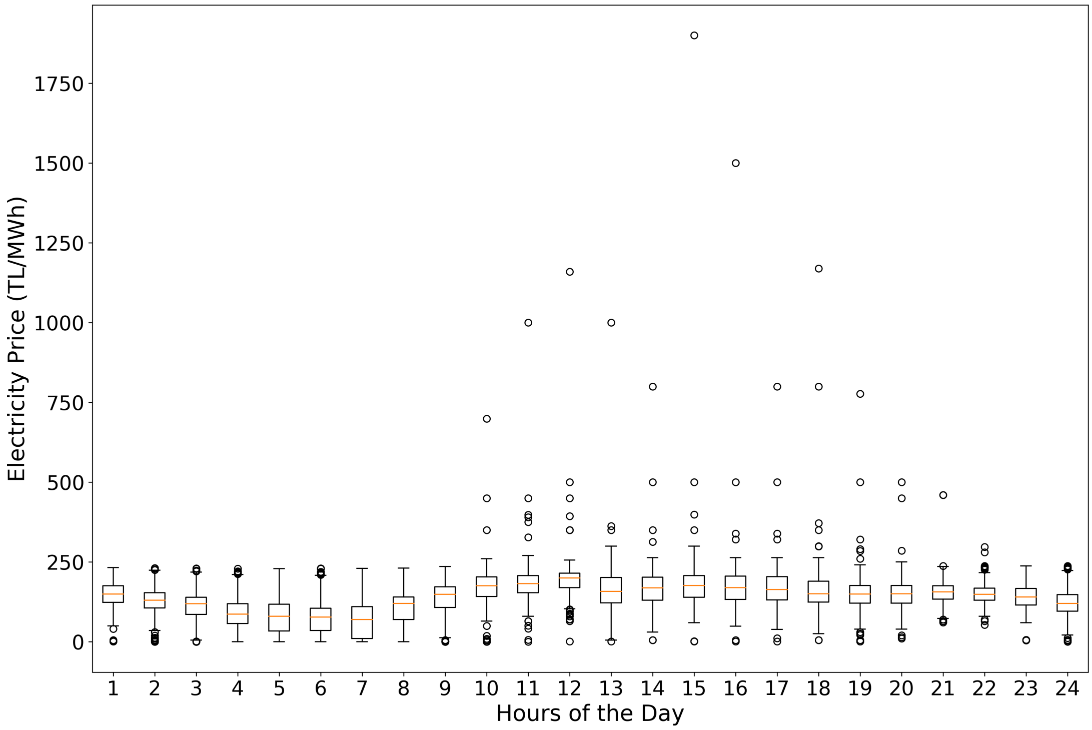

Figure 4.21. Variations in Electricity Prices in 2016

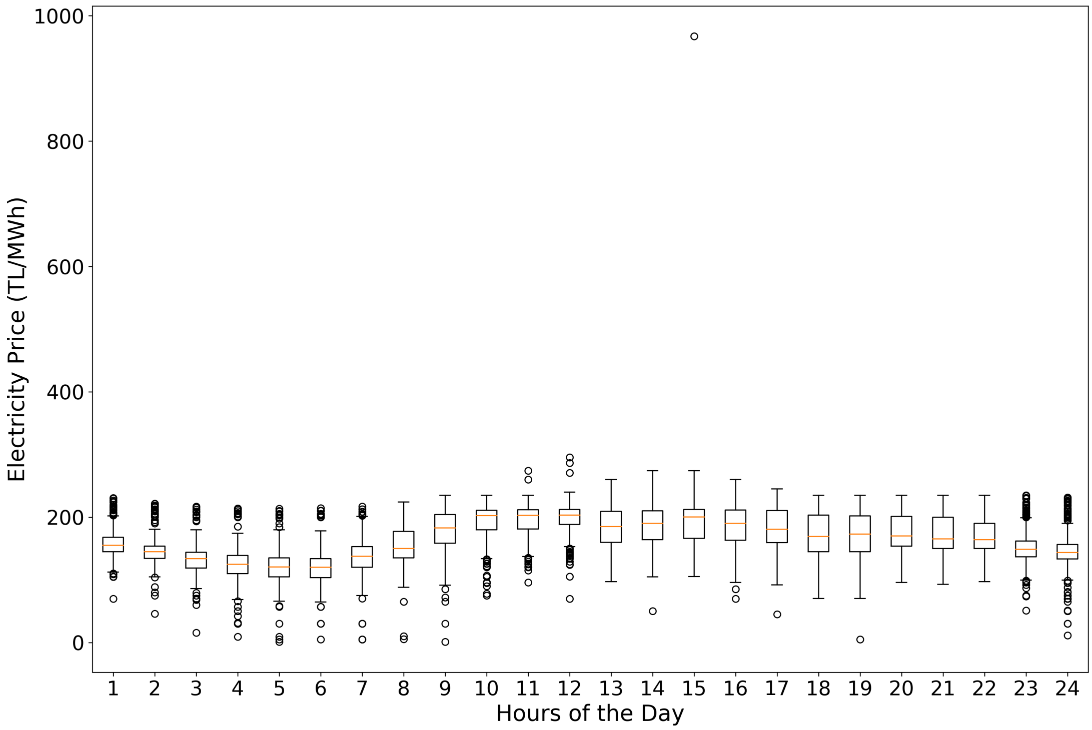

Figure 4.22. Variations in Electricity Prices in 2017

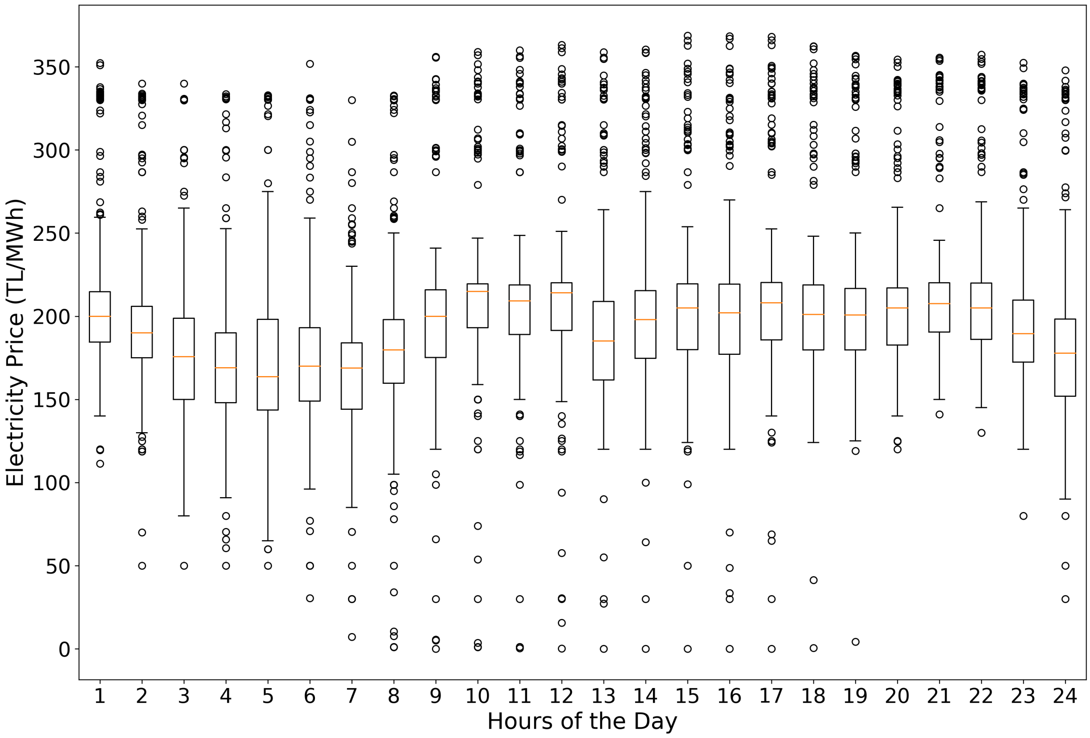

Figure 4.23. Variations in Electricity Prices in 2018

To better understand the change in electricity prices through time, monthly average values are calculated and presented in Figure 4.24. As shown in Figure 4.24, there are many abrupt variations in electricity prices. Especially, the last slope of the curve in 2018 is considerably sharp. These abrupt changes in the electricity prices may be due to different factors such as fuel prices, availability in generating units, hydro or wind generation of the country and network congestions (Dong, Li, Wallin, Avelin, Zhang and Yu, 2019).

Mean electricity prices, for each month, are shown in Figure 4.25 and used to investigate the seasonal effect. It is clear that electricity prices in the winter and the summer seasons are higher than those in the spring and the autumn seasons.

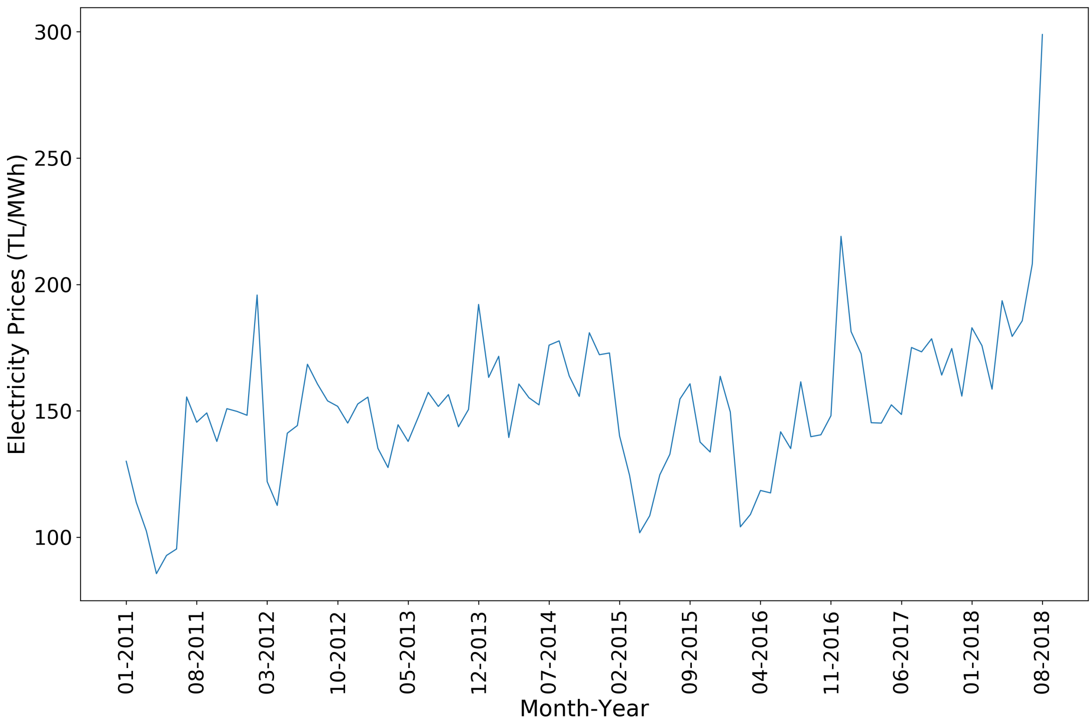

Figure 4.24. Monthly Averaged Electricity Prices

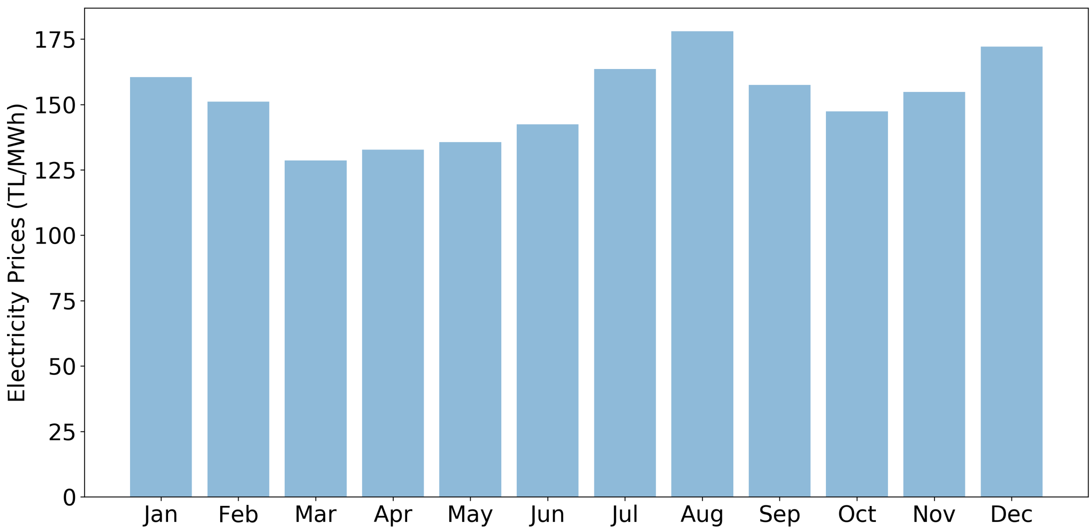

Figure 4.25. Monthly Mean Electricity Prices

Mean electricity prices for each day of the week are presented in Figure 4.26. Except Sunday, other days have similar mean electricity prices. Due to low demand in Sunday, it has the lowest mean electricity price.

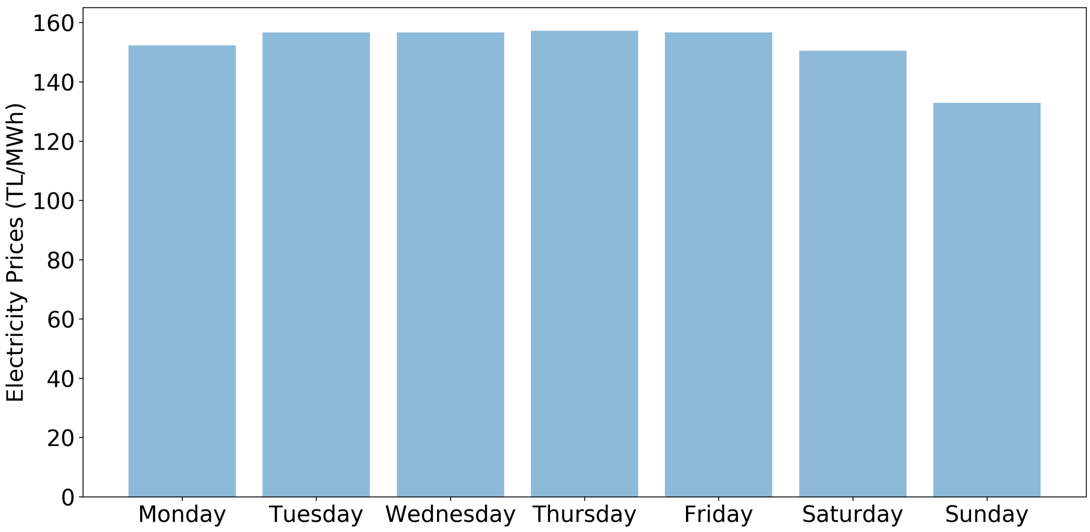

Figure 4.26. Daily Mean Electricity Prices

To see the relation between hourly electricity prices, the variation of the correlations between prices of the previous hours is plotted in Figure 4.27. As can be seen from Figure 4.27, the curve follows a cyclic pattern, and electricity prices have high correlations around multiplication of 24 hours (i.e., same hours of the previous days). This correlation graph is used in selecting the inputs of variables of the LSTM network that is explained in Section 4.4.

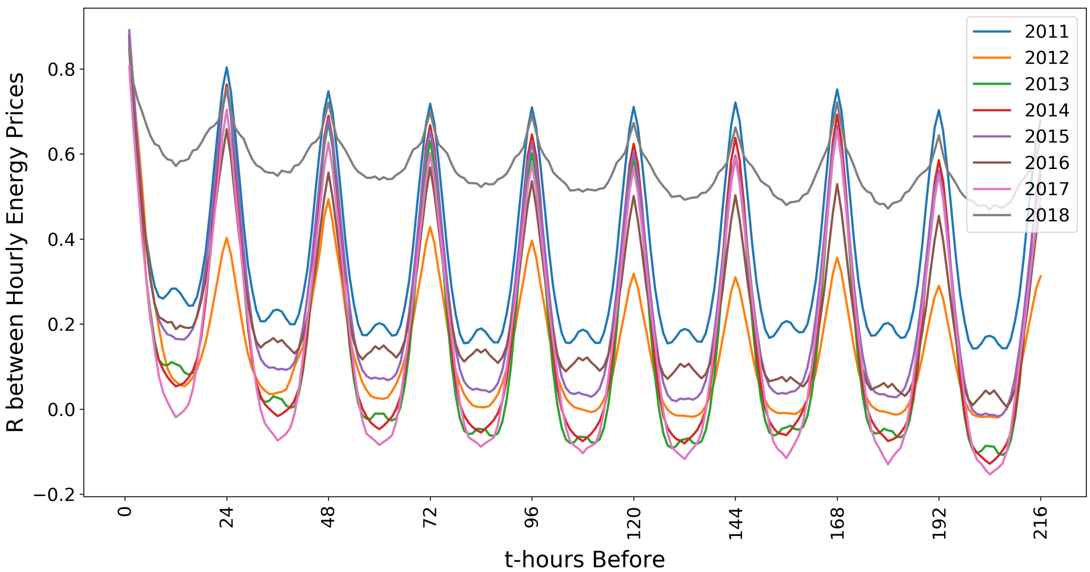

Figure 4.27. Variation of Electricity Price Correlation Coefficient with respect to Previous Hours

4.3 Hourly Wind Energy Estimations

The wind energy is the second input of the optimization model. In the scope of the case study, the 2.5 MW wind turbine, which is manufactured by General Electric (GE), is used. To obtain the available hourly wind energy, the power curve of the wind turbine is acquired from General Electric (n.d.), and presented in Figure 4.28. The wind turbine has 103 meters rotor diameter, 85 meters hub height, 3 m/s cut-in speed and 25 m/s cut-out speeds (General Electric, n.d.).

To calculate available hourly wind energy, a curve is fitted to the power curve, as shown in Figure 4.29. This curve is composed of five parts as given in Equation (4.2). The first part is constrained by the cut-in speed, 3.0 m/s. The middle segment of the curve includes two polynomial functions to express the power curve in a more accurate way. The polynomial functions are given in Equation (4.2) where x is the wind speed and $f(x)$ is the hourly wind energy. The last part of the curve is constrained by the cut-out speed, 25 m/s as given in Equation (4.2). Wind speed data, between September 2017 and August 2018, which is first extrapolated to a height of 85 meters, is converted to the available hourly wind power by using the power equation given in Equation (4.2). Lastly, the available hourly wind energy is obtained by multiplying the available hourly wind power by one hour.

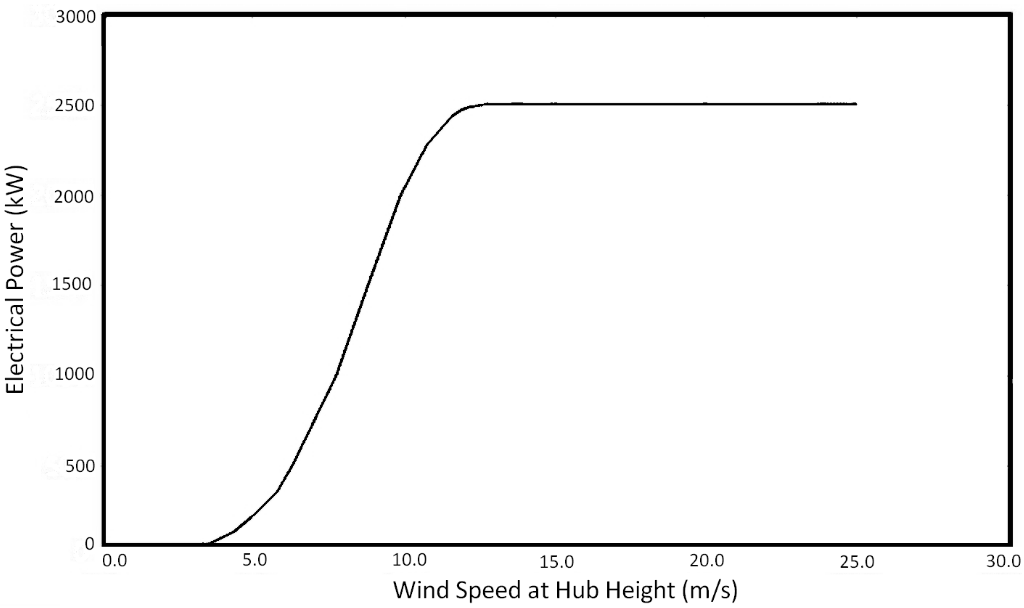

Figure 4.28. GE 2.5 MW Wind Turbine Power Curve (General Electric, n.d.)

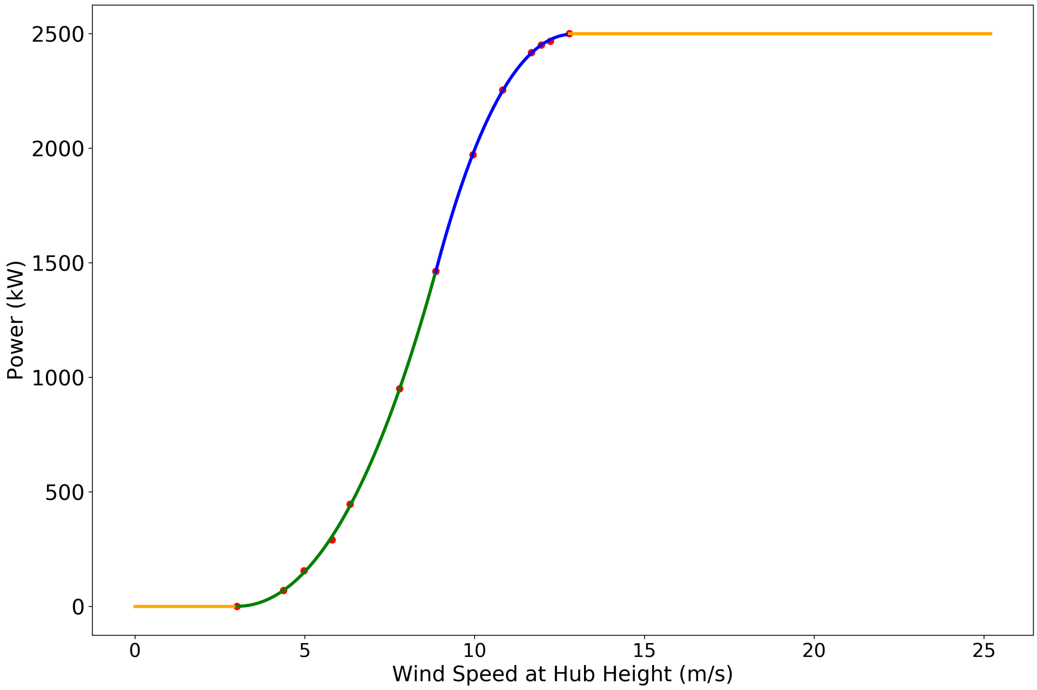

Figure 4.29. Power Curve of the Wind Turbine

$$f(x) = \begin{cases} 0 & x \leq 3 \\ 0.001x^3 + 0.025x^2 - 0.182x + 0.291 & 3 < x \leq 8.859 \\ 0.003x^3 - 0.168x^2 + 2.83x - 12.511 & 8.859 < x \leq 12.791 \\ 2.5 & x > 12.791 \\ 0 & x > 25 \end{cases} \tag{4.2}$$

4.4 The LSTM Network

The LSTM network that is developed in this study is used to forecast electricity prices in the Turkish day-ahead spot electricity market. The obtained electricity price data is split into three parts, such as training, validation and test data. The intervals of the training, validation, and test data are from 01.01.2011 to 31.08.2016, from 01.09.2016 to 31.08.2017 and from 01.09.2017 to 31.08.2018, respectively. After the validation process (i.e., determination of the hyperparameters) is completed, the validation data is added to the training data. In this way, the LSTM network can perform better since it can learn from the most recent observations.

In the day-ahead market, the electricity providers must submit their bids until 12:30 of the bidding day for all the hourly prices of the next day (i.e., from 00:00 to 24:00). So, we should forecast the electricity price of each hour in the next day by using the hourly electricity price data before 12:30 of the bidding day. Thus, 24 different LSTM models are developed with the same architecture, to forecast electricity price for each hour in the next day.

During the validation process of the LSTM network, different number of epochs, time series size, batch sizes, number of LSTM units, and number of features are evaluated. After many simulations, the number of epochs is fixed to 5000 with an early stopping value of 25, the time series size is set to 48, and the number of LSTM units is set to three by considering the performance of the LSTM network and the simulation time. Once the number of epochs and the number of LSTM units are fixed, 24 different models are generated using different batch sizes, number of features and seed values to determine the hyperparameters of the final LSTM network. Batch size values of 16, 32, 64 and 128; the number of features 4 and 16; the seed value of 20, 350 and 2019 are simulated. Indeed, the seed is not a hyperparameter of the LSTM network. It is a random value to initialize the initial weights of the LSTM network. However, to see the effects of the initial weight assignment, three different seeds are tried. Last 24 simulations are evaluated based on the errors.

4.4.1 The Architecture of the LSTM Network

The time series size of the LSTM network is selected as 48 hours. It means that each of the 24 LSTM networks takes as the unlagged time series, the electricity prices of the previous 48 hours in the day-ahead market as inputs, and forecasts the electricity price of the 24 each hours in the next day. For example, to forecast the electricity prices of each hour for February 15, the bid should be submitted on February 14 at 12:00. Since 48 hours prior electricity prices are going to be used for the LSTM network, the first input of the unlagged series for the LSTM network is the electricity price at 12:00 of February 12. Following 47 hours are used as the remaining inputs of the LSTM network. To summarize, the LSTM networks use the electricity prices on February 12 at 12:00 and February 14 at 12:00 to forecast each hourly electricity price on February 15 from 00:00 to 24:00.

The number of features of the LSTM network equals to four. These features are composed of one unlagged and three lagged (i.e., 23-hours lagged, 24-hours lagged, and 168-hours lagged) hourly electricity price time series. These lagged prices are selected based on the correlation coefficients between the hourly electricity price and their values in previous hours in 2011 data. As shown in Figure 4.27, the variation of electricity price correlation coefficient plots show similar trends for all the years. To identify the inputs of the LSTM network, the variation of the electricity price correlation coefficient in 2011 is investigated in detail. The value of 0.75 is used as the threshold. According to Figure 4.27, the correlation coefficients between the electricity price at time t and $t - 23$, $t - 24$ and $t - 168$ are equal or greater than 0.75, so they are selected as input features of the LSTM network. For the example given in the previous paragraph, to forecast the electricity prices of February 15, following time intervals of the electricity price input time series are used as inputs for the LSTM network: from 12:00 of February 12th to 12:00 of February 14th; from 13:00 of February 11th to 13.00 of February 13th; from 12:00 of February 11th to 12.00 of February 13; from 12:00 of February 4th to 12:00 of February 6th.

The LSTM network architecture is shown in Figure 4.30. The first subscript of the h is the LSTM unit number, the second subscript of h, and x is the time step in the time series, and the first subscript of the x is the feature number.

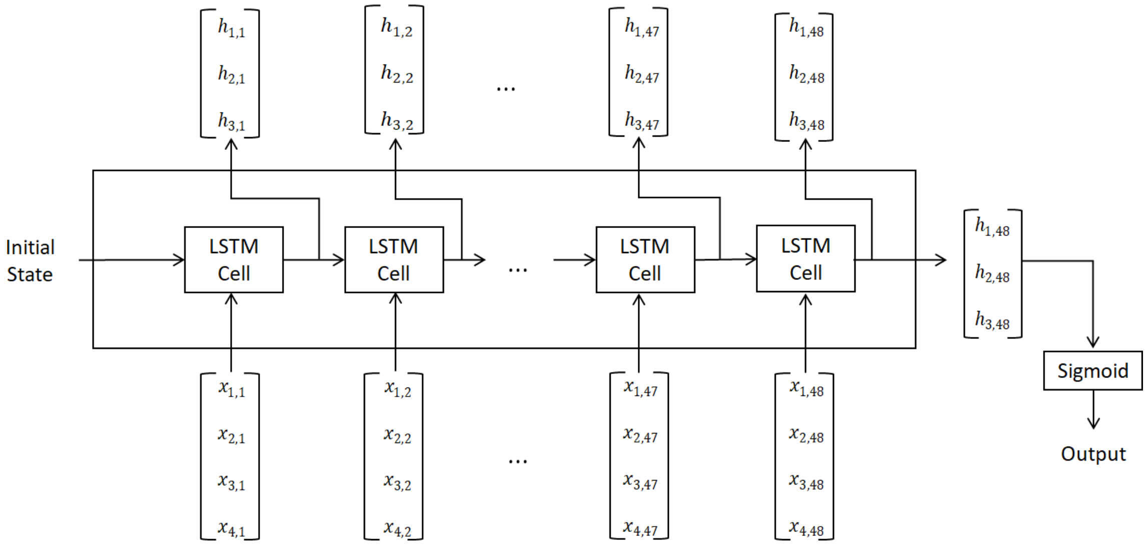

Figure 4.30. The LSTM Network Flow Diagram

4.5 The Optimization Model

The developed optimization model that is introduced in Chapter 3 is used to determine optimum operation strategies for the WHHS. The optimization model aims to maximize the daily revenue of the WHHS. The optimum operating schedules of wind turbines, the hydro turbine, the pump, and the energy trade with the grid that maximize the daily revenue are found. The optimization model uses available hourly wind energies and hourly electricity prices in the day-ahead market as inputs. Hourly electiricity prices are estimated by 24 LSTM networks. The optimization model is run from September 2017 to August 2018. To evaluate the performance of the LSTM network and the optimization model, different scenarios (see Section 5.2.1) are tested.

4.5.1 Parameters of the Optimization Model

The optimization model has eight parameters, which are the maximum energy that can be generated by wind turbines in an hour, the maximum energy that can be generated by the hydro turbine in an hour, the maximum energy that can be bought from the grid in an hour, the maximum energy that can be consumed by the pump in an hour, the minimum energy level in the upper reservoir, the maximum energy level that can be stored in the upper reservoir, the efficiency for the turbine mode and the efficiency for the pump mode. The maximum energy that can be generated by the wind turbines p^{w}_{max} in an hour equals to the available hourly wind energy. Its calculation is explained in Section 4.3.

Currently, the installed capacity of the hydro turbine in the Uluabat Hydropower Plant is 100 MW (Akenerji, 2005). We used the same installed capacity by changing the hydro turbine with a hydro pump-turbine. So, for this case study, the system can work either as a hydro turbine or a pump. Thus, the maximum energy that can be generated by the hydro turbine in an hour p^{hydro}_{max} and the maximum energy that can be consumed by pumping in an hour p^{pump}_{max} equal to 100 MWh.

The maximum energy that can be bought from the grid in an hour is not limited. Thus, this parameter equals positive infinity. The schematic view of Çınarcık Dam, Uluabat Hydropower Plant, and Lake Uluabat are shown in Figure 4.31. The minimum energy level in the upper reservoir and the maximum energy level that can be stored in the upper reservoir is computed based on the elevation-area curve of the dam by using the following expression:

$$E_p = 2.778 \times 10^{-10} \;\; pghV \tag{4.3}$$

where E_p is the potential energy of the fluid in MWh, V is the volume of the fluid in m^3, p is the density of the fluid in kg/m^3, g is the acceleration due to gravity in m/s^2, h is the height of the fluid in m. The minimum energy level in the upper reservoir E_{min}, and the maximum energy level that can be stored in the upper reservoir E_{max} are computed as 138233.8 MWh and 298624.1 MWh, respectively. The initial energy level $E^{initial}$ is fixed to E_{min}, 138233.8 MWh.

The efficiency of the turbine mode and the efficiency of the pump mode are assumed as 0.88 and 0.85, respectively, based on the study by Cruz et al. (2014).

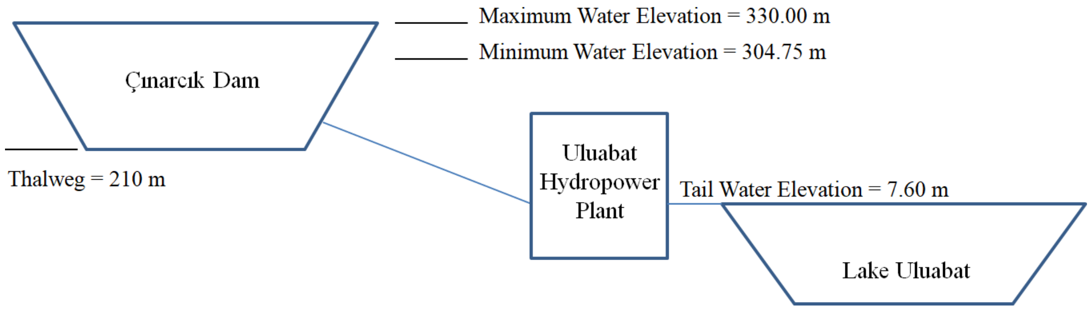

Figure 4.31. The Schematic View of Çınarcık Dam, Uluabat Hydropower Plant and Lake Uluabat

CHAPTER 5

RESULTS AND DISCUSSIONS

In this chapter, the results of the LSTM network and the optimization model are presented and discussed. In this study, the LSTM network is developed to forecast electricity prices as accurately as possible. After the most accurate electricity prices are obtained, they are used in the optimization model to identify the best operation schedule for WHHS that maximizes the daily revenue.

5.1 The LSTM Network Results

As discussed in Section 4.4, 24 simulations for each hour of the bidding day are executed to determine the hyperparameters of the final form of the LSTM network. Twenty-four simulations using various combinations of four batch size values (i.e., 16, 32, 64, and 128), two numbers of features (i.e., 4 and 16), and three seed values (i.e., 20, 350 and 2019) are carried out and the results are shown in Table 5.1. Thus, each row in Table 5.1 summarizes results of 24 simulations.

Table 5.1. The Summary Table of 24 LSTM Network Simulations

Run No	Batch Size	Seed	Number of Features	Min.[1] MSE [2] (Training)	Min. MSE (Validation)	Max.[3] MSE (Training)	Max. MSE (Validation)	Avg.[4] MSE (Training)	Avg. MSE (Validation)
1	16	2019	16	470.32	485.26	2124.14	14638.36	837.28	2874.21
2	32	2019	16	480.59	421.46	2141.85	15373.73	813.99	2418.33
3	64	2019	16	447.13	461.64	2062.25	9524.69	846.61	2122.03
4	128	2019	16	460.80	443.25	2120.31	9812.39	925.71	2261.13
5	16	2019	4	479.14	421.29	1975.88	9712.53	991.12	2255.25
6	32	2019	4	461.97	414.50	2427.10	14638.15	1037.76	2535.76
7	64	2019	4	495.02	421.34	2356.12	8891.80	1084.21	2144.29
8	128	2019	4	497.96	449.04	2186.21	9153.45	1105.26	2128.56
9	16	350	16	385.92	461.91	1018.99	24398.91	673.02	3063.89
10	32	350	16	424.59	455.49	1257.14	11789.21	707.61	2900.81
11	64	350	16	464.91	438.71	1241.98	8383.21	722.05	2096.21
12	128	350	16	457.58	492.67	1309.37	13413.79	781.42	2534.72
13	16	350	4	488.56	423.91	2536.85	12180.83	1039.91	2518.60
14	32	350	4	504.78	421.43	2631.57	11292.51	1032.36	2437.35
15	64	350	4	500.22	414.04	2376.22	12336.05	1038.39	2440.82
16	**128**	**350**	**4**	**507.61**	**453.20**	**2213.65**	**8270.37**	**1101.43**	**1986.28**
17	16	20	16	412.48	462.91	1036.81	19783.35	668.04	2912.49
18	32	20	16	460.70	474.46	1333.74	15510.65	721.43	3170.12
19	64	20	16	461.87	479.00	1556.57	11349.75	758.20	2663.02
20	128	20	16	464.78	443.31	1952.34	13582.81	893.14	2375.31
21	16	20	4	428.48	465.79	2182.64	13067.01	886.76	2767.95
22	32	20	4	464.41	432.19	2662.72	14872.81	969.29	3200.57
23	64	20	4	493.22	403.10	1860.99	13050.23	923.56	2495.37
24	128	20	4	509.18	395.12	1652.58	12105.63	952.39	2439.02

[1] Minimum, [2] Mean Square Error, [3] Maximum, [4] Average

In Table 5.1, Min. MSE (Training) column shows the minimum mean square error (MSE) for training data set among all 24 LSTM configurations. Other columns represent maximum and average MSE for training and validation data sets among all 24 configurations. The final LSTM network hyperparameters are selected based on the average MSE of the validation (i.e., last column of Table 5.1). Thus, hyperparameters of **Run No** = 16 are selected for the final LSTM hyperparameters. That is, the batch size equals 128, and the number of features equals four. Although the seed is not a hyperparameter, we select the seed value in **Run No** = 16, which is 350. To check if overfitting occurs, the number of epochs versus error for the training and validation periods are plotted for **Run No** =16 and t = 12 hr, as shown in Figure 5.1. As can be seen from Figure 5.1, there are not enough weights in the LSTM network to cause overfitting.

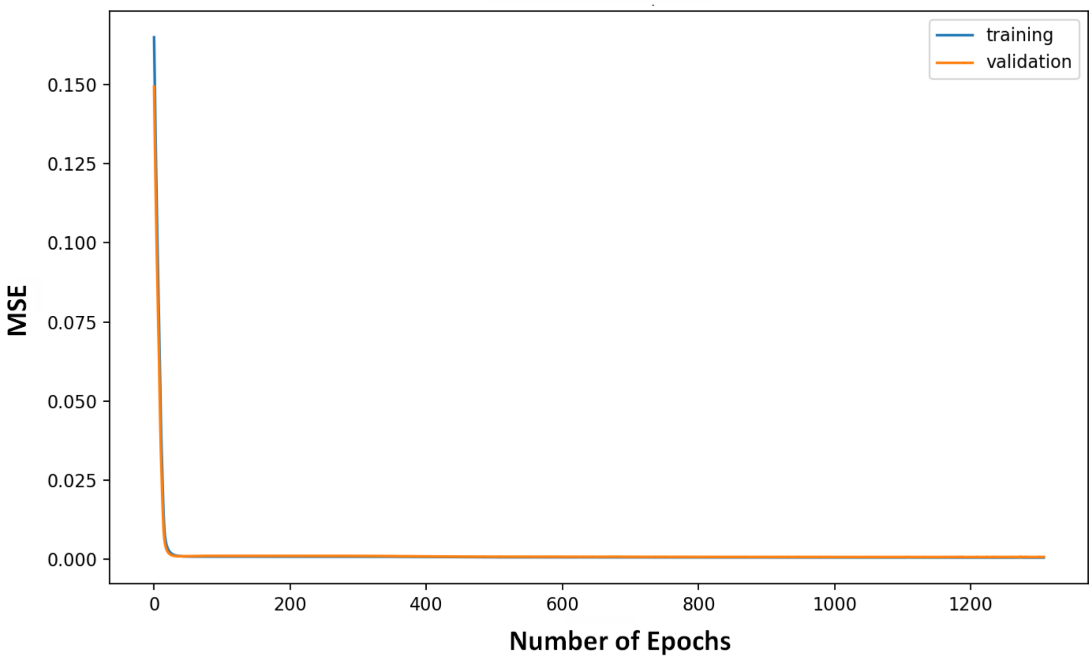

Figure 5.1. MSE vs. Number of Epochs Curve

The final form of the LSTM network is run 24 times for the bidding day (i.e., run once for each hour of the bidding day) to forecast the test data, and results are presented in Table 5.2. It can be noticed that each hour has a different number of epochs due to the early stopping property. For example, the LSTM network at t = 20 hr reaches the tolerance in 733 epochs, whereas the LSTM network at t = 7 hr reaches the tolerance in 1802 epochs. The summary statistics of these 24 runs is given in Table 5.3. It can be noticed that training errors are different when compared to the training errors in **Run No** = 16 in Table 5.1. The reason for this discrepancy is that different training data is used in these runs. The training data in the final LSTM network includes the initial training data set plus the validation data set. The validation data is added to the training data to introduce the behaviour of the most recent data in the calibration process.

Table 5.2. The Summary Table of the Final LSTM Network Hourly Simulations

t (hr)	Batch Size	Seed	Number of Features	Number of Epochs	MSE (Training)	MSE (Test)
01	128	350	4	1122	525.29	1717.73
02	128	350	4	1173	640.02	1482.01

Table 5.2 continued from previous page

t (hr)	Batch Size	Seed	Number of Features	Number of Epochs	MSE (Training)	MSE (Test)
03	128	350	4	998	873.26	1086.9
04	128	350	4	1282	952.27	848.18
05	128	350	4	1411	902.65	1371.27
06	128	350	4	1370	831.15	1061.03
07	128	350	4	1802	1017.17	1543.33
08	128	350	4	1139	1364.29	1910.7
09	128	350	4	1001	1299.68	2136.89
10	128	350	4	912	1179.12	1578.4
11	128	350	4	1173	2087.84	5267.77
12	128	350	4	1308	2251.82	8403.58
13	128	350	4	1062	1249.4	1368.17
14	128	350	4	1436	1374.37	3948.69
15	128	350	4	1098	2727.56	9495.05
16	128	350	4	818	1738.99	1176.83
17	128	350	4	818	1320.92	1262.46
18	128	350	4	829	1858.65	1038.31
19	128	350	4	792	1330.89	855.58
20	128	350	4	733	763.37	1301.49
21	128	350	4	842	555.3	1258.04
22	128	350	4	1198	491.69	1815.07
23	128	350	4	881	582.97	1317.89
24	128	350	4	1003	718.9	1592.61

Table 5.3. The Summary Table of the Final LSTM Network Simulation

Batch Size	Seed	Number of Features	Min. MSE (Training)	Min. MSE (Test)	Max. MSE (Training)	Max. MSE (Test)	Avg. MSE (Training)	Avg. MSE (Test)
128	350	4	491.69	848.18	2727.56	9495.05	1193.23	2284.92

MSE (Training) and **MSE (Test)** columns of Table 5.2 are plotted in Figure 5.2. As can be seen from this plot, the LSTM network has the largest MSE at t = 15 hr in both training and test processes. The minimum MSE is at t = 4 hr for the test process, and at t = 22 hr for the training process. As expected the performance of training is better than that of test. Actually, for t = 11, 12, 14 and 15 hours trained LSTM perform very poorly (i.e., errors are at least doubled from training to test for these hours).

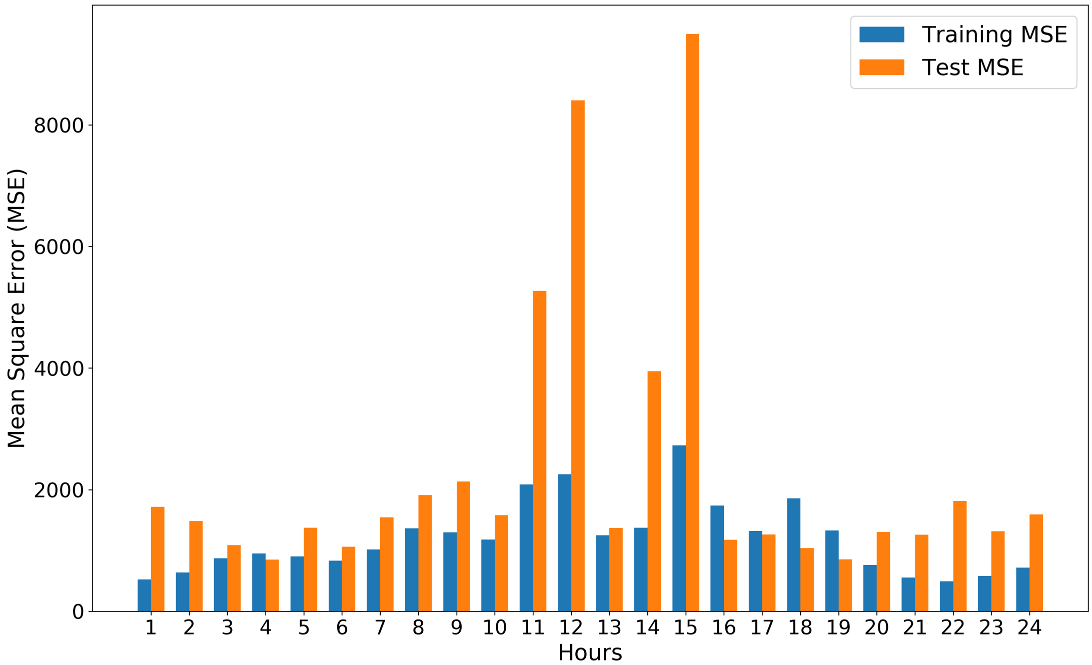

Figure 5.2. The Final LSTM Network Hourly MSE Plot

Figure 5.3 shows the forecasted and real electricity prices in the training process for t = 22 hr. Although t = 22 hr is the best LSTM network based on the training results, it does not perform with the same efficiency for the test data. In terms of the test data, t = 4 hr has the best results, and they are presented in Figure 5.4. Especially before day 250, the forecasted values follows the trend of real values, and it estimates many peak values successfully. However, after day 250, the real values change abruptly, and the LSTM network does not perform well in forecasting these peaks. The real electricity prices are affected by many factors, such as fluctuations in the price of the dollar, change in the contribution of various types of power plants to the energy budget of the country, other economic and political issues. These unexpected issues result in abrupt changes in the price of electricity which makes it very hard to predict.

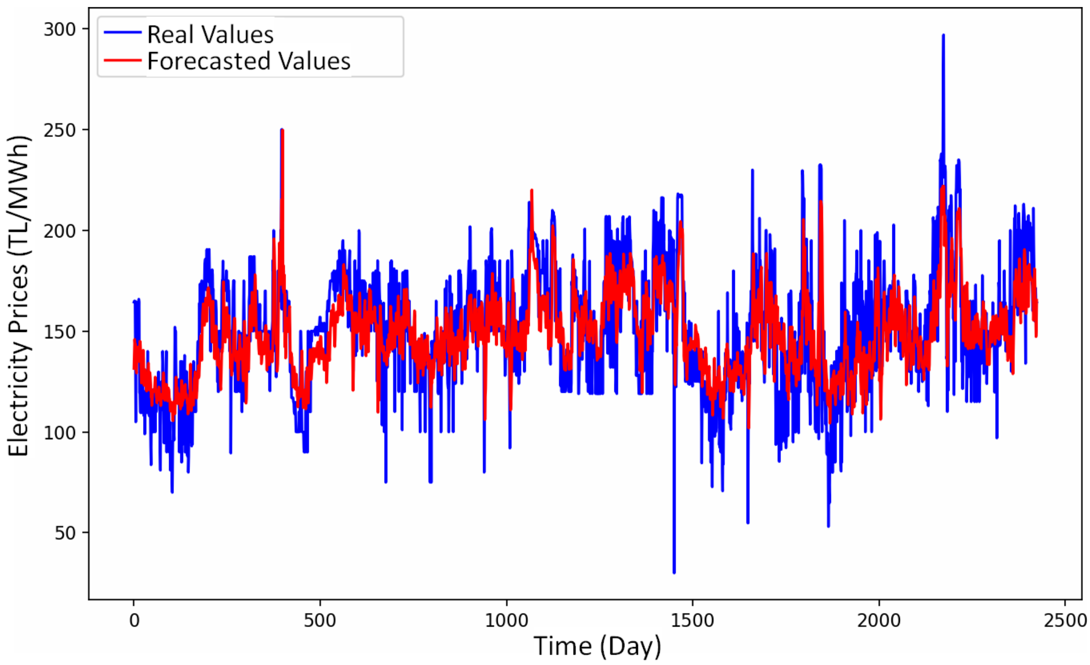

Figure 5.3. Training Process Results of the LSTM Network for t = 22 hr

In Figure 5.5, the results of the LSTM network for the worst performing hour of the training process is shown, which is t = 15 hr. At this hour of the training days, there are many extreme values that lead to low training performance. Nevertheless, forecasts follow the general trend, and some of the extreme values are simulated correctly. Also, the test process has the worst performance at t = 15 hr, and the results are presented in Figure 5.6. As can be seen from Figure 5.6, it underestimates real prices almost every day at t = 15 hr.

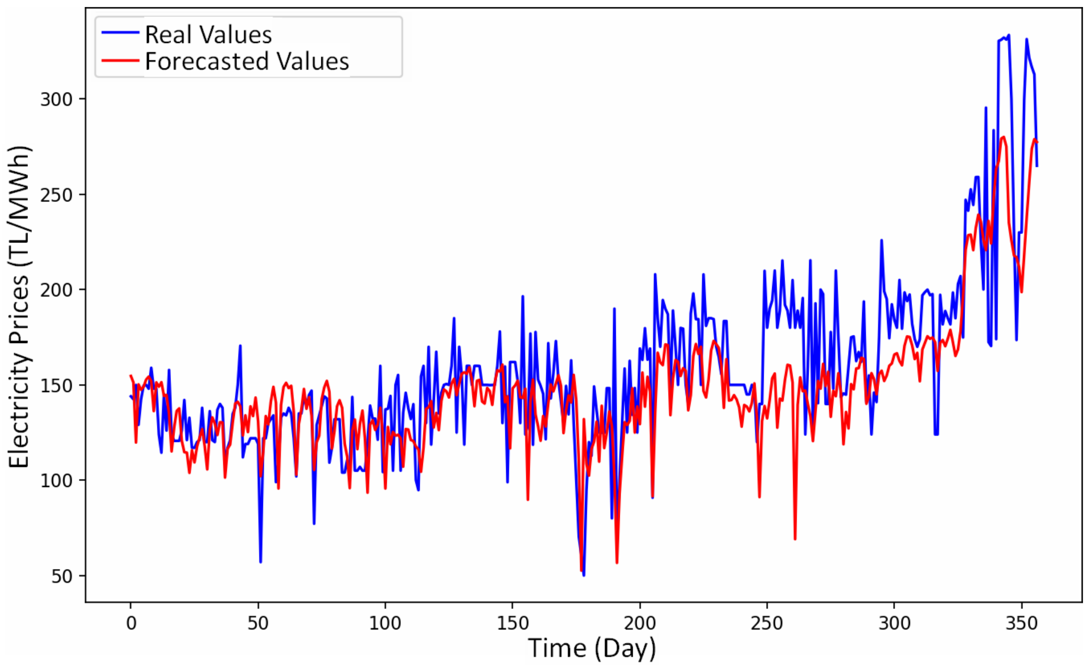

Figure 5.4. Test Process Results of the LSTM Network for t = 4 hr

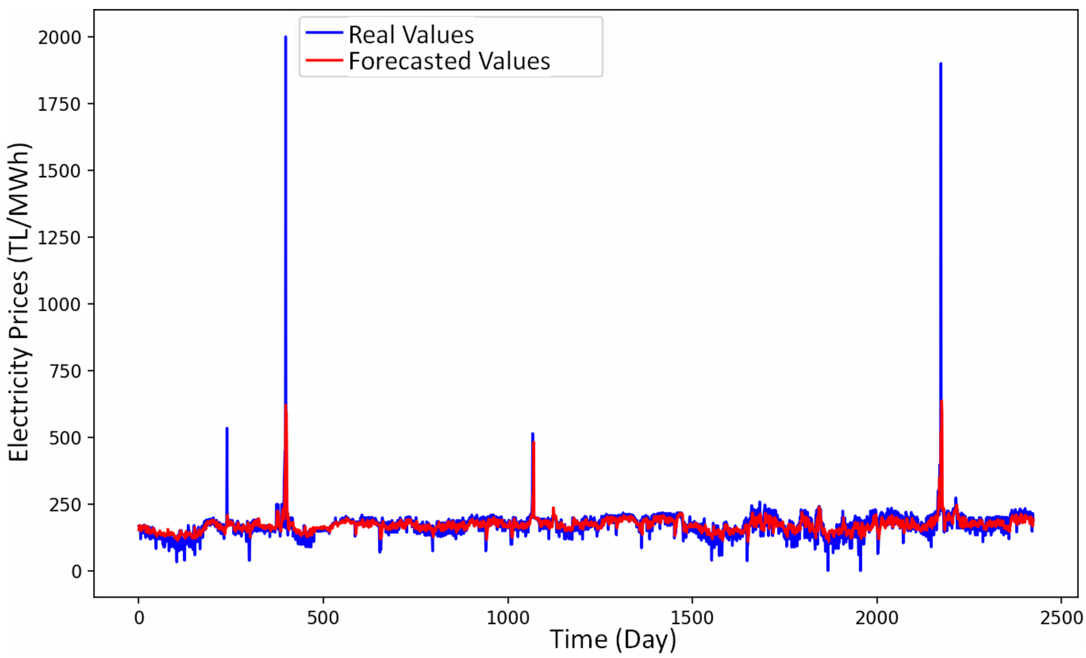

Figure 5.5. Training Process Results of the LSTM Network for t = 15 hr

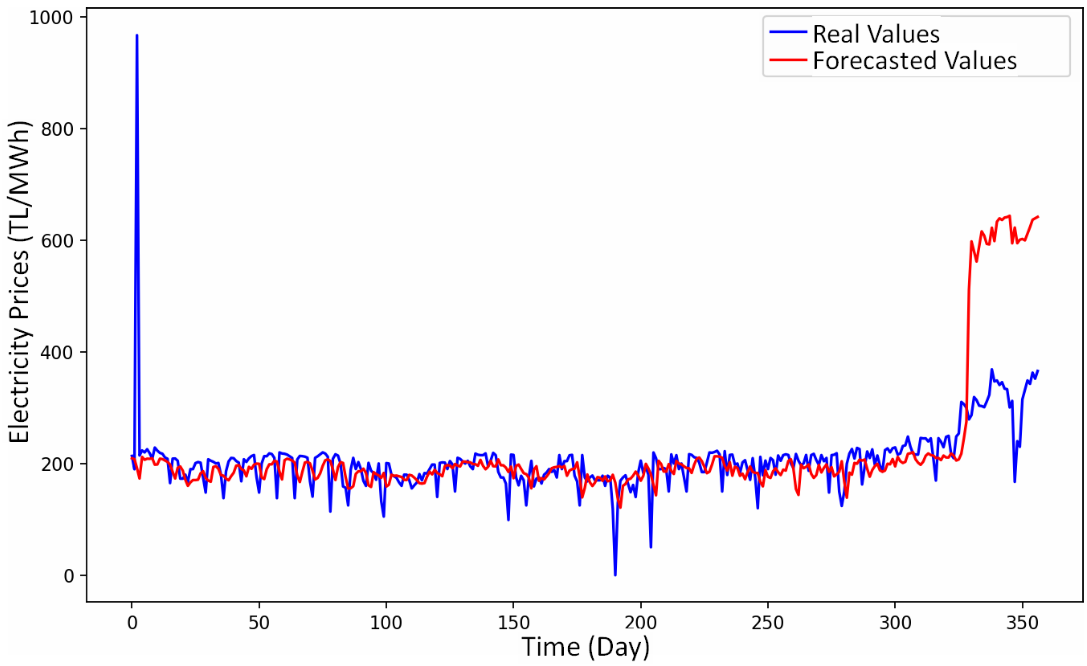

Figure 5.6. Test Process Results of the LSTM Network for t = 15 hr

In Figure 5.7, the forecasted electricity prices versus the corresponding real prices are presented for the test process of the LSTM network. Especially, the prices at the noon hours could not be forecasted well. As can be seen from Figure 4.23, there are many outliers in these hours. However, most of the hours, the forecasted prices are close to real prices.

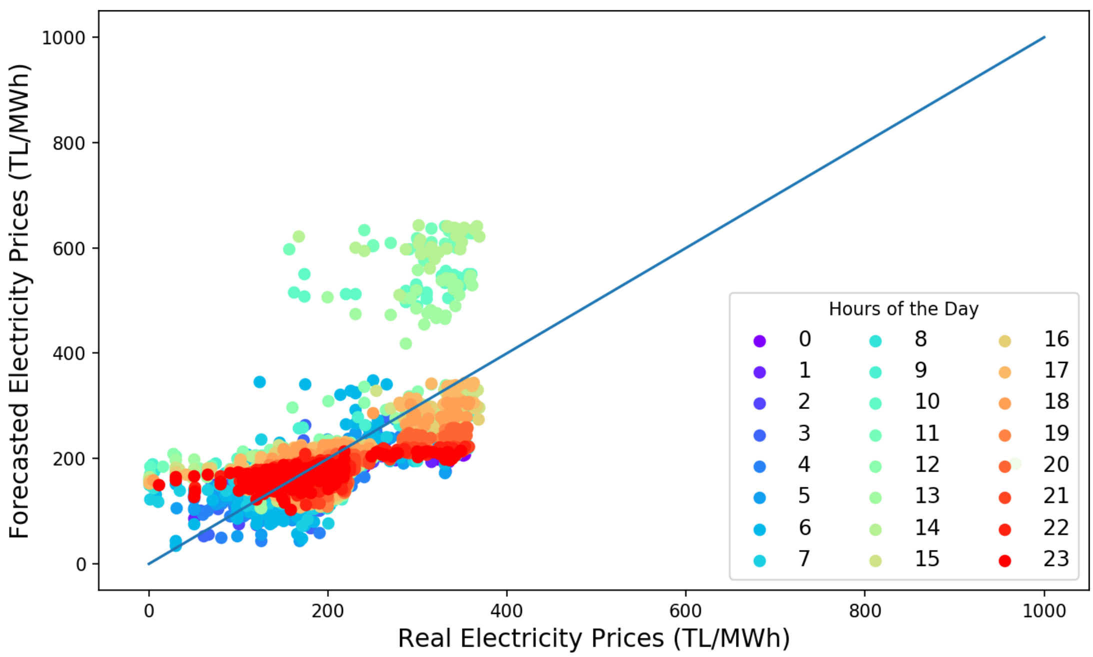

Figure 5.7. Scatter Plot of Forecasted and Real Prices

5.2 The Optimization Model Results

In this section, the scenarios of the optimization models are introduced, and the results for these scenarios are represented for the pumped storage hydropower plant and the WHHS. After the results are represented for each scenario, they are discussed.

5.2.1 The Scenarios

In order to explain the scenarios some definitions are provided first:

The bidding day: As explained in Section 2.2, the power plant owner submits bids for each hour of the next day. Thus, the day in which the bids are submitted is referred to as the bidding day.

The operation day: This is the day on which the bids are submitted, and it follows the bidding day.

The previous day: In the bidding day, the most recent realized electricity prices belongs to this day. In other words, if an LSTM network is not available to estimate the bidding day's electricity prices, the electricity prices of this day (i.e., the previous day) would be available to the operator of the power plant to decide on the bids for the bidding day (i.e., the next day).

For example, if today is 5th of May 2020 and this is the bidding day, then the operation day will be the 6th of May 2020 (i.e., tomorrow). The electricity prices of 4th of May 2020 are the most recent realized electricity prices, and these prices can be used by the operator of the power plant to decide on the bids (i.e., the operation schedule of the power plant) of the bidding day (i.e., 6th of May 2020) if the LSTM network is not available to predict the prices.

The optimization model is run to determine the optimum operation schedule for the system. In order to evaluate the performance of the LSTM network's electricity price estimations, three different scenarios are considered:

1. Scenario 1: Ideal_Opt

This scenario corresponds to an ideal case, where the realized prices of the operation day are assumed to be known in the bidding day. The revenue obtained for this case presents the upper bound of the revenue. Of course, it is not possible to make this revenue in real life since the operation day's prices are not known in the bidding day. This ideal revenue will be referred to as the Ideal-Revenue from here after.

2. Scenario 2: PrevDay_Opt

   This scenario considers the following situation: An LSTM network is not available to the operator of the power plant. So the most recent realized electricity prices (i.e., electricity prices of the previous day) are used in the optimization model to generate the optimum operation schedule for the power plant. The revenue of the power plant based on the previous day's electricity prices will be referred to as PrevDay-Revenue from here after. PrevDay-Revenue is a hypothetical revenue as well since the realized prices will be different than previous day's prices. The real revenue of the power plant that will occur in the operation day (i.e., the revenue that will occur due to the execution of the optimized operation schedule of PrevDay_Opt with realized electricity prices of the operation day) will be referred to as the PrevDay-RealRevenue.

3. Scenario 3: LSTM_Opt

   This scenario considers the following situation: In the bidding day, the LSTM network is run and electricity prices of the operation day are estimated. Then the optimization model is run, and the optimum operation schedule for the power plant is obtained. The revenue of the power plant based on LSTM price estimations and the optimization model is only a hypothetical revenue, and it will be referred to as LSTM-Revenue from here after. In real life, the realized electricity prices will be different than those estimated by the LSTM network; thus the real revenue of the power plant will be different than LSTM-Revenue. The real revenue of the power plant that will occur in the operation day (i.e., the revenue that will occur due to the execution of the optimized operation schedule of LSTM_Opt with realized electricity prices of the operation day) will be referred to as the LSTM-RealRevenue from here after.

All three scenarios and the revenues corresponding to different sets of prices are depicted in Figure 5.8. In addition to these, all scenarios are run with different number of wind turbines. First, the revenue of the system without a wind turbine (i.e., pumped storage hydropower plant) is evaluated. Then different number of wind turbines (i.e., 10, 50, and 200 each 2.5 MW) are used to see the effect of the installed capacity of wind turbines on the revenue.

Developed optimization models generate the daily schedule of the WHHS to maximize the daily revenue of the system. For each scenario, eight plots are prepared using the results of the optimization models. These eight plots are hourly electricity price (i.e., price used in the optimization model), the pumping energy input (i.e., the energy consumed for pumping the water from the lower reservoir to the upper reservoir), the wind turbines output (i.e., the energy generated by the wind turbines), the hydro turbine output (i.e., the energy generated by the hydro turbine), the energy bought from the grid, the net energy output injected to the grid (i.e., the net energy sold to the grid), the energy stored in the upper reservoir and the daily revenue. The test period is selected as one year (from 9th of Sep 2017 to 31st of Aug 2018). Thus, these eight plots represent the change of these variables with respect to time (i.e., for each hour of the test period).

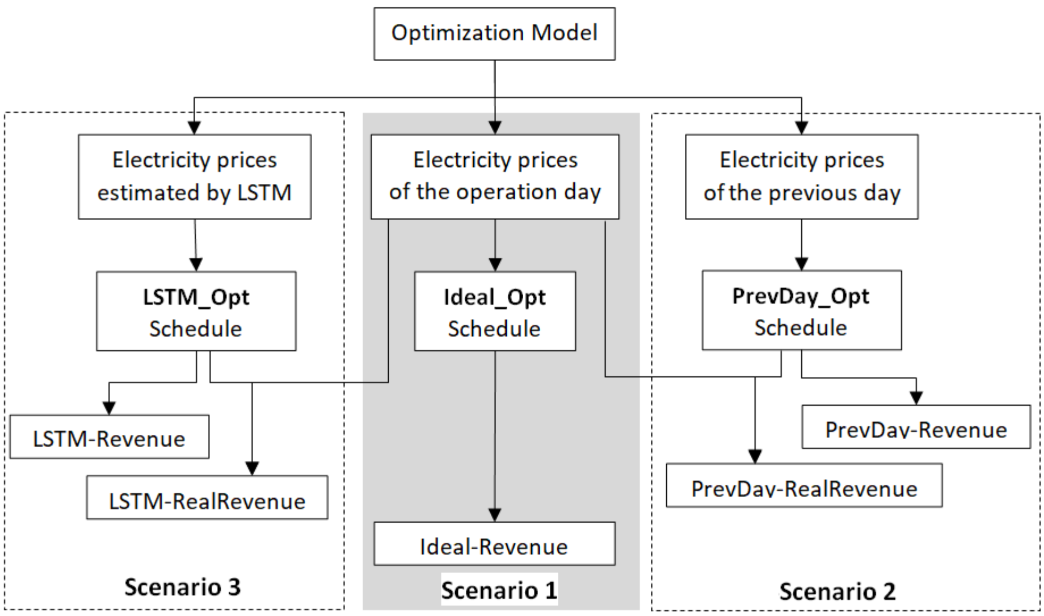

Figure 5.8. Optimization Model Scenarios

5.2.2 Pumped Storage Hydropower Plant Results

Here, the results of the optimization model for the pumped storage hydropower plant (i.e., no wind turbine case) are presented for all three scenarios.

5.2.2.1 Results of Ideal_Opt

The results of the ideal case (i.e., the case where the real prices of the operation day are assumed to be known in the bidding day) are presented in Figure 5.9. As can be seen in Figure 5.9(c), since there are no wind turbines for this case, the wind turbine output is zero all the time, and hydro turbine output given in Figure 5.9(d) represents the positive output in the net energy output injected to the grid in Figure5.9(f). As can be seen from Figure 5.9(b), the pump operates at its maximum capacity in most of the hours during pump mode, while turbine works at varying capacities during turbine mode as shown in Figure 5.9(d). Also, there are many hours when the plant is idle. The net energy output injected to the grid is negative at some hours (i.e., pumped storage hydropower plant buys electricity from the grid in these hours) and positive in others (i.e., pumped storage hydropower plant sells electricity to the grid in these hours) as can be seen in Figure 5.9(f). According to the schedule given in Figure 5.9(h), the total revenue of the pumped storage hydropower plant in the test period of one year is 3,975,820 TL. This revenue is the upper bound of the revenue since real prices are assumed to be known in the bidding day. In practice, the real electricity prices of the operation day would be unknown to the operator of the system, and the optimization model cannot be run using the real values. If an LSTM network to predict the operation day's electricity prices does not exist, the second-best set of prices that can be used in the optimization model are the electricity prices of the previous day. The results for this case are given in the following sub-section.

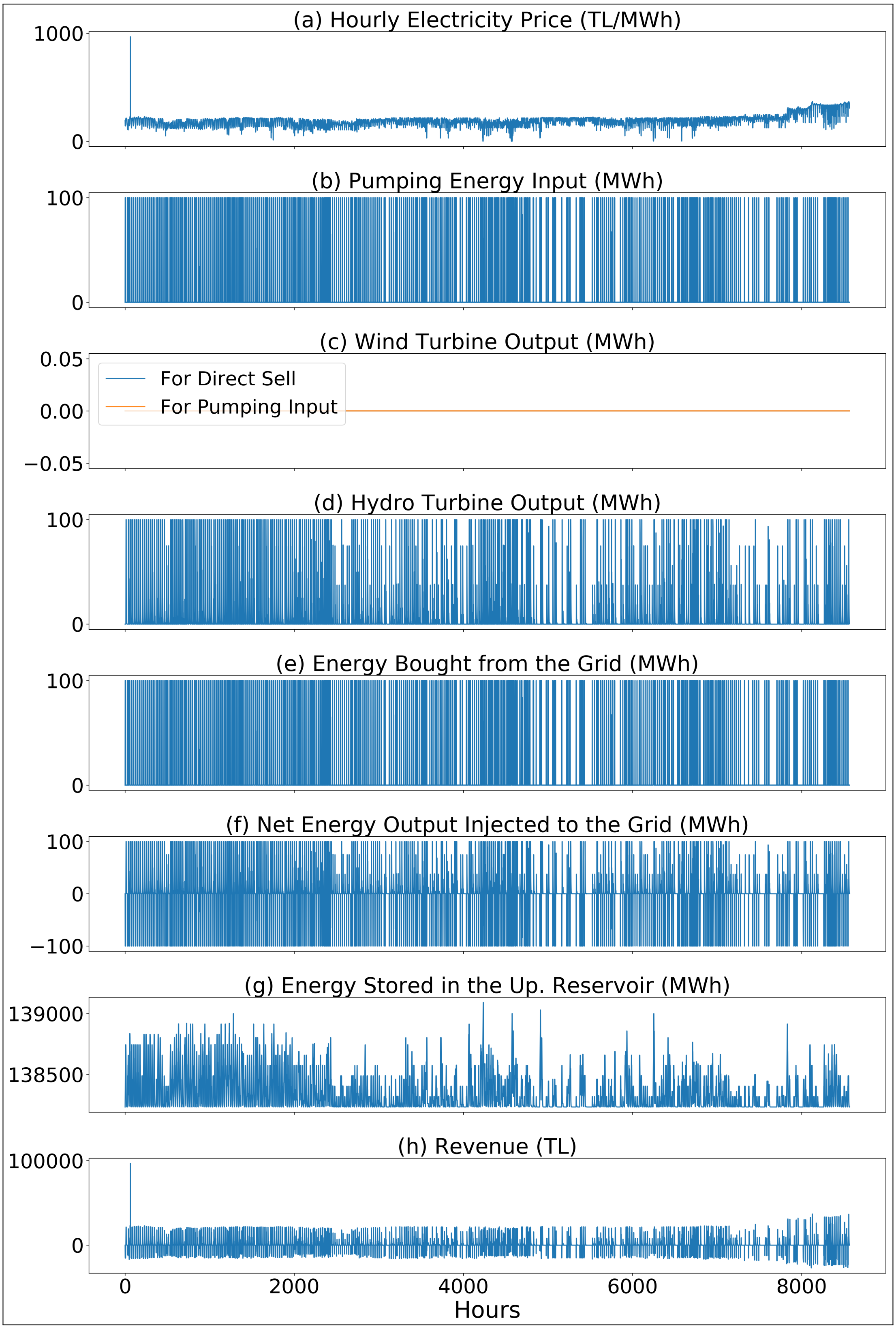

Figure 5.9. Results of Ideal_Opt for the Pumped Storage Hydropower Plant

5.2.2.2 Results of PrevDay_Opt

In this scenario, the optimization model is run for the pumped storage hydropower plant using the electricity prices of the previous day, and the optimum schedule and the revenue corresponding to this schedule are obtained (these are represented as PrevDay_Opt schedule and PrevDay-Revenue, respectively in Figure 5.8). The results of this case are presented in Figure 5.10. In Figure 5.10(a), the plotted hourly electricity price is two days shifted version of the prices that are used in Figure 5.9(a). As shown in Figure 5.8, a second revenue, PrevDay-RealRevenue is calculated for this scenario for comparison purposes. The optimum schedule obtained from the optimization model (i.e., PrevDay_Opt schedule) is simulated using the realized prices of the operation day to calculate PrevDay-RealRevenue. In real life, the revenue of the system will be PrevDay-RealRevenue since the execution of the optimum schedule will be realized with the electricity prices of the operation day instead of the previous day's electricity prices which were used in the optimization model. Thus, in Figure 5.10(h) the results of PrevDay-RealRevenue are given in orange in addition to PrevDay-Revenue for comparison purposes. The results for the whole test period are summarized in Table 5.4.

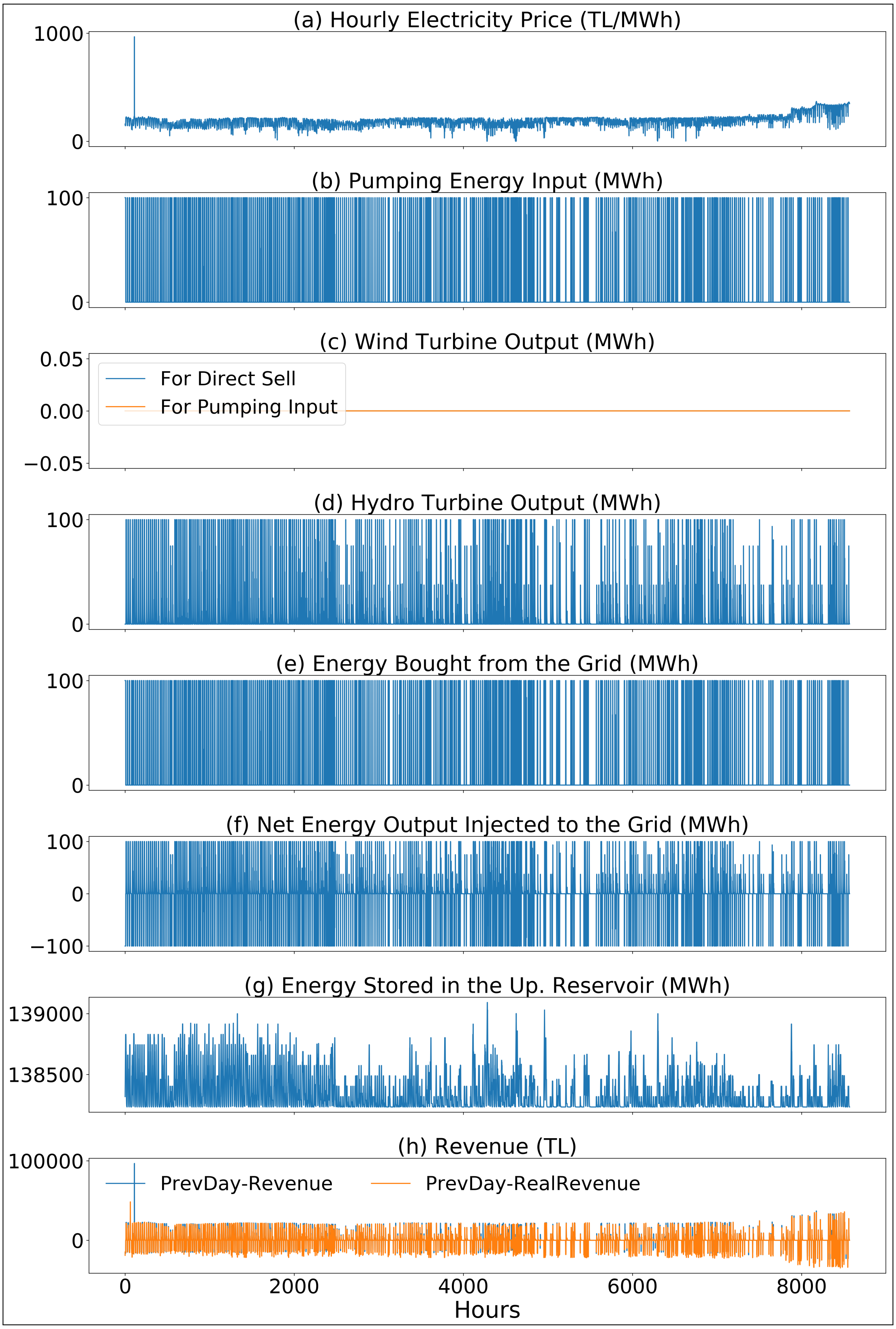

Figure 5.10. Result of PrevDay_Opt for the Pumped Storage Hydropower Plant

Table 5.4. Revenues of PrevDay_Opt and Ideal_Opt

PrevDay-Revenue (TL)	PrevDay-RealRevenue (TL)	Ideal-Revenue (TL)	Error in real revenue with respect to the estimated revenue (%)	Error in real revenue with respect to the ideal revenue (%)
3,978,708	-955,905	3,975,820	124	124

When the operation schedules of Ideal_Opt and PrevDay_Opt (i.e., Figure 5.9 and 5.10) are compared, it can be noticed that they are quite similar. The reason for this similarity is hourly electricity prices that are used in PrevDay_Opt and Ideal_Opt. There is two days difference between the inputs of PrevDay_Opt and Ideal_Opt, so two days difference exists in the schedules, as well. PrevDay_Opt follows the Ideal_Opt from two days behind. For instance, the schedule of energy stored in upper reservoirs for both Ideal_Opt and PrevDay_Opt is shown in Figure 5.11 where the similarity can be seen clearly. In addition to this, although PrevDay_Opt uses the electricity prices that are realized two days ago, it presents a rather incorrect optimum schedule. As can be seen in Table 5.4, PrevDay-Revenue is higher than Ideal-Revenue. That is, PrevDay_Opt can misguide the operator to determine the operation schedule of the pumped storage hydropower plant. For example, as shown in Figure 5.11, the use of the electricity prices that are realized two days ago in the schedule of the upper reservoir leads to a significant error in the revenue estimation although only two days lag exist in the prices.

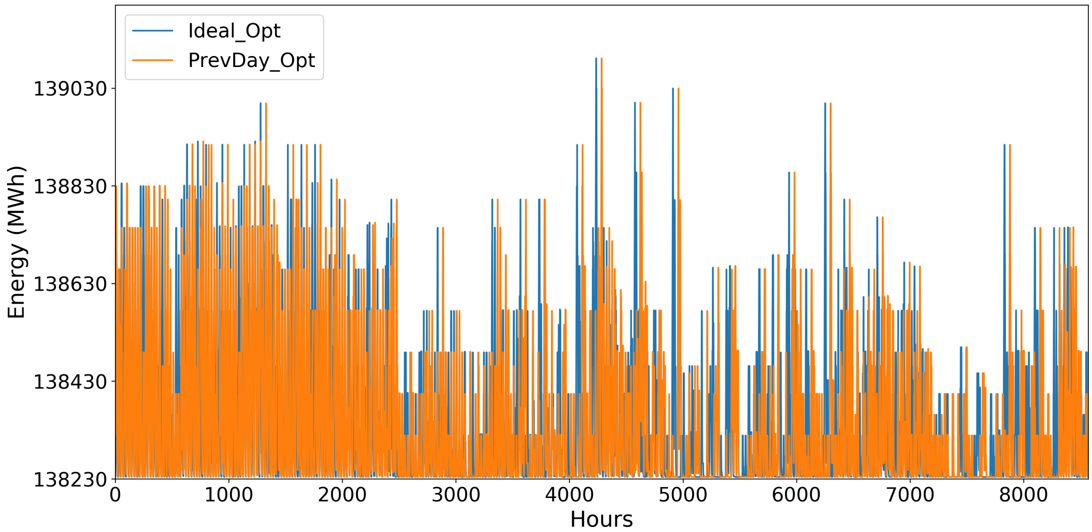

Figure 5.11. Energy Stored in the Upper Reservoir in Ideal_Opt and PrevDay_Opt

The errors in Table 5.4 are calculated using the following equation:

$$\frac{|\sum_n x - \sum_n y|}{\sum_n y} \times 100 \tag{5.1}$$

where x is PrevDay-RealRevenue, and y is PrevDay-Revenue and Ideal-Revenue for the 4th and 5th columns of Table 5.4, respectively and n is the total number of hours in the test period.

As can be seen in Table 5.4, when the previous day's electricity prices are used in the optimization model, the total revenue (i.e., PrevDay-Revenue) is estimated as 3,978,708 TL. However, the realized revenue of the system is -955,905 TL. This shows that the utilization of the previous day's electricity prices leads to 124% error in the revenue estimation. In other words, the owner of the system was hoping to make 3,978,708 TL but actually loses 955,905 TL in one year of the test period (from 9th of Sep 2017 to 31st of Aug 2018). As can be seen in Table 5.4, for the ideal case, the revenue of the system (i.e., Ideal-Revenue) is 3,975,820 TL, which is an upper bound for the revenue and the model error with respect to the ideal case is 124% as well. These results indicate that the utilization of the previous day's electricity prices results in misleading revenues.

5.2.2.3 Results of LSTM_Opt

The optimization model is run for the pumped storage hydropower plant using the electricity prices that are forecasted by the LSTM network in this scenario. The optimum schedule (i.e., LSTM_Opt in Figure 5.8) and the corresponding schedule (i.e., LSTM-Revenue in Figure 5.8) are obtained. The results of the obtained schedule are represented in Figure 5.12. In addition to LSTM-Revenue, the optimum schedule (i.e., LSTM_Opt schedule) is simulated using the realized prices to obtain LSTM-RealRevenue. To compare LSTM-Revenue and LSTM-RealRevenue, the results of LSTM-RealRevenue are given in orange in Figure 5.12(f). It can be noticed that in the last part of Figure 5.12(f) (i.e., around t = 8000 hr), there is a significant discrepancy between LSTM-Revenue and LSTM-RealRevenue. The reason for this discrepancy is that the LSTM network cannot forecast this part successfully due to abrupt changes in the electricity prices in this time duration (see Figure 4.24). Also, the summary of the results for the whole test period is given in Table 5.5.

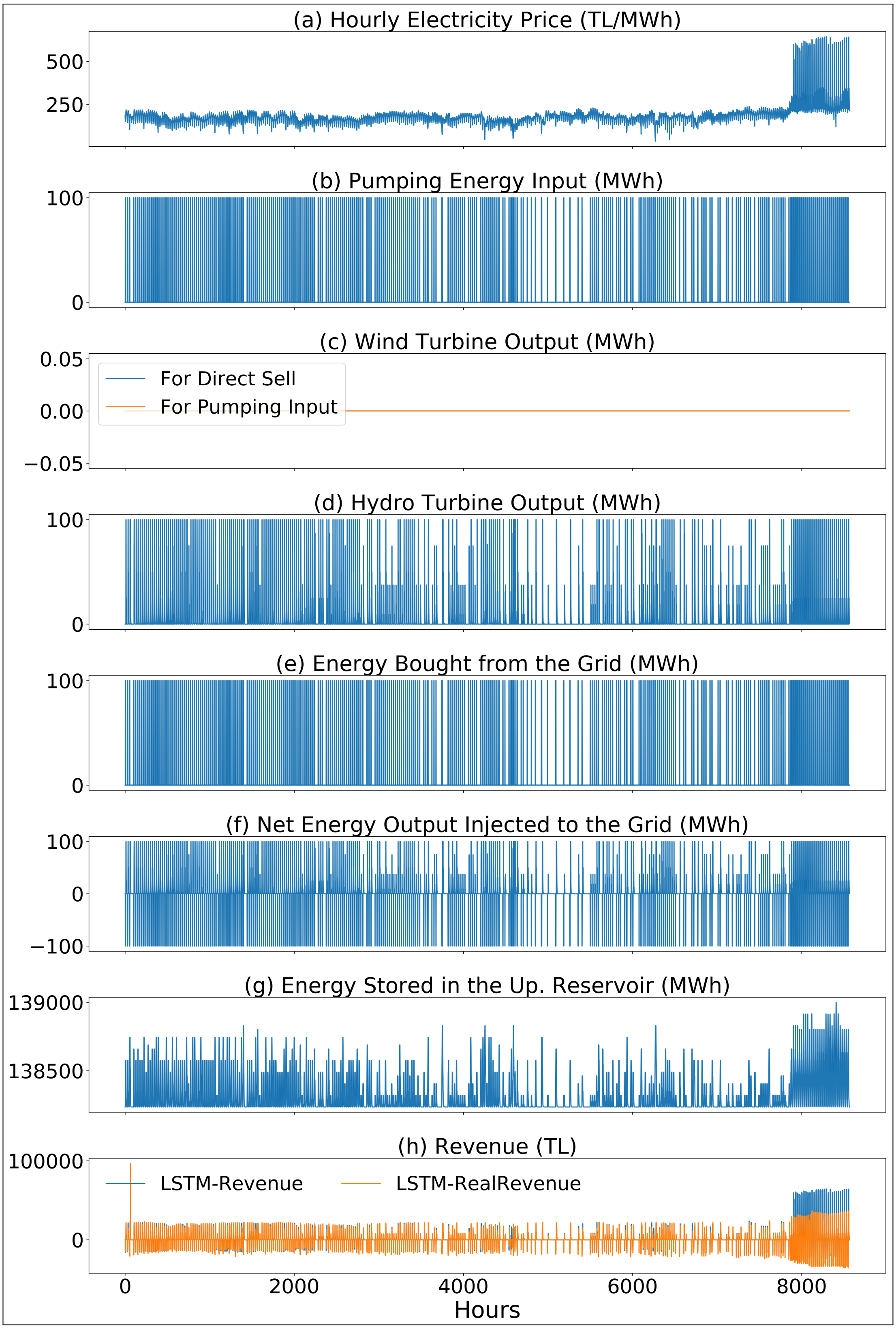

Figure 5.12. Result of LSTM_Opt for the Pumped Storage Hydropower Plant

Table 5.5. Revenues of LSTM_Opt and Ideal_Opt

LSTM-Revenue (TL)	**LSTM-RealRevenue (TL)**	**Ideal-Revenue (TL)**	**Error in real revenue with respect to the estimated revenue (%)**	**Error in real revenue with respect to the ideal revenue (%)**
4,339,821	-757,083	3,975,820	117.5	119.0

The errors are calculated using the Equation (5.1) where x is LSTM-RealRevenue and y is LSTM-Revenue and Ideal-Revenue for the 4th and 5th columns of Table 5.5, respectively.

According to Table 5.5, the total revenue (i.e., LSTM-Revenue) is estimated as 4,339,821 TL when the electricity prices that are forecasted by the LSTM network are used in the optimization model. Besides, the real revenue of the system is -757,083 TL. It can be inferred that the use of the LSTM network leads to 117.5% error in the revenue estimation. As shown in the Table 5.5, the revenue of the ideal case (i.e., Ideal-Revenue) is 3,975,820 TL. When the error is calculated with respect to the ideal case, it equals to 119%. So, these results indicate that the utilization of the LSTM prices does not improve the results significantly compared to the utilization of the previous day's electricity prices when the system does not have any wind turbine (i.e., only pumped storage hydropower).

To investigate the effects of the wind turbine integration to the pumped storage hydropower plant, similar simulations are conducted for the WHHS and presented in the next section.

5.2.3 WHHS Results

In this subsection, the results of the optimization model of the WHHS are presented for Ideal_Opt, PrevDay_Opt and LSTM_Opt, respectively.

5.2.3.1 Results of Ideal_Opt

The results of the ideal case are presented for the WHHS with 10, 50 and 200 wind turbines in Figures 5.13, 5.14, 5.15, respectively. As can be seen in Figures 5.13(c), 5.14(c) and 5.15(c), since wind turbines outputs exist in these scenarios, they contribute to the WHHS both for pumping and direct energy selling. Negative values of the net energy output injected to the grid are decreasing as the number of wind turbines are increasing as can be seen in Figures 5.13(f), 5.14(f), 5.15(f). It can be noticed that the schedule of pumping energy input, hydro turbine output, and energy stored in the upper reservoir are not affected by the number of wind turbines. They are the same in all three figures. The reason is that the operations of the pumped storage hydropower plant is governed by the electricity prices, and there is an upper bound - dictated by the capacity of the upper reservoir - of the revenue of the pumped storage hydropower plant with the given electricity prices. Wind turbines prevent the pumped storage hydropower plant from buying the energy from the grid. According to the optimum operation, if the system decided to pump water to the upper reservoir, it accomplishes this by buying the energy from the grid or taking it from the wind turbines if it is available. After wind turbines provide the necessary energy to the system, if extra wind energy exists, then it is sold to the grid. Thus, as the number of wind turbines increases, the revenue that is provided by the direct sell of wind energy increases as expected, and the energy bought from the grid decreases. According to the schedules given in Figures 5.13, 5.14 and 5.15, the total revenues are 11,278,263 TL, 40,488,038 TL and 150,024,694 TL, respectively. These revenues are the upper bounds of the revenues of the WHHS.

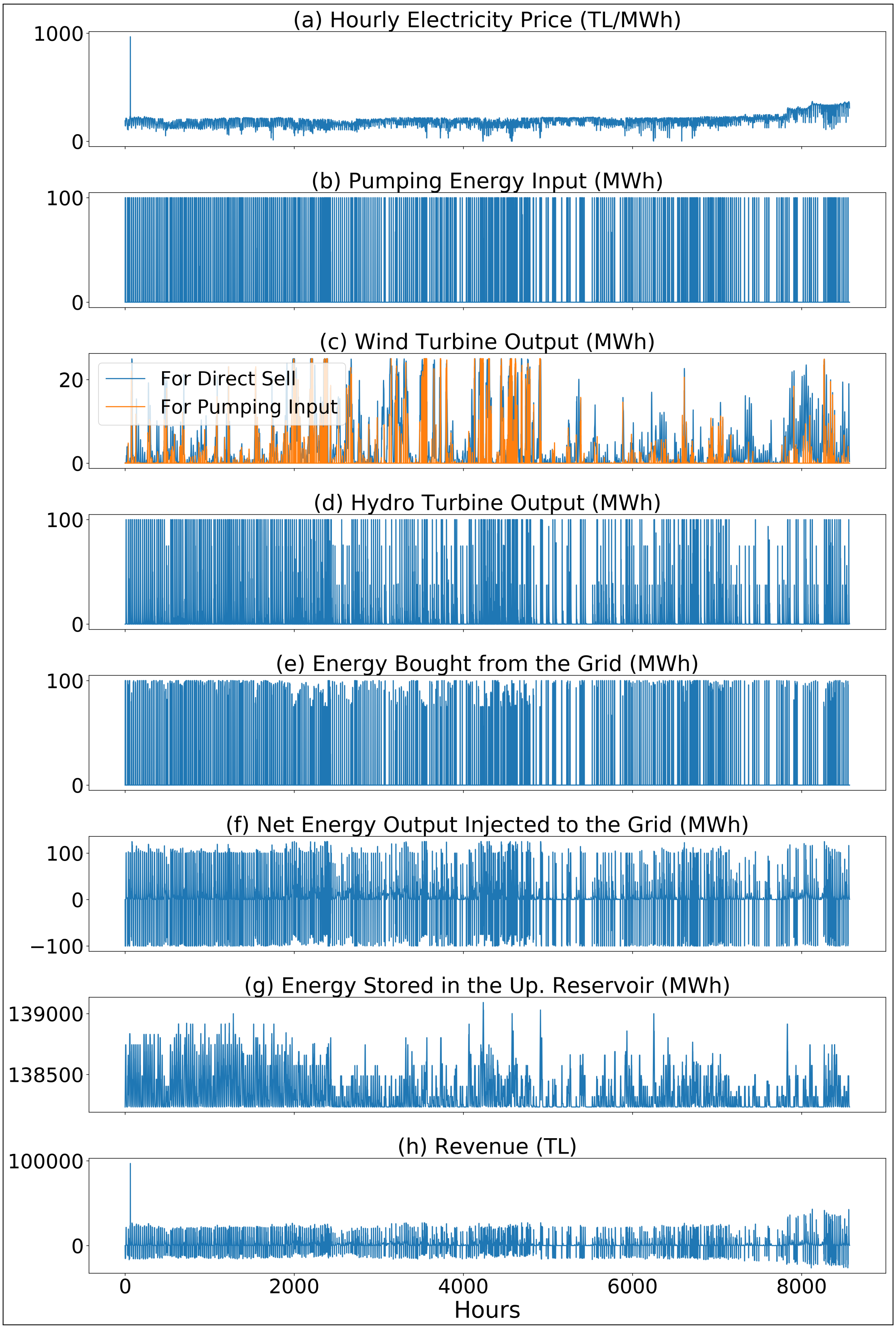

Figure 5.13. Results of Ideal_Opt for the WHHS with 10 Wind Turbines

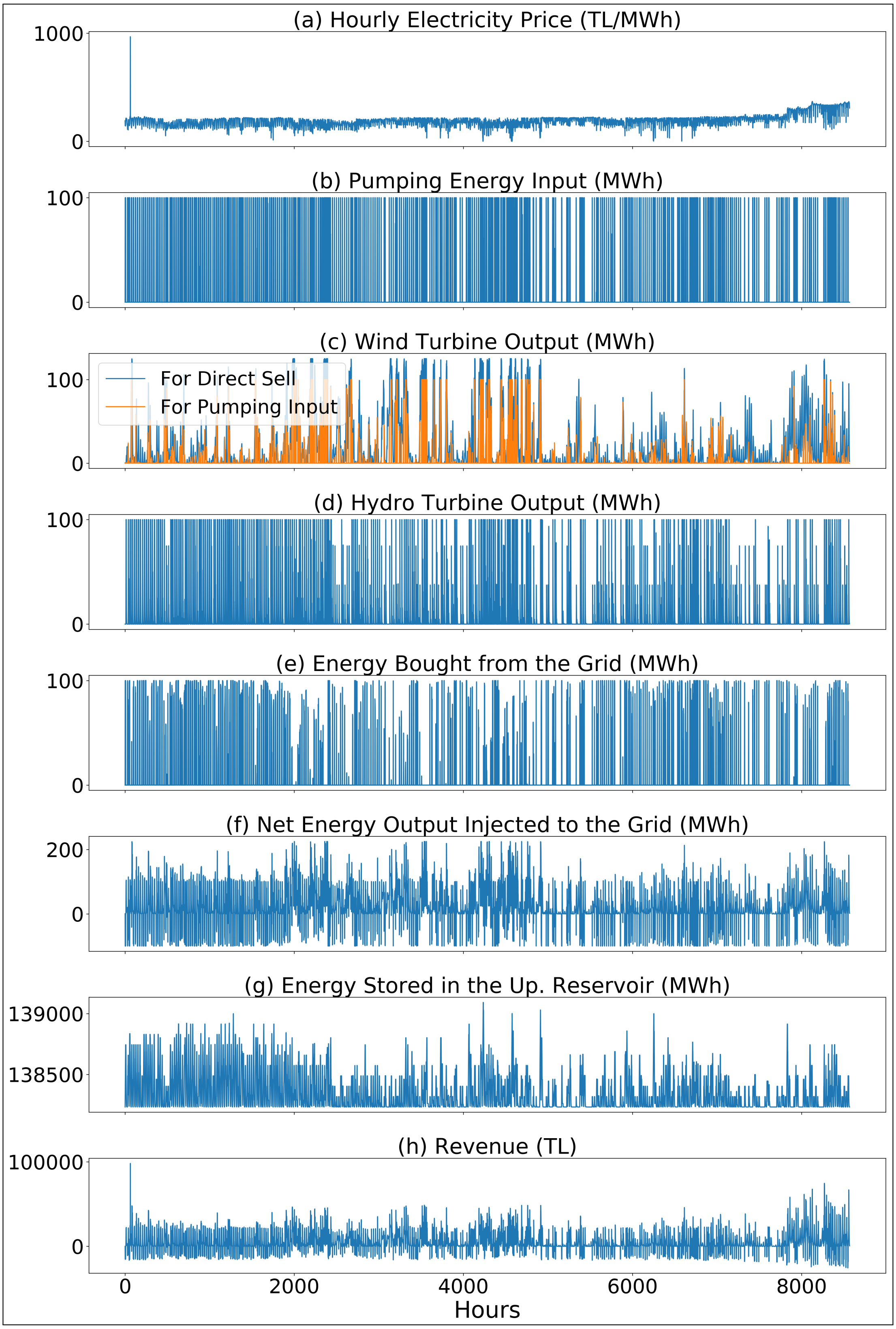

Figure 5.14. Results of Ideal_Opt for the WHHS with 50 Wind Turbines

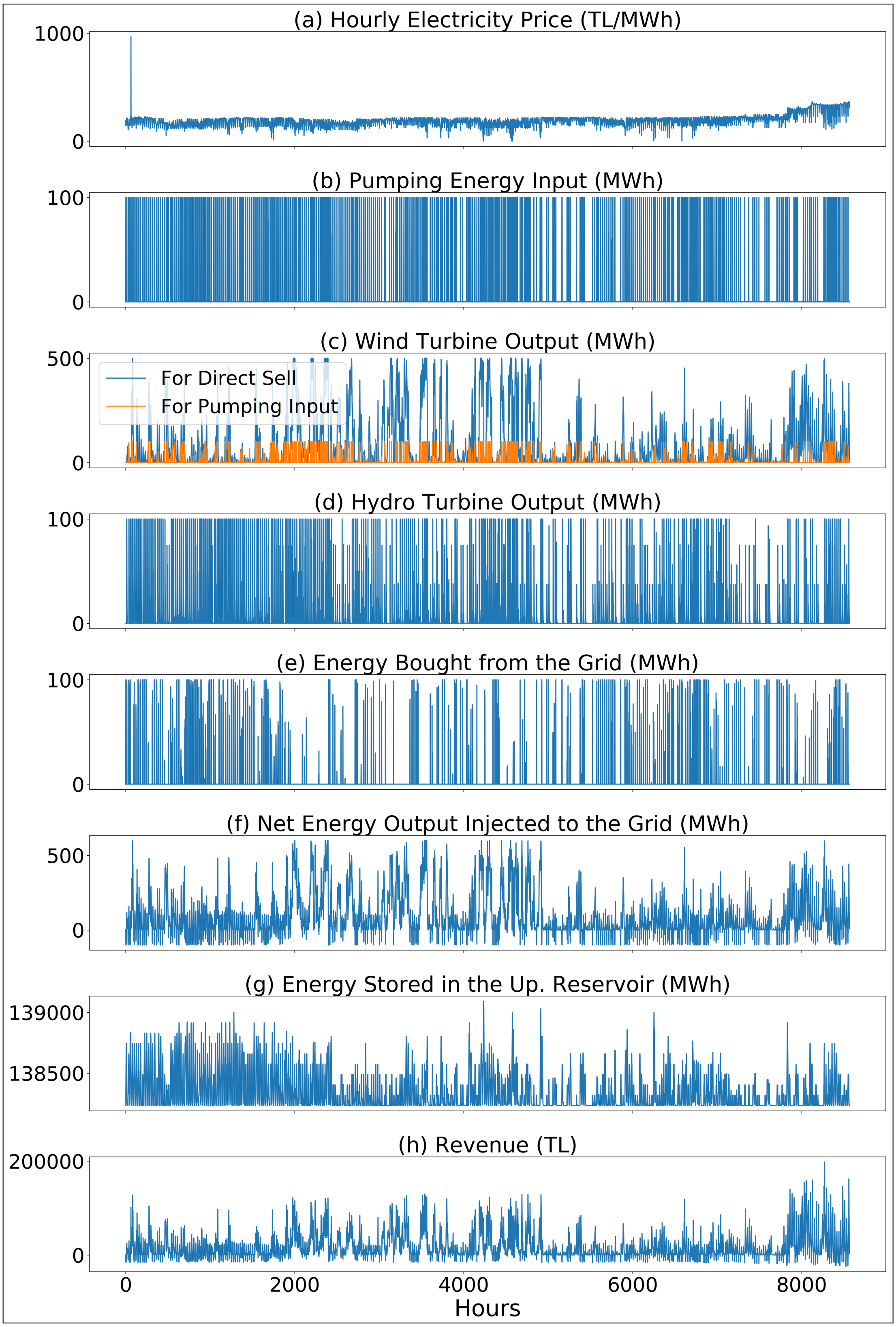

Figure 5.15. Results of Ideal_Opt for the WHHS with 200 Wind Turbines

5.2.3.2 Results of PrevDay_Opt

In this scenario, the optimization model is run for the WHHS with 10, 50, 200 wind turbines using the electricity prices of the previous day, and the optimum schedules and the revenues corresponding to these schedules are obtained. The results of these schedules are presented in Figures 5.16, 5.17 and 5.18, respectively. The obtained optimum schedules are simulated using the realized prices of the operation day, and PrevDay-RealRevenues are calculated. The orange line in Figures 5.16(h), 5.17(h) and 5.18(h) shows the results of PrevDay-RealRevenue. The summary of the results is presented in Table 5.6.

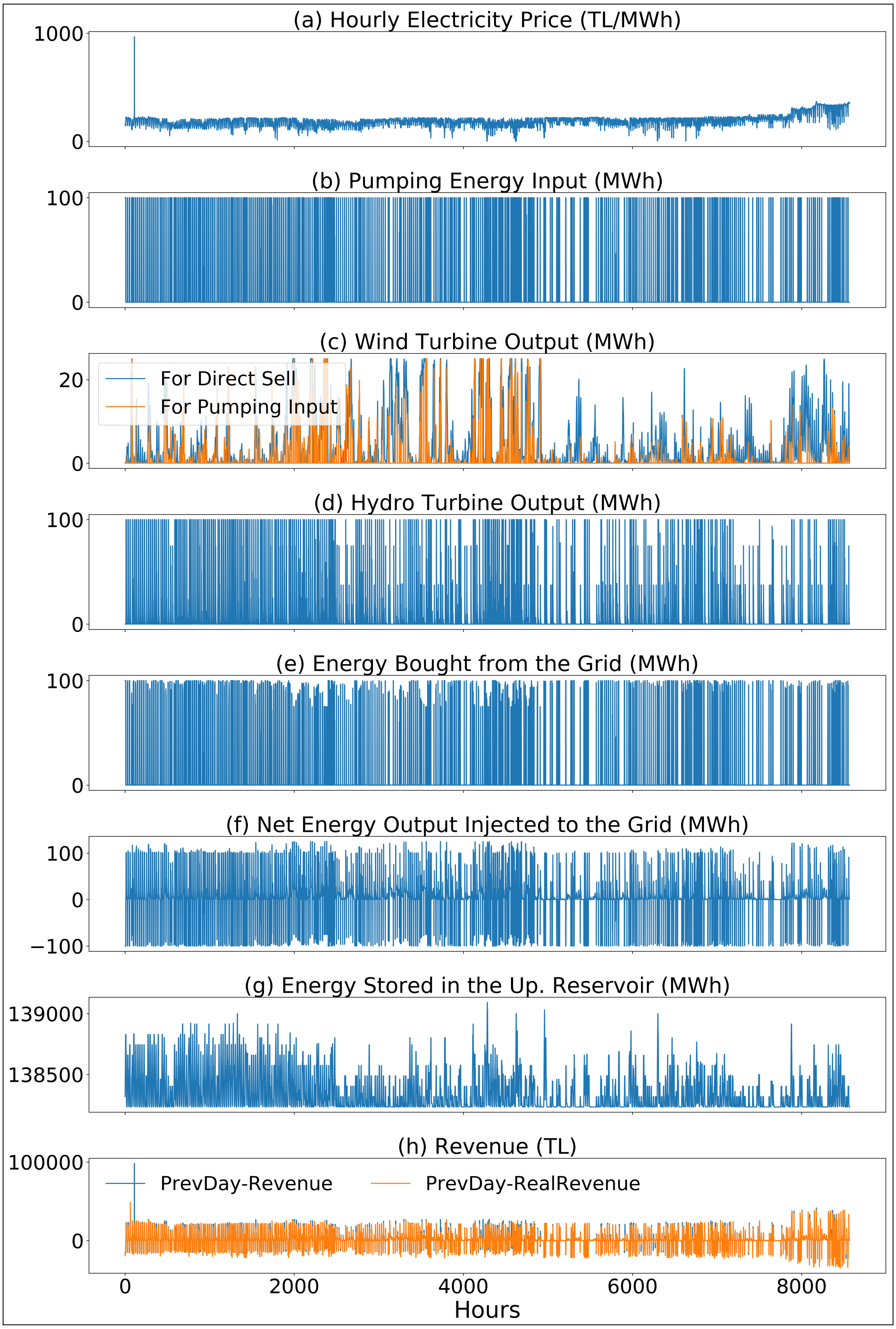

Figure 5.16. Result of PrevDay_Opt for the WHHS with 10 Wind Turbines

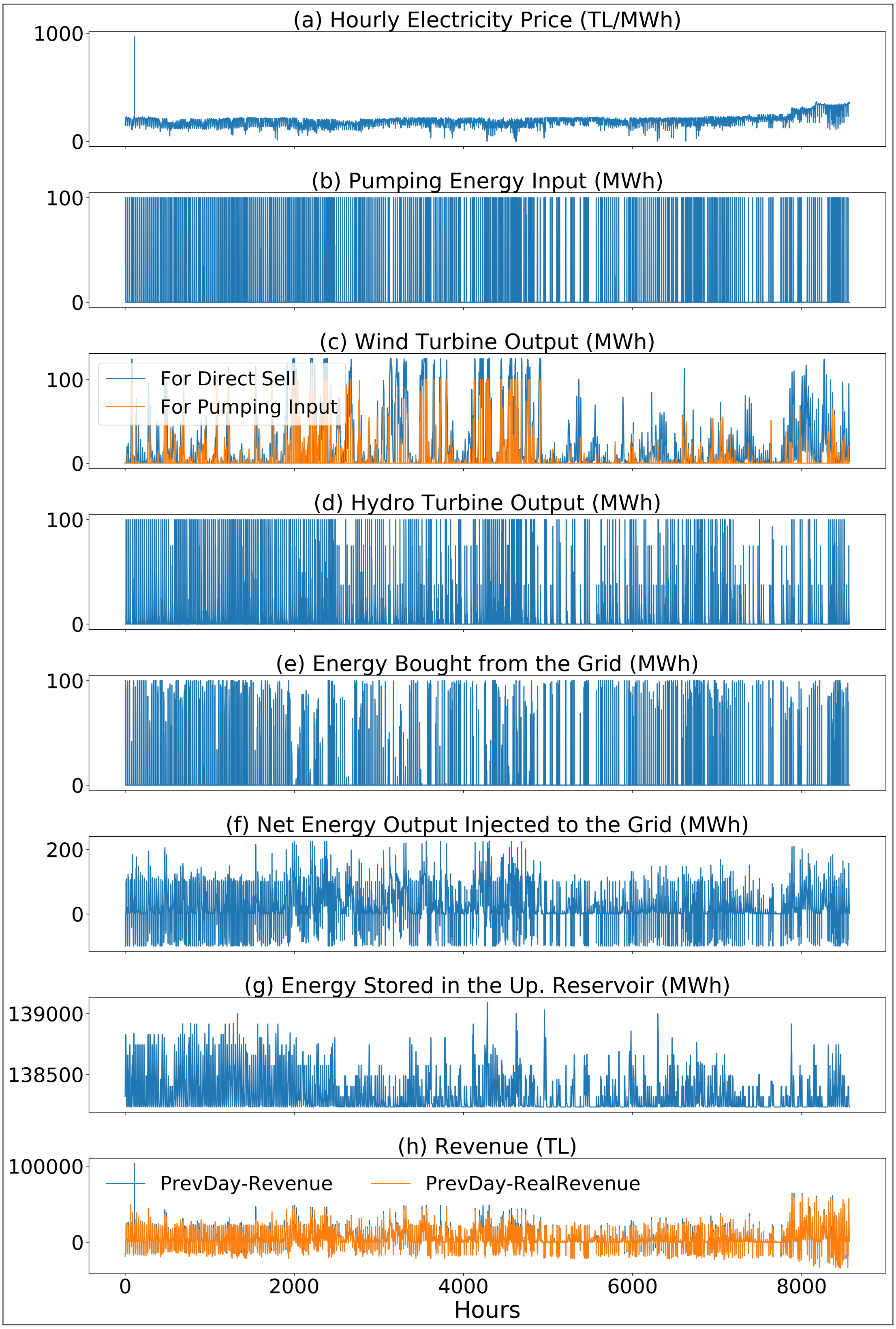

Figure 5.17. Result of PrevDay_Opt for the WHHS with 50 Wind Turbines

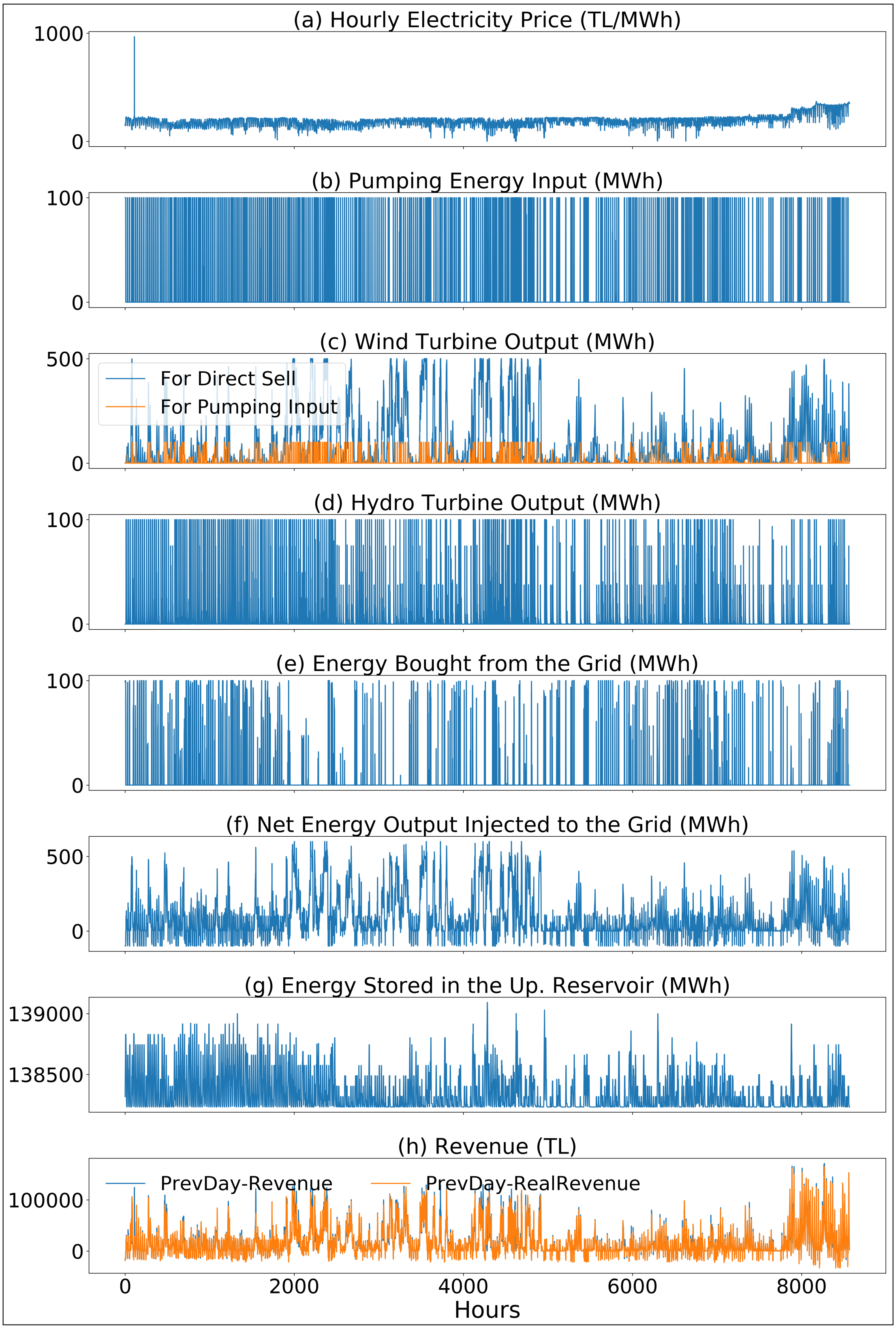

Figure 5.18. Result of PrevDay_Opt for the WHHS with 200 Wind Turbines

Table 5.6. Revenues of PrevDay_Opt and Ideal_Opt

Number of Wind Turbine	PrevDay-Revenue (TL)	PrevDay-RealRevenue (TL)	Ideal-Revenue (TL)	Error in real revenue with respect to the estimated revenue (%)	Error in real revenue with respect to the ideal revenue (%)
10	11,659,180	6,326,841	11,278,263	45.7	43.9
50	42,381,067	35,531,262	40,488,038	16.2	12.2
200	157,588,146	144,911,061	150,024,694	8.0	3.5

As shown in Table 5.6, the total revenues (i.e., PrevDay-Revenues) are estimated as 11,659,180 TL, 42,381,067 TL and 157,588,146 TL for 10, 50 and 200 wind turbines, respectively. On the other hand, the realized revenues of the WHHS are 6,326,841 TL for 10 wind turbines, 35,531,262 TL for 50 wind turbines and 144,911,061 TL for 200 wind turbines. These results correspond to 45.7%, 16.2%, and 8.0% errors in the revenue estimation for 50, 100, and 200 wind turbines, respectively. Also, Ideal-Revenues are shown in Table 5.6, and the errors with respect to the ideal case are 43.9%, 12.2%, and 3.5% for 10, 50 and 200 wind turbines, respectively. It can be inferred that increasing integration of the wind turbines decreases the errors. There are two main reasons for this. Firstly, a higher number of wind turbines provide higher revenues such that the share of the pumped storage hydropower operations in revenue becomes very small compared to the share of the wind turbine operations. Since the errors are originated from the pumped storage hydropower operations, they can be reduced with the decreasing share of the pumped storage hydropower in the revenue. The operation of the wind turbine does not affect the error directly since after the energy need of the WHHS is provided, the energy generated by the wind turbine is sold to the grid regardless of the electricity prices. Secondly, the energy bought from the grid at incorrect hours leads to the loss. However, if the WHHS takes the energy from the wind turbines instead of the grid, the loss is prevented. In this way, the wind turbine compensates for the error emerging from an incorrect schedule of the WHHS.

5.2.3.3 Results of LSTM_Opt

The optimization model is run for the WHHS with 10, 50 and 200 wind turbines using the electricity prices that are forecasted by the LSTM network in this scenario. The optimum schedules and the revenues corresponding to these schedule are obtained. The optimum schedules correspond to 10, 50 and 200 wind turbines are presented in Figures 5.19, 5.20 and 5.21, respectively. In addition to LSTM-Revenue, LSTM-RealRevenue is calculated for all wind turbine cases, and they are shown in orange in Figures 5.19(h), 5.20(h) and 5.21(h). In Table 5.6, the summary of the results is presented.

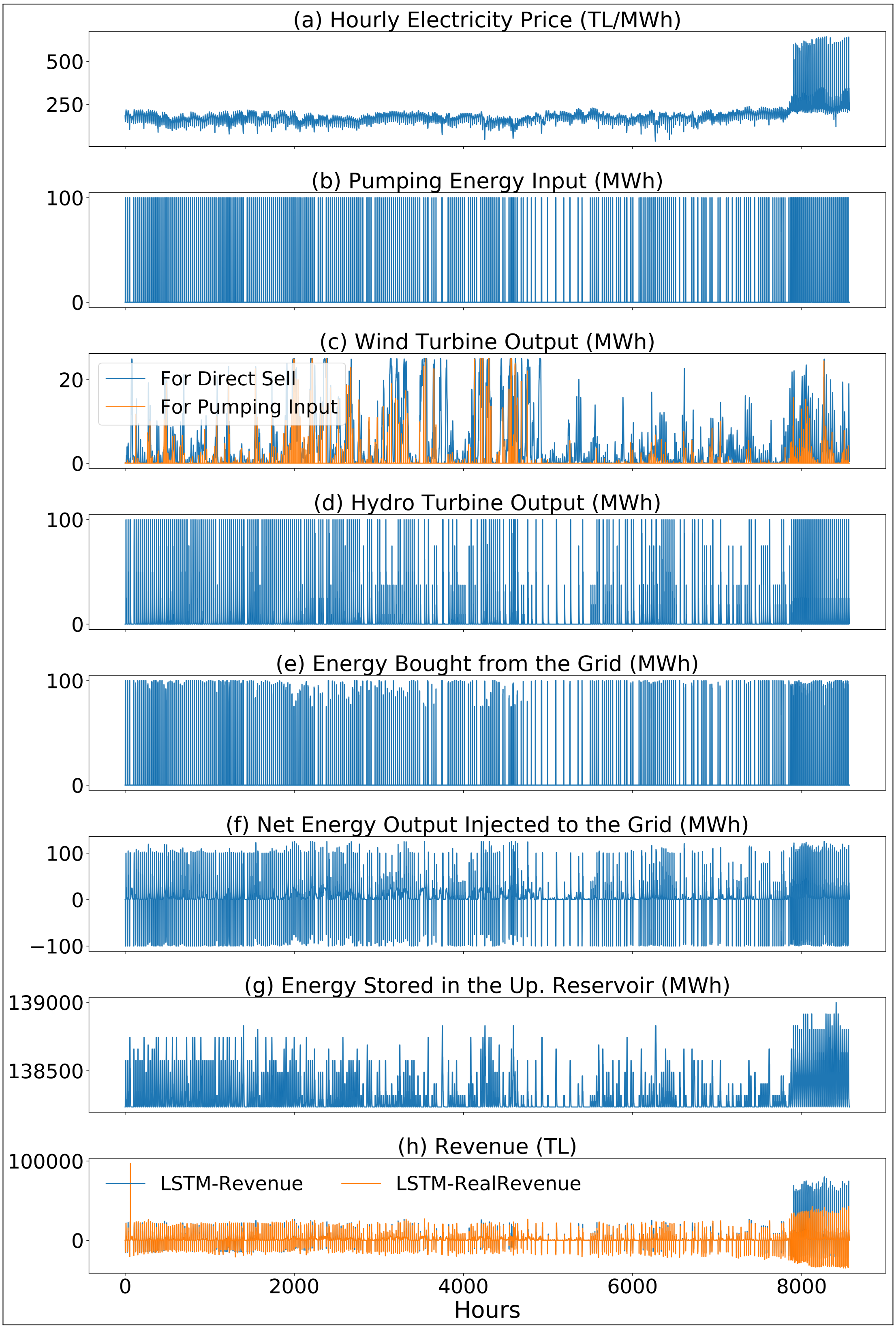

Figure 5.19. Result of LSTM_Opt for the WHHS with 10 Wind Turbines

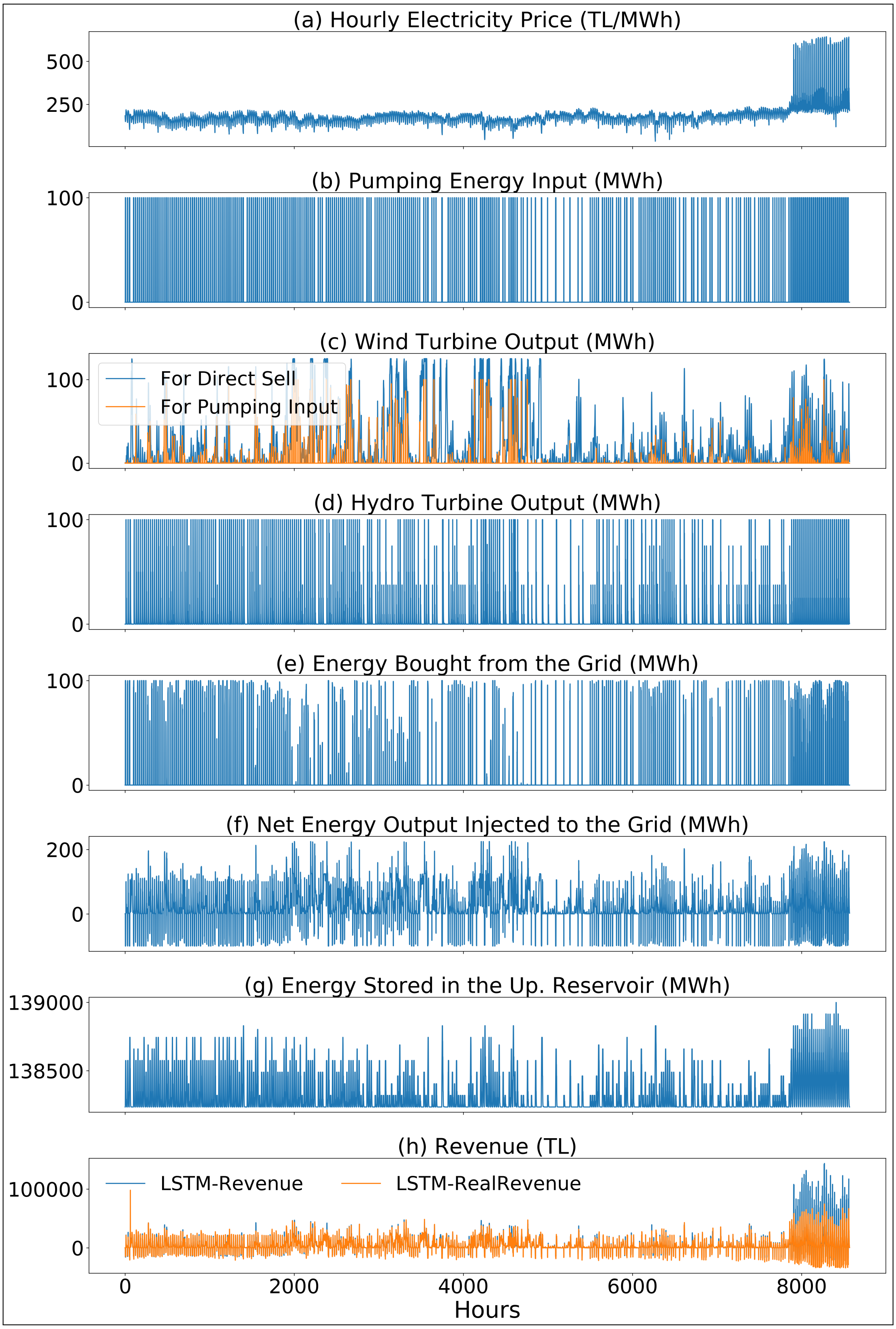

Figure 5.20. Result of LSTM_Opt for the WHHS with 50 Wind Turbines

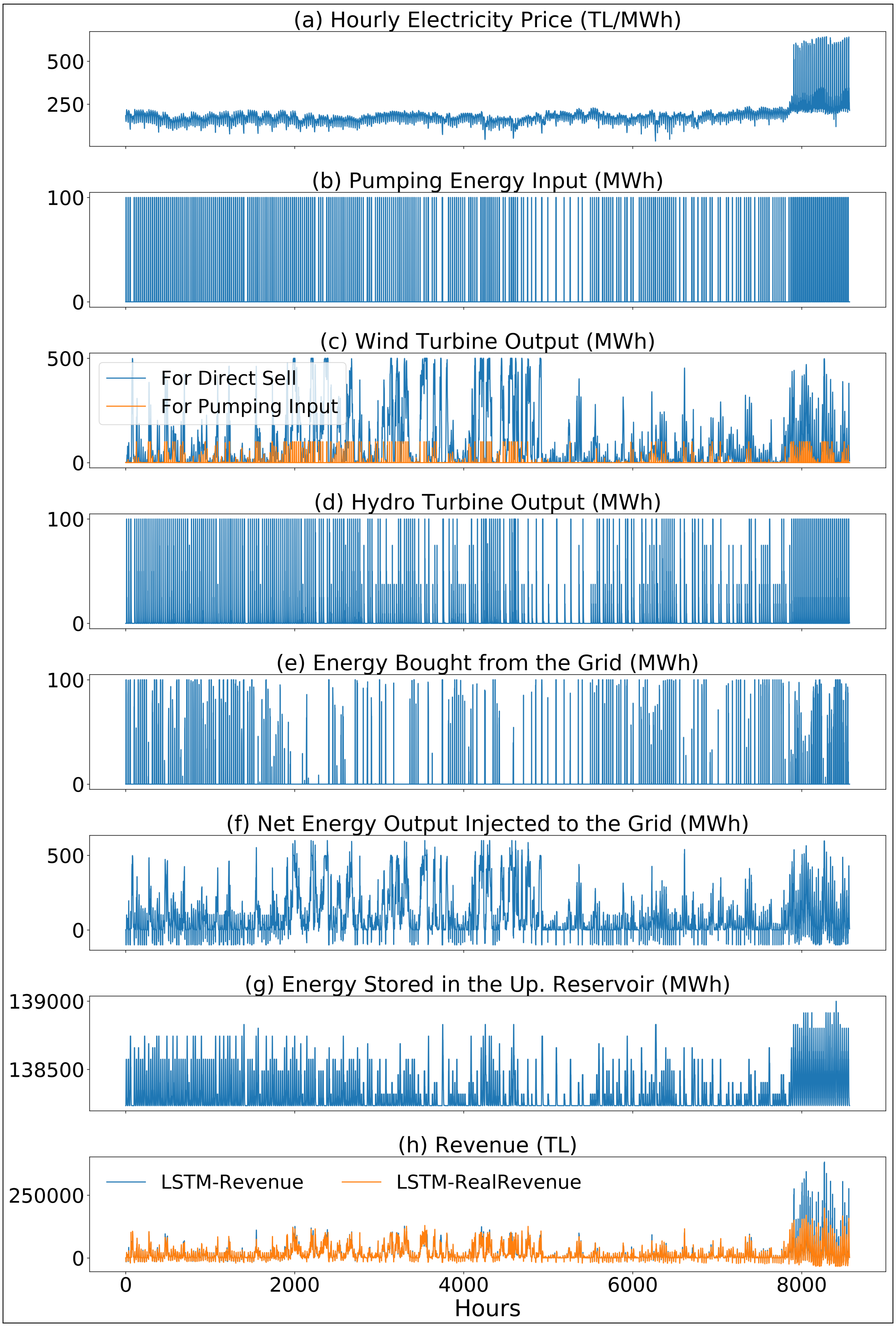

Figure 5.21. Result of LSTM_Opt for the WHHS with 200 Wind Turbines

Table 5.7. Revenues of LSTM_Opt and Ideal_Opt

Number of Wind Turbine	LSTM-Revenue (TL)	LSTM-RealRevenue (TL)	Ideal-Revenue (TL)	Error in real revenue with respect to the estimated revenue (%)	Error in real revenue with respect to the ideal revenue (%)
10	11,986,931	6,545,361	11,278,263	45.4	42.0
50	42,575,370	35,755,136	40,488,038	16.0	11.7
200	157,282,016	145,291,791	150,024,694	7.6	3.2

According to Table 5.7, the total revenues (i.e., LSTM-Revenues) are estimated as 11,986,931 TL, 42,575,370 TL and 157,282,016 TL for 10, 50 and 200 wind turbines, respectively. The realized revenues of the WHHS are 6,545,361 TL for 10 wind turbines, 35,755,136 TL for 50 wind turbines and 145,291,791 TL for 200 wind turbines. The errors in revenue estimations are computed as 45.4%, 16.0%, and 7.6% for 10, 50, and 200 wind turbines, respectively. In addition to this, the errors with respect to the ideal case are 42.0% for 10 wind turbines, 11.7% for 50 wind turbines and 3.2% for 200 wind turbines. So, the increase in the number of wind turbines decreases both errors. Apart from this, when the error columns of Tables 5.6 and 5.7 are compared, it can be seen that the errors in the scenario of LSTM_Opt are smaller than PrevDay_Opt even if the differences are small. Therefore, to use the LSTM_Opt in the operation of the WHHS is beneficial theoretically. However, when the computational load of the LSTM network is considered, its performance is not successful enough compared to PrevDay_Opt. Especially the time durations when abrupt changes occur in electricity prices, LSTM_Opt results in poor performance compared to PrevDay_Opt. This is because the LSTM network is not trained by the data that includes these abrupt changes, or its architecture is not powerful to catch the abrupt changes. Thus, it is beneficial to use PrevDay_Opt when unusual trends in electricity prices are observed. Nevertheless, if a more comprehensive LSTM network (i.e., the LSTM network includes input features that creates abrupt changes in electricity prices) is used in LSTM_Opt, it is expected to perform better than the current one and PrevDay_Opt.

5.2.4 Comparison of Pumped Storage Hydropower Plant and WHHS

Results of Ideal_Opt, PrevDay_Opt and LSTM_Opt are summarized and given in Tables 5.8, 5.9 and 5.10, respectively. It can be inferred that the schedules are not affected by the change in the number of wind turbines. The schedules change with the electricity prices that are used in the optimization model. Therefore, they are different in each scenario (i.e., Ideal_Opt, PrevDay_Opt and LSTM_Opt). It can be noticed that different number of wind turbines corresponds to different total pump and turbine hours in the schedule for a each scenario. The minor changes in total pump and turbine hours as the number of wind turbines change is due to round-off errors that occur in the optimization process.

Table 5.8. Summary Schedule of Ideal_Opt

Number of Wind Turbine	Pumping Input Energy (MWh)	Wind Energy for Direct Sell (MWh)	Wind Energy for Pumping (MWh)	Hydro Turbine Output (MWh)	Energy Bought from Grid (MWh)	Net Energy Injected to Grid (MWh)	Total Pump Hours	Total Turbine Hours
0	137848.77	0.00	0.00	103110.64	137848.77	-34738.13	1400	3763
10	137848.77	32766.75	7895.90	103110.64	129952.87	5924.52	1423	3793
50	137848.77	167185.31	36527.97	103110.64	101320.80	168975.15	1421	3792
200	137848.77	746743.67	66909.45	103110.64	70939.32	778914.99	1411	3792

Table 5.9. Summary Schedule of PrevDay_Opt

Number of Wind Turbine	Pumping Input Energy (MWh)	Wind Energy for Direct Sell (MWh)	Wind Energy for Pumping (MWh)	Hydro Turbine Output (MWh)	Energy Bought from Grid (MWh)	Net Energy Injected to Grid (MWh)	Total Pump Hours	Total Turbine Hours
0	138548.77	0.00	0.00	103634.33	138548.77	-34914.44	1407	3767
10	138548.77	34368.18	6304.74	103634.33	132244.03	5758.48	1423	3803
50	138548.77	173689.65	29974.95	103634.33	108573.82	168750.16	1422	3803
200	138548.77	752279.80	61578.58	103634.33	76970.19	778943.95	1418	3803

Table 5.10. Summary Schedule of LSTM_Opt

Number of Wind Turbine	Pumping Input Energy (MWh)	Wind Energy for Direct Sell (MWh)	Wind Energy for Pumping (MWh)	Hydro Turbine Output (MWh)	Energy Bought from Grid (MWh)	Net Energy Injected to Grid (MWh)	Total Pump Hours	Total Turbine Hours
0	111198.64	0.00	0.00	83176.19	111198.64	-28022.45	1157	4126
10	111198.64	35974.41	4779.97	83176.19	106418.67	12731.94	1157	4192
50	111198.64	181175.38	22596.54	83176.19	88602.10	175749.48	1157	4192
200	111198.64	767456.36	47631.35	83176.19	63567.29	787065.26	1157	4192

5.2.5 Further Comparisons

Bar plots of three realized revenues (i.e., LSTM-RealRevenue, PrevDay-RealRevenue and Ideal-Revenue) with no wind turbine case and three different numbers (i.e., 10, 50 and 200) of wind turbines are shown in Figure 5.22. The integration of the wind turbines to the system clearly decreases the negative effect induced by the difference between the estimated prices and occurred prices. This is because the share of the pumped storage hydropower operations in the revenue is reducing with the increasing number of wind turbines. In other words, the importance of the electricity price forecasting disappears. As a result, the owner of the pumped storage hydropower plant has two choices. First, he or she can have a very powerful LSTM network to forecast electricity prices with high accuracy. Second, he or she can have enough number of the wind turbines so that the errors in consequence of the incorrect schedule of the pumped storage hydropower plant can be compensated by wind turbines.

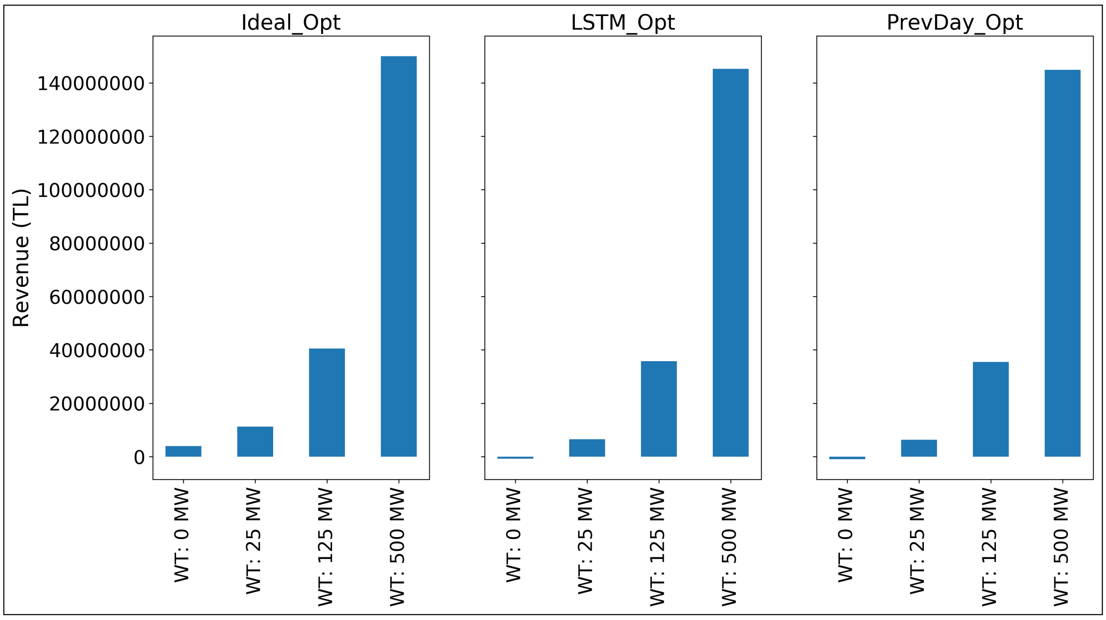

Figure 5.22. Revenues of LSTM-RealRevenue, Prevday-RealRevenue and Ideal-Revenue (TL)

Error variations through hours of the year in revenues of LSTM-RealRevenue with respect to Ideal-Revenue, and PrevDay-RealRevenue with respect to Ideal-Revenue are computed, and presented in Figure 5.23. We can say that the error ranges of the LSTM-RealRevenue are smaller than PrevDay-RealRevenue. Also, the positive effect of the wind integration can be seen in these figures, as well. In other words, errors are decreasing with the number of wind turbines.

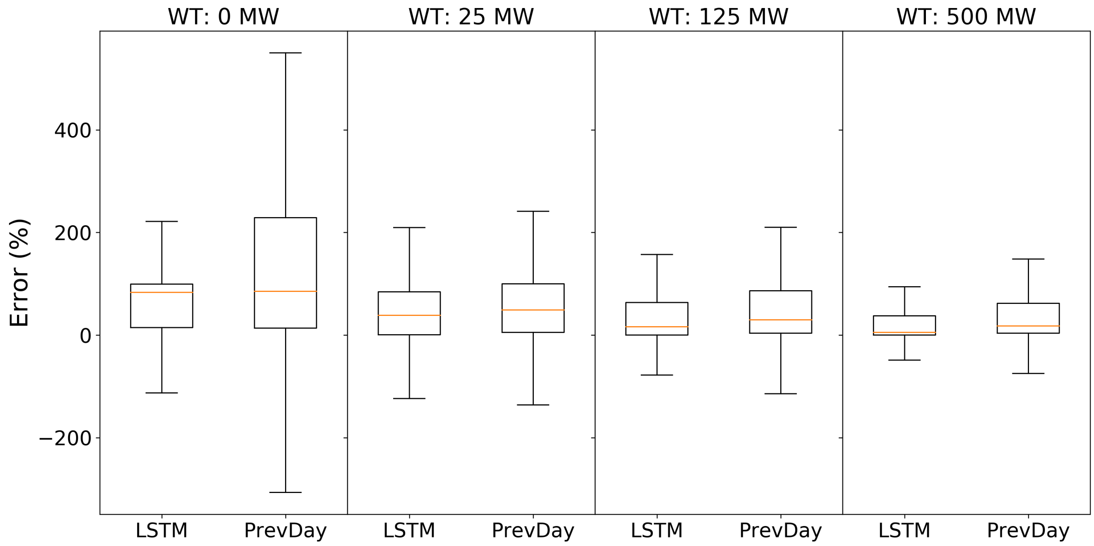

Figure 5.23. Error Variations of LSTM-RealRevenue and PrevDay-RealRevenue with respect to Ideal-Revenue

In addition to yearly analysis of the revenues, monthly analyses are conducted as well to see the effect of the seasonal change in the electricity price and presented in Figure 5.24. In the first plot (i,e., there is no wind turbine), monthly revenues are negative from January to August since both LSTM_Opt and PrevDay_Opt cannot predict the real price accurate enough. This leads to purchase of electricity in wrong hours (i.e., when the prices are high) and consequently results in revenue loss. Especially, the loss of LSTM-RealRevenue is very high in August due to abrupt changes in the electricity prince in this month (see Figure 4.24). The integration of wind turbines turns the loss into the positive revenue. However, abrupt changes in the electricity price in August lead to the lowest revenues of LSTM-RealRevenue in all wind turbine scenarios (i.e., 10, 50, and 200). Apart from August, LSTM-RealRevenue brings more revenue than PrevDay_Opt-RealRevenue in all months and wind turbine scenarios. The WHHS has more revenue in January, February, March, December, and August than other months in all three optimization scenarios (i.e., Ideal_Opt, PrevDay_Opt and LSTM_Opt).

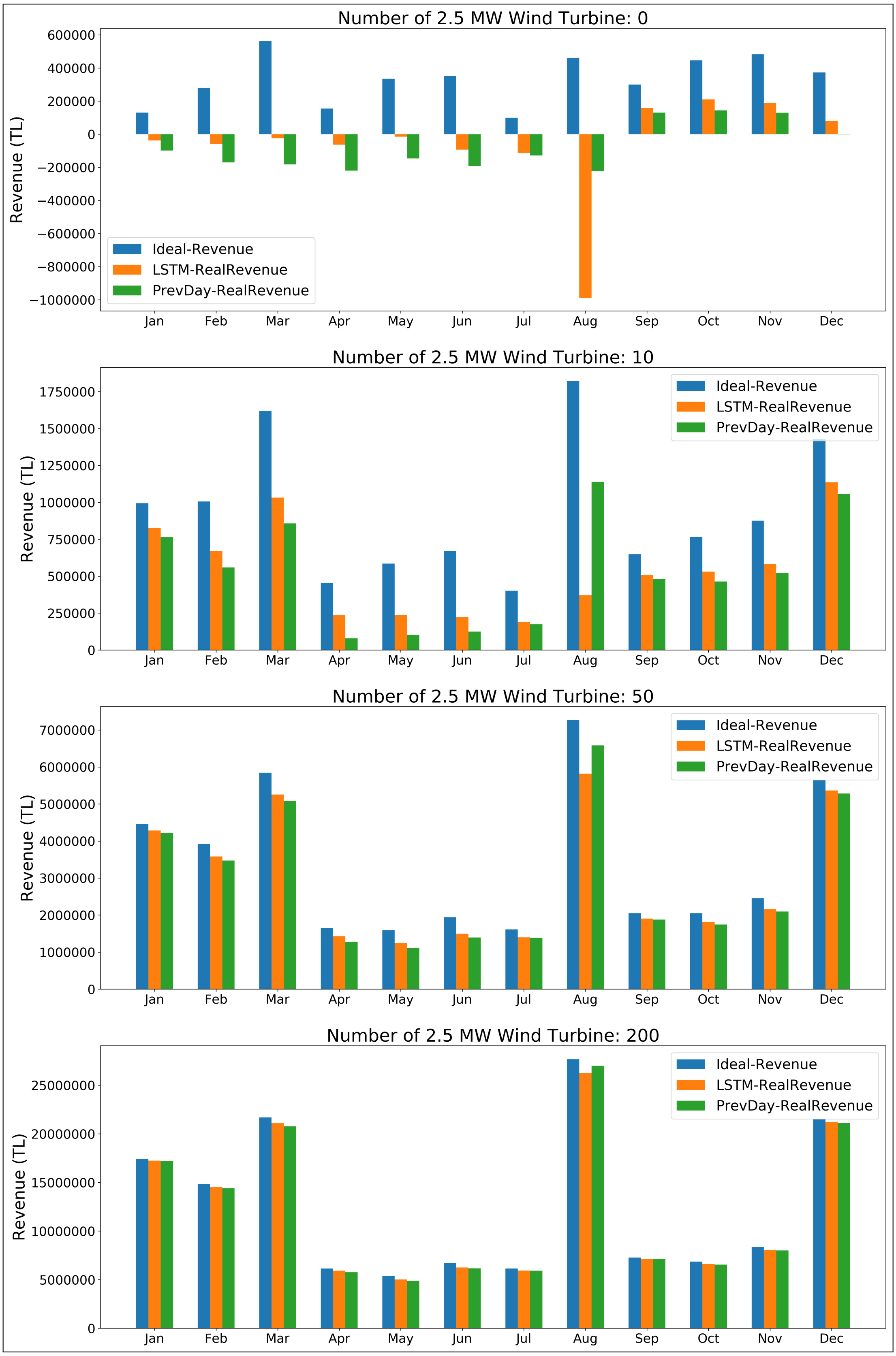

Figure 5.24. Monthly Revenues of Ideal-Revenue, LSTM-RealRevenue and PrevDay-RealRevenue (TL)

Another important point is that electricity prices affect the pump need of the WHHS directly. Each optimization model scenario uses a different amount of pumping energy according to their schedule. Input energy for the pump and its sources (i.e., from the grid or wind turbines) are plotted and represented in Figure 5.25. For all three optimization model scenarios, the pump operation does not change as the number of wind turbines increases. However, the dependency of the WHHS to the grid decreases with an increasing number of wind turbines. Plots in Figure 5.25 show that if a sufficient number of wind turbines is provided, the WHHS may not buy the energy from the grid at all.

The schedule of the pump energy input of the WHHS changes according to the optimization model scenario. For all three optimization model scenarios, the schedule of the pump input energy is presented in Figure 5.26. Each optimization model scenario has different schedules of pump input energy. The important point is that the schedule does not change with the number of wind turbines. It is same for no wind turbine case and all wind turbine numbers (i.e., 10, 50, 200). The number of wind turbines only changes the source of the pump input energy (i.e., from the grid or wind turbines).

Apart from the scenarios discussed in the previous sub-sections, the optimization model simulated using only wind turbines by ignoring all turbine and pump operations, as well. In other words, all energy generated by wind turbines is sold directly to the grid. This is not a common practice in electricity spot markets. Because the amount of energy to be sold to the grid is specified in advance, and wind power plant operators must obey these amounts. Otherwise, they will be penalized. This scenario is simulated to compare it with the hybrid system. As expected, only the wind turbine scenario has lower revenue than the scnearios of the WHHS. For example, the revenue of Ideal_Opt of the WHHS with 10 wind turbines is 11.3 million TL, whereas the revenue of 10 wind turbines is 7.3 million TL in a year.

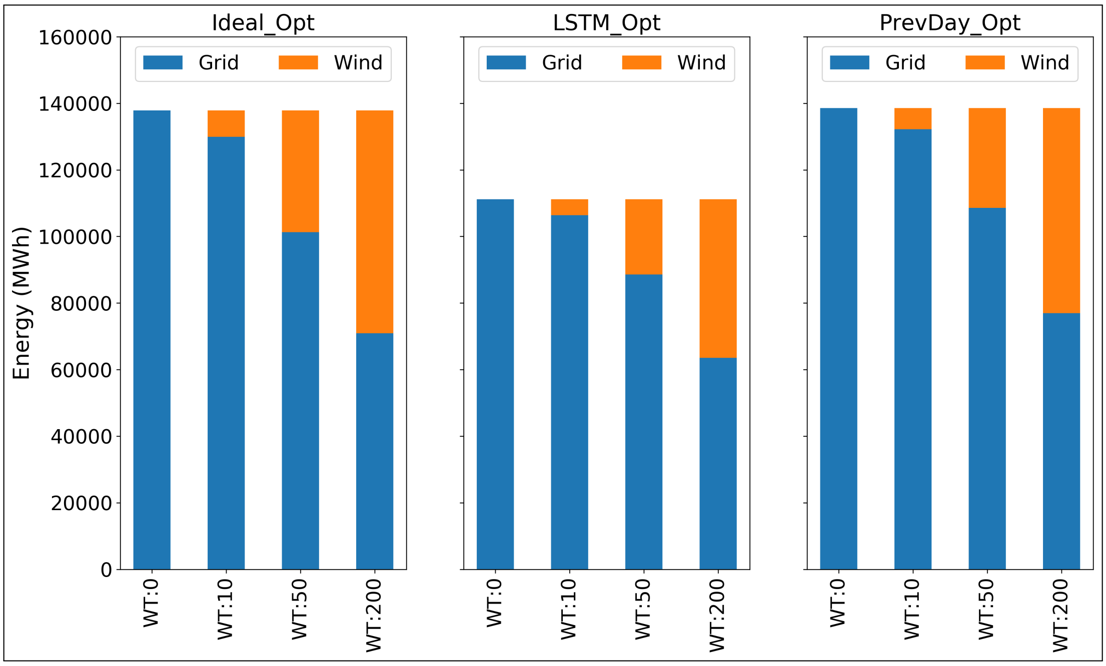

Figure 5.25. Plots for the Input Energy of the Pump in the Scenarios

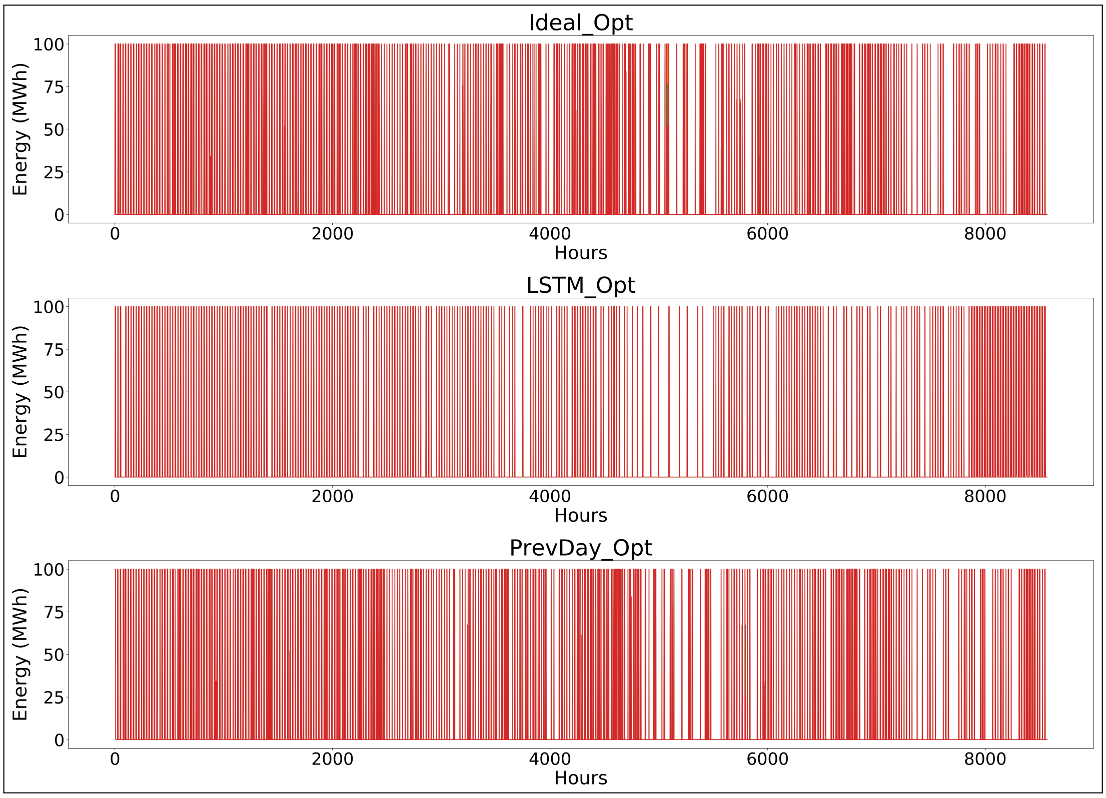

Figure 5.26. Schedules of the Pump Input Energy in the Scenarios

CHAPTER 6

CONCLUSION

In this thesis, the optimum operation schedule of a WHHS is investigated. In the scope of the thesis, first, an LSTM network is developed to forecast the electricity prices in the day-ahead spot electricity market. Then, an optimization model is developed to maximize the revenues of the WHHS. To investigate the optimization model and the LSTM network, different scenarios are created and run. Optimum operation schedules of the WHHS are obtained with these runs.

The significant findings of this thesis are given below:

- When the proposed LSTM network is used to estimate electricity prices, closer to actual revenues are obtained compared to those obtained by using previous day prices at most of the times. However, it brings a computational load.
- LSTM network does not perform effectively for periods where abrupt changes occur. In Turkey, the electricity prices are affected from many reasons, so it highly oscillates at certain time intervals. Therefore, using the previous days' prices is more beneficial than the prices forecasted by the LSTM network for these intervals in the optimization model. However, since it is not possible to know the exact timing of these abrupt changes, the overall efficiency of the model has to be considered.
- Especially, in the case of the pumped storage hydropower plant, poor forecasting of the electricity prices considerably affects the revenue of the energy seller. Although a profit is estimated for the operation day, a loss may occur.
- Increase in the number of wind turbines provides higher revenue since the WHHS buys less energy from the grid, and the surplus energy is directly sold

to the grid after the pump's need is met. Therefore, the integration of the wind turbines to the WHHS decreases the grid dependency of the WHHS.

- The number of wind turbines in the WHHS does not change the operation schedules of the pump input, the hydro turbine output and the energy stored in the upper reservoir within the studied range of installed capacities. This is because these schedules are determined based on the electricity price, which is the input of the optimization model.

- The integration of the wind power to the pumped storage hydropower plant reduces two types of estimation errors. The first one is the error between the planned revenue and the realized revenue. The second one is the error between the maximum revenue in the ideal condition and the realized revenue. The first reason for the decrease in these errors is that the energy generated by wind turbines increases the total revenue, so the share of the pump and the hydro turbine operations in the revenue decreases. Since the majority of these errors are originated from the pumping cost, when its contribution decreases, the total error decreases, as well. Furthermore, the pump has a chance to use energy from wind turbines instead of using the energy from the grid in incorrectly predicted hours (i.e., the hours when the schedule of the pump operation is determined incorrectly). In this way, the loss is prevented, so the errors are decreased.

- Since it is challenging to predict future electricity prices with high accuracy, some buffer should be introduced to the calculated installed capacity of a wind power plant when a WHHS is designed. This provides compensation for the inefficient operation of the pumped storage hydropower plant due to the unpredictable electricity price oscillations. In addition to this, the additional energy generated from wind turbines will be sold in the grid, which will increase the revenue.

Some recommendations for the future studies are listed below:

- In this study, the MERRA-2 database is used for wind speed data. If better wind speed forecasts are available, then more realistic schedules can be predicted.

The optimization model can be run with a range of wind speed predictions in a stochastic manner, and a range of revenues can be obtained.

- The LSTM network, which is used to forecast electricity prices, can be improved by including more input features and a more extended training data set.

- In the scope of this study, an investigation of the initial cost to build a WHHS is not conducted. For further study, feasibility research can be carried out, and the rate of return for the WHHS may be calculated to convert existing cascade hydropower plant to a WHHS or build a WHHS from scratch.

- The studied optimization model in this thesis is based on 24 hours of simulations. However, this time interval can be extended to investigate the behavior of the optimization model in the long term (i.e., seasons of a year). To carry out the described investigation may be challenging due to the curse of dimensionality since it will include a lot more variable than the studied optimization model in this thesis.

- The losses in the hydraulic equipment of the WHHS (pump, hydro turbine, pipelines, etc.) are not evaluated explicitly in this study. For future research, hydraulic calculations may be carried out. Then, the design values of the hydraulic equipment can be determined to obtain the maximum revenue and operational schedule of the WHHS.

- In this study, a closed-system system is taken into consideration, so all inflows and outflows from and to the reservoir are ignored. The inclusion of inflows and outflows from the reservoir will result in more realistic representations of hybrid systems.

REFERENCES

Aeronautics, N. and Information, D. (2017). README Document for MERRA2 Data Products, pp. 1–62.

Akenerji (2005). Çınarcık HES Gerekçe Raporu.

Aksoy, S. A., Eryigit, E., Hashimova, N., Isbilir, M., Avsar, Z. M., Koksal, G. and Terciyanli, E. (n.d.). Ruzgar Gucu Uretimi icin Tahmin ve Teklif Sistemi Tasarimi, pp. 3–4.

Al Zohbi, G., Hendrick, P., Renie, C., Bouillard, P. and Zohbi, G. A. (2015). Wind-hydro pumped storage systems to meet lebanese electricity demand, *Revue des Energies Renouvelables* **18**: 3–375.

Anagnostopoulos, J. S. and Papantonis, D. E. (2012). Study of hybrid wind-hydro power plants operation and performance in the autonomous electricity system of Crete Island, pp. 239–246.

Anbazhagan, S. and Kumarappan, N. (2013). Day-ahead deregulated electricity market price forecasting using recurrent neural network, *IEEE Systems Journal* **7**(4): 866–872.

Angarita, J. M. and Usaola, J. G. (2007). Combining hydro-generation and wind energy. Biddings and operation on electricity spot markets, *Electric Power Systems Research* **77**(5-6): 393–400.

Antal, B. A. (2014). Pumped Storage Hydropower: A Technical Review in the area of Hydrologic and Hydraulic Engineering, (May).

Benitez, L. E., Benitez, P. C. and van Kooten, G. C. (2008). The economics of wind power with energy storage.

Bueno, C. and Carta, J. A. (2006). Wind powered pumped hydro storage systems, a means of increasing the penetration of renewable energy in the Canary Islands, *Renewable and Sustainable Energy Reviews* **10**(4): 312–340.

Castronuovo, E. D. and Lopes, J. A. (2004a). On the optimization of the daily operation of a wind-hydro power plant, *IEEE Transactions on Power Systems* **19**(3): 1599–1606.

Castronuovo, E. D. and Lopes, J. A. (2004b). Optimal operation and hydro storage sizing of a wind-hydro power plant.

Chollet, F. et al. (2015). Keras.
URL: *https://keras.io*

Crespo-Vazquez, J. L., Carrillo, C., Diaz-Dorado, E., Martinez-Lorenzo, J. A. and Noor-E-Alam, M. (2018). A machine learning based stochastic optimization framework for a wind and storage power plant participating in energy pool market, *Applied Energy* **232**(October): 341–357.

Cruz, P., Pousinho, H., Melício, R. and Mendes, V. (2014). Optimal Coordination on Wind-Pumped-Hydro Operation, *Procedia Technology* **17**: 445–451.
URL: *http://linkinghub.elsevier.com/retrieve/pii/S2212017314004897*

Deane, J., Gallachóir, B. . and McKeogh, E. (2010). Techno-economic review of existing and new pumped hydro energy storage plant, *Renewable and Sustainable Energy Reviews* **14**(4): 1293 – 1302.
URL: *http://www.sciencedirect.com/science/article/pii/S1364032109002779*

Dong, S., Li, H., Wallin, F., Avelin, A., Zhang, Q. and Yu, Z. (2019). Volatility of electricity price in denmark and sweden, *Energy Procedia* **158**: 4331 – 4337. Innovative Solutions for Energy Transitions.
URL: *http://www.sciencedirect.com/science/article/pii/S1876610219308264*

Dursun, B., Alboyaci, B. and Gokcol, C. (2011). Optimal wind-hydro solution for the Marmara region of Turkey to meet electricity demand, *Energy* **36**(2): 864–872.
URL: *http://dx.doi.org/10.1016/j.energy.2010.12.028*

Fischer, T. and Krauss, C. (2017). Deep learning with long short-term memory networks for financial market predictions, *Technical report*.

Forrest, J., Ralphs, T., Vigerske, S., LouHafer, Kristjansson, B., Jpfasano, Edwin-Straver, Lubin, M., Santos, H. G., Rlougee and Saltzman, M. (2018). coin-

or/cbc: Version 2.9.9.
URL: *https://doi.org/10.5281/zenodo.1317566*

García-González, J., de la Muela, R. M. R., Santos, L. M. and Gonzalez, A. M. (2008). Stochastic joint optimization of wind generation and pumped-storage units in an electricity market, *IEEE Transactions on Power Systems* **23**(2): 460–468.

Garrido, O. a. (2012). Short Term Load Forecasting with Neural Netwoks, **53**(1): 17–23.

General Electric (n.d.). GE Power & Water, Wind Turbine Series 2 .5mw.

Ghaisi Rad, M., Rahmani, M., Gharghabi, P., Zoghi, A., Hossein Hosseinian, S. and Hossein, S. (2017). Scheduling a Wind Hydro-Pumped-Storage Unit Considering the Economical Optimization, *American Journal of Electrical and Electronic Engineering* **5**(1): 16–22.
URL: *http://pubs.sciepub.com/ajeee/5/1/3*

Gimeno-Gutiérrez, M. and Lacal-Arántegui, R. (2013). *Assessment of the European potential for pumped hydropower energy storage storage potential.*

Global Modeling and Assimilation Office (GMAO) (2015). MERRA-2 tavg1_2d_slv_Nx: 2d, 1-Hourly, Time-Averaged, Single-Level, Assimilation, Single-Level Diagnostics V5.12.4, Greenbelt, MD, USA, Goddard Earth Sciences Data and Information Services Center (GES DISC), Accessed: 2019-09-05, 10.5067/VJAFPLI1CSIV.

Goodfellow, I., Bengio, Y. and Courville, A. (2016). *Deep Learning*, MIT Press.
URL: *http://www.deeplearningbook.org*

Greff, K., Srivastava, R. K., Koutnik, J., Steunebrink, B. R. and Schmidhuber, J. (2017). Lstm: A search space odyssey, *IEEE Transactions on Neural Networks and Learning Systems* **28**(10): 2222–2232.
URL: *http://dx.doi.org/10.1109/TNNLS.2016.2582924*

GWEC (Wind Global Council Energy) (2019). Global wind energy report 2018, (April): 1–61.
URL: *www.gwec.net*

Hering, P., Mošna, J., Janecek, E. and Hrycej, D. (2013). Optimal scheduling of a pumped-storage hydro power plant operation, *2013 13th International Conference on Environment and Electrical Engineering, EEEIC 2013 - Conference Proceedings* pp. 166–171.

Hochreiter, S. and Schmidhuber, J. (1997). Long Short-Term Memory, *Neural Computation* **9**(8): 1735–1780.

Hogeboom, R. J., Knook, L. and Hoekstra, A. Y. (2018). The blue water footprint of the world's artificial reservoirs for hydroelectricity, irrigation, residential and industrial water supply, flood protection, fishing and recreation, *Advances in Water Resources* **113**: 285 – 294.
URL: *http://www.sciencedirect.com/science/article/pii/S030917081730307X*

Hong, Y. Y. and Hsiao, C. Y. (2001). Locational marginal price forecasting in deregulated electric markets using a recurrent neural network, *Proceedings of the IEEE Power Engineering Society Transmission and Distribution Conference* **2**(WINTER MEETING): 539–544.

Ibrahim, H., Ghandour, M., Dimitrova, M., Ilinca, A. and Perron, J. (2011). Integration of wind energy into electricity systems: Technical challenges and actual solutions, *Energy Procedia* **6**: 815–824.
URL: *http://dx.doi.org/10.1016/j.egypro.2011.05.092*

IHA (2018). The world's water battery: Pumped hydropower storage and the clean energy transition, *IHA Working Paper* **1**(December): 1–15.

IRENA (2019). *Future of wind - deployment, investment, technology, grid integration and socio-economic aspects*.

James F. Manwell, Jon G. McGowan, A. L. R. (2009). *Wind Energy Explained: Theory, Design and Application*, second edi edn, Wiley.

Jaramillo, O. A., Borja, M. A. and Huacuz, J. M. (2004). Using hydropower to complement wind energy: A hybrid system to provide firm power, *Renewable Energy* **29**(11): 1887–1909.

Jiang, L. and Hu, G. (2018). Day-Ahead Price Forecasting for Electricity Market using Long-Short Term Memory Recurrent Neural Network, *2018 15th International Conference on Control, Automation, Robotics and Vision, ICARCV 2018* pp. 949–954.

Justus, C. (1978). *Winds and wind system performance*, Solar Series, Franklin Institute Press.
URL: *https://books.google.com.tr/books?id=a-RSAAAAMAAJ*

Kaldellis, J. K. and Kavadias, K. A. (2001). Optimal wind-hydro solution for Aegean Sea islands' electricity-demand fulfilment, *Applied Energy* **70**(4): 333–354.

Kapsali, M. and Kaldellis, J. K. (2010). Combining hydro and variable wind power generation by means of pumped-storage under economically viable terms, *Applied Energy* **87**(11): 3475–3485.
URL: *http://dx.doi.org/10.1016/j.apenergy.2010.05.026*

Kaya, M. N. (2012). *Design and Optimization of a Wind-Pumped Hydro Hybrid Power System Mehmet*, PhD thesis.

Kentel, E. and Alp, E. (2013). Hydropower in turkey: Economical, social and environmental aspects and legal challenges, *Environmental Science & Policy* **31**: 34 – 43.
URL: *http://www.sciencedirect.com/science/article/pii/S1462901113000361*

Korpaas, M., Holen, A. T. and Hildrum, R. (2003). Operation and sizing of energy storage for wind power plants in a market system, *International Journal of Electrical Power and Energy System* **25**(8): 599–606.

Kose, F. and Kaya, M. N. (2013). Analysis on meeting the electric energy demand of an active plant with a wind-hydro hybrid power station in Konya, Turkey: Konya water treatment plant, *Renewable Energy* **55**: 196–201.
URL: *http://dx.doi.org/10.1016/j.renene.2012.12.047*

Kragh, K. and Fleming, P. (2012). Rotor speed dependent yaw control of wind turbines based on empirical data, *Proceedings*, American Institute of Aeronautics and Astronautics.

Kur, B. (2019). Turkish Power Markets, (January).

Long Short-Term Memory Networks (n.d.). Accessed: 2020-03-23.
URL: *https://www.mathworks.com/help/deeplearning/ug/long-short-term-memory-networks.html;jsessionid=2c3026a6353544f6aebc47d5d882*

Loutan, C. and Hawkins, D. (2007). Integration of renewable resources, (November): 231.

Mandal, P., Senjyu, T., Member, S. and Urasaki, N. (2007). Price Forecasting for Day-Ahead Electricity Market.

Merity, S., Keskar, N. S. and Socher, R. (2017). Regularizing and optimizing LSTM language models, *CoRR* **abs/1708.02182**.
URL: *http://arxiv.org/abs/1708.02182*

Miller, R. (2009). Opportunities in Pumped Storage Hydropower: Supporting Attainment of Our Renewable Energy Goals By: Rick Miller, P.E., Senior Vice President, Hydropower Division, HDR|DTA and Maureen Winters, Corporate Consultant, Hydropower Division, HDR|DTA, pp. 1–9.
URL: *http://www.hydro.org/Pumped Storage Paper April 2009.pdf*

OECD (2019). Fossil Fuel Support Country Note, Turkey, *Technical Report April*.

Olauson, J. and Bergkvist, M. (2015). Modelling the Swedish wind power production using MERRA reanalysis data, *Renewable Energy* **76**: 717–725.
URL: *http://dx.doi.org/10.1016/j.renene.2014.11.085*

Panwar, N., Kaushik, S. and Kothari, S. (2011). Role of renewable energy sources in environmental protection: A review, *Renewable and Sustainable Energy Reviews* **15**(3): 1513 – 1524.
URL: *http://www.sciencedirect.com/science/article/pii/S1364032110004065*

Papaefthymiou, S. V., Karamanou, E. G., Papathanassiou, S. A. and Papadopoulos, M. P. (2010). A wind-hydro-pumped storage station leading to high RES penetration in the autonomous island system of Ikaria, *IEEE Transactions on Sustainable Energy* **1**(3): 163–172.

Pascanu, R., Mikolov, T. and Bengio, Y. (2012). On the difficulty of training recurrent neural networks, *30th International Conference on Machine Learning, ICML 2013* .

Presidency of the Republic of Turkey (2019). Eleventh Development Plan (2019-2023), *Technical report*.

Ragheb, M. (2012). Global wind power status.

Ritter, M., Shen, Z., Cabrera, B. L., Odening, M. and Deckert, L. (2015). A New Approach to Assess Wind Energy Potential, *Energy Procedia* **75**: 671–676.
URL: *http://dx.doi.org/10.1016/j.egypro.2015.07.485*

Roche, J. and Mcnally, S. (2016). Predicting the price of Bitcoin using Machine Learning Sean McNally Supervisor :, *Technical report*.

Sak, H., Senior, A. and Beaufays, F. (2014). Long Short-Term Memory Based Recurrent Neural Network Architectures for Large Vocabulary Speech Recognition, (Cd).
URL: *http://arxiv.org/abs/1402.1128*

Sivakumar, N., Das, D., Padhy, N., Kumar, A. and Bisoyi, N. (2013). Status of pumped hydro-storage schemes and its future in india, *Renewable and Sustainable Energy Reviews* **19**: 208 – 213.
URL: *http://www.sciencedirect.com/science/article/pii/S1364032112006090*

Smola, A. and Vishwanathan, S. (2008). *INTRODUCTION TO MACHINE LEARNING*, Vol. 1107, Cambridge University Press.

Somaraki, M. (2003). *A Feasibility Study of a Combined Wind - Hydro Power Station in Greece A thesis submitted for the degree of Master in Science In " Energy Systems and the Environment " Department of Mechanical Engineering*, PhD thesis.

Song, W., Zhang, K., Li, L., Zeng, M. and Zhang, G. (2013). Optimization model of the Joint operation of Pumped-Storage Hydro Plant and Wind Farm: Considering the Imbalances of Wind Power Output, *Przegląd Elektrotechniczny* **R. 89 NR 3**(3): 207–211.
URL: *http://pe.org.pl/articles/2013/3b/58.pdf*

Tan, M., Xiang, B. and Zhou, B. (2015). Lstm-based deep learning models for non-factoid answer selection, *CoRR* **abs/1511.04108**.
URL: *http://arxiv.org/abs/1511.04108*

Timmons, D., Harris, J. M. and Roach, B. (2014). The economics of renewable energy, *Global Development And Environment Institute, Tufts University* **52**: 1–52.

U.S. Army Corps of Engineers (2009). Technical Analysis of Pumped Storage and Integration with Wind Power in the Pacific Northwest Final Report U . S . Army Corps of Engineers Northwest Division Hydroelectric Design Center, (August): 166.

Veselý, K., Burget, L. and Grézl, F. (2010). Parallel Training of Neural Networks, *Technical Report 102*.

Yang, C. J. and Jackson, R. B. (2011). Opportunities and barriers to pumped-hydro energy storage in the United States, *Renewable and Sustainable Energy Reviews* **15**(1): 839–844.

Yarici, M. (2018). World Energy Council Turkish National Committee.

Zayas, J., Derby, M., Gilman, P., Ananthan, S., Lantz, E., Cotrell, J., Beck, F. and Tusing, R. (2015). Enabling Wind Power Nationwide, (DOE/EE-1218): 43.